



HAL
open science

Production and decay properties of neutron deficient isotopes with $N < 126$ and $74 \leq Z \leq 92$ at SHIP

Julio Antonio Heredia Cardona

► **To cite this version:**

Julio Antonio Heredia Cardona. Production and decay properties of neutron deficient isotopes with $N < 126$ and $74 \leq Z \leq 92$ at SHIP. Nuclear Experiment [nucl-ex]. Goethe Universität Frankfurt Allemagne, 2012. English. NNT: . tel-01139498

HAL Id: tel-01139498

<https://theses.hal.science/tel-01139498>

Submitted on 9 Apr 2015

HAL is a multi-disciplinary open access archive for the deposit and dissemination of scientific research documents, whether they are published or not. The documents may come from teaching and research institutions in France or abroad, or from public or private research centers.

L'archive ouverte pluridisciplinaire **HAL**, est destinée au dépôt et à la diffusion de documents scientifiques de niveau recherche, publiés ou non, émanant des établissements d'enseignement et de recherche français ou étrangers, des laboratoires publics ou privés.

Copyright

Production and decay properties of neutron deficient isotopes with $N < 126$ and $74 \leq Z \leq 92$ at SHIP



Dissertation
zur Erlangung des Doktorgrades
der Naturwissenschaften

vorgelegt beim Fachbereich Physik
der Johann Goethe Universität
in Frankfurt am Main von

MSc. Julio Antonio Heredia Cardona
geboren in Havanna, Kuba

Frankfurt am Main, 2012

Vom Fachbereich Physik der
Johannes Goethe Universität als Dissertationen angenommen

Dekan: Prof.Dr. Michael Huth
Erster Gutachter: Prof.Dr. Sigurd Hofmann
Zweiter Gutachter: Prof.Dr. Rene Reifarth
Datum der Disputation: 2012

Zusammenfassung

Kerne sind quantenmechanische Systeme, bei denen die Wechselwirkungen zwischen Nukleonen so komplex sind, daß die theoretischen Modelle, die ihre experimentell gemessenen Eigenschaften zu beschreiben versuchen, sie nicht alle gleichzeitig für alle Kerne wiedergeben können. Diese Modelle erklären besonders gut die wesentlichen Eigenschaften der Kerne in der Nähe der Stabilitätslinie, aber tun sich schwer mit zunehmender Entfernung davon, zum Beispiel im Bereich der Protonenabbruchkante. Es ist daher verständlich, daß man versuchen sollte, so viele Daten wie möglich über diese exotischen Kerne zu kompilieren, um die bestehenden theoretischen Modelle zu verbessern und um vielleicht eines Tages in der Lage zu sein, ein universelles Modell, das alle Eigenschaften aller Kerne beschreibt, zu erhalten. Zu diesem Zweck muß man diese Kerne gründlich studieren und ihre Eigenschaften messen. Natürlich ist die schwierigste experimentelle Herausforderung, daß sowohl Halbwertszeiten wie Wirkungsquerschnitte sich verringern, je weiter diese Kerne von der Stabilitätslinie entfernt sind.

Die wissenschaftliche Problemstellung dieser Arbeit war es, wie weit man die Erforschung neuer exotischer neutronenarmer Kerne im Bereich $N < 126$ und $74 \leq Z \leq 92$ weiter ausdehnen kann, um damit nukleare theoretische Modelle zu verbessern. Darüber hinaus muss es möglich sein, diese neuen Isotope spektroskopisch zu studieren. Der erste Schritt hierfür ist: Synthese und Nachweis. Unser Hauptziel ist es daher, vorherzusagen, welche neue neutronenarme Kerne mit $N < 126$ und $74 \leq Z \leq 92$ durch Verdampfungs-Fusionsreaktionen synthetisiert und anschließend mit Rückstoß-Separatoren nachgewiesen und identifiziert werden können, in dem man die wahrscheinlichsten Werte ihrer Halbwertszeiten und Wirkungsquerschnitte mit heutigen Modellen berechnet.

Zwei Experimente zur Synthese von neutronenarmen Isotopen in vollständigen Fusionsreaktionen wurden bei der GSI im Jahre 2008 durchgeführt,

nämlich Experiment R263 (^{64}Ni auf $^{147,150,152}\text{Sm}$) und Experiment R266 (^{40}Ca auf ^{144}Sm). Beide Strahlen wurden durch den UNILAC (Universal Linear Accelerator) beschleunigt. In diesen Experimenten wurde das Geschwindigkeitsfilter SHIP verwendet (siehe Abbildung 1). Es dient dazu, Verdampfungsrestkerne (VR) aufgrund ihrer Geschwindigkeitsunterschiede von den Projektilen zu trennen. Sein Detektor-System besteht aus drei Flugzeit-Detektoren, acht identischen 16-Streifen Silizium-Wafern (einem, um die Ionen zu stoppen, sechs rückwärts Detektoren und einem weiteren, der als Veto-Detektor verwendet wird) und einem klee-artigen Vier-Kristall-Germanium-Detektor. Die Positionsempfindlichkeit der Silizium-Detektoren gibt uns die Möglichkeit, das Zeit-, Positions- und Energie-Korrelationsverfahren anzuwenden.

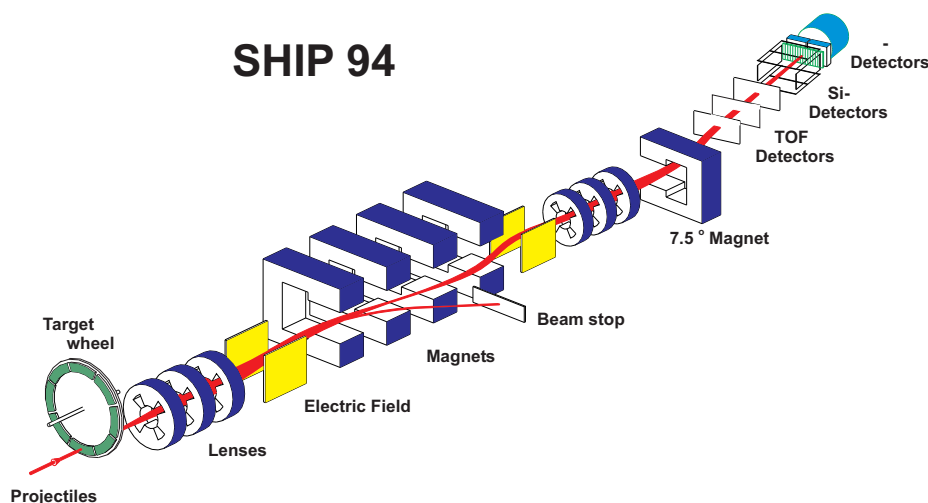


Abbildung 1: Separator for Heavy ion Reaction Products (SHIP) - Separator für Produkte von Schwerionenreaktionen

Die neuen neutronenarmen Isotope ^{208}Th und ^{179}Pb wurden in den vollständigen Fusionsreaktionen $^{64}\text{Ni} + ^{147}\text{Sm} \rightarrow ^{208}\text{Th} + 3n$ beziehungsweise $^{40}\text{Ca} + ^{144}\text{Sm} \rightarrow ^{179}\text{Pb} + 5n$ produziert. Die gemessenen Energien und Halbwertszeitwerten beim Alphazerfall von ^{208}Th sind 8044(30) keV beziehungsweise $1.7_{-0.6}^{+1.7}$ ms. Die von ^{179}Pb lauten 7350(20) keV beziehungsweise $3.5_{-0.8}^{+1.4}$ ms. Verbesserte Daten für den Alphazerfall von $^{209,210,212}\text{Th}$, $^{208g,208m,209}\text{Ac}$

und ^{208}Ra wurden mit den vollständigen Fusionsreaktionen von ^{64}Ni auf $^{147,150,152}\text{Sm}$ Targets ermittelt (siehe Tabelle 1). Verbesserte Daten für den Alphazerfall von $^{180,181}\text{Pb}$, ^{181g}Tl , ^{177g}Au , $^{174,172}\text{Pt}$ und ^{177}Hg wurden mit den vollständigen Fusionsreaktionen von ^{40}Ca auf ^{144}Sm Targets ermittelt (siehe Tabelle 1). Die neuen und auch die verbesserten Werte bilden schon jetzt eine wichtige Erweiterung der Basis von Messwerten, die von Modellen zur Vorhersage von Halbwertszeiten und Wirkungsquerschnitten herangezogen werden können.

Tabelle 1: Ergebnisse von Experimenten R263 und R266 - Gemessene Energien der α -Teilchen und Halbwertszeiten der Aktivitäten der Mutterkerne sowie α -Verzweigungsverhältnisse.

Kerne	E_α /keV	$T_{1/2}$ /ms	Kerne	E_α /keV	$T_{1/2}$ /ms	Kerne	b_α /%
^{212}Th	7809(5)	31.7(1.3)	^{208}Ra	7133(5)	1110(45)	^{208}Ra	87(3)
^{210}Th	7917(6)	16.0(3.6)	^{181}Pb	7016(15)	36(2)	^{177}Hg	100(5)
^{209}Th	8123(25)	$2.5^{+1.7}_-0.7^a$	^{180}Pb	7254(10)	4.2(5)	^{177g}Au	40(6)
^{208}Th	8044(30)	$1.7^{+1.7}_-0.6$	^{179}Pb	7350(20)	$3.5^{+1.4}_-0.8$	^{174}Pt	67(2)
^{209}Ac	7580(10)	77^{+8}_-7	^{181g}Tl	6181(7)	a	^{172}Pt	97(3)
^{208m}Ac	7747(10)	$23.6^{+8.6}_-5.0$	^{177g}Au	6161(7)	1530(70)		
^{208g}Ac	7566(10)	100^{+16}_-12					

^a Aufgrund der hohen Implantationsrate von VR konnte keine Halbwertszeit abgeleitet werden.

Um die totalen Halbwertszeiten der neuen neutronenarmen Isotope mit $N < 126$ und $74 \leq Z \leq 92$ vorherzusagen, verwendet man nukleare Massen aus theoretischen Berechnungen (Möller-Nix und Goriely *et al.*) und semi-empirische Formeln, um die partiellen Alpha-, β^+/EC - und Protonen Halbwertszeiten zu berechnen. Am SHIP können Isotope mit Halbwertszeiten zwischen 1 μs und 1 s getrennt, nachgewiesen und identifiziert werden, indem das Erfassungssystem mit schneller Elektronik benutzt wird.

Für schwere Kerne ist die Emission geladener Alpha-Teilchen ein spezifischer Zerfallsmodus. Drei semi-empirische Formeln wurden für die theoretische Berechnung der partiellen Halbwertszeiten für den Alphazerfall verwendet: die von Viola-Seaborg, Royer und Parkhomenko-Sobiczewski. Speziell für

neutronenarme Isotope mit $N < 126$ und $74 \leq Z \leq 92$, wurden neue Parameter der drei oben genannten semi-empirischen Formeln ermittelt. Dafür wurden 137 Isotope benutzt, von denen zwei neu produziert wurden (^{208}Th und ^{179}Pb) und zehn, bei denen die Zerfallswerte verbessert wurden. Der Abschirmungseffekt der Bahnelektronen hat keinen Einfluß auf die Qualität der Vorhersagen. Um die partielle Halbwertszeit für den Alphazerfall zu berechnen, wurde der geometrische Durchschnitt der drei semi-empirischen Formeln benutzt. Für den Q_α -Wert wurde der arithmetische Durchschnitt von den berechneten Werten aus den nuklearen Massen von Möller-Nix und Goriely *et al.* genommen. Einige partielle Halbwertszeiten für den β^+/EC -Zerfall wurden schon von Möller berechnet. Für die restlichen nicht berechneten Isotopen wurden diese partielle Halbwertszeiten durch die semi-empirische Formel von Zhang berechnet. Für die unbekanntesten neutronenarmen Isotope mit gerader Protonenzahl, $N < 126$ und $74 \leq Z \leq 92$, berechnet man die totalen Halbwertszeiten $T_{\frac{1}{2}}$ aus den partiellen Halbwertszeiten für den Alpha- und β^+/EC -Zerfall, da es keinen anderen konkurrierenden Zerfallsmodus gibt. Es konnten 73 bislang unbekannteste Isotope festgestellt werden, bei denen $1\mu\text{s} < T_{\frac{1}{2}} < 1\text{s}$ ist oder sogar 84, wenn $0.1\mu\text{s} < T_{\frac{1}{2}} < 1\text{s}$ ist (siehe Abbildung 2). In Abbildung 3 sind sie in rot, orange und gelb gefärbt.

Sehr neutronenarme Isotope mit ungerader Protonenzahl können nicht nur durch α oder β^+/EC Kanäle zerfallen, sondern auch durch Protonenzerfall. Diese Möglichkeit muß berücksichtigt werden, um die totale Halbwertszeit bestimmen zu können. Zwei semi-empirische Formeln zur Berechnung der partiellen Halbwertszeit für den Protonenzerfall wurden von Dong, Zhang und Royer ermittelt. Die partielle Protonen-Halbwertszeit erhöht sich um 3 bis 4 Größenordnungen, wenn der übertragene Drehimpuls Δl sich von null auf fünf ändert. Sie ist somit sehr empfindlich auf den Drehimpulswert l der emittierten Protonen. Deshalb wurde eine untere, $T_{\frac{1}{2},p}^L$, und eine obere, $T_{\frac{1}{2},p}^U$, Grenze für die partielle Halbwertszeit der Protonenzerfälle berechnet, die den Extremwerten von Δl , das heißt $\Delta l = 0$ beziehungsweise $\Delta l = 5$ entsprechen. Um die partielle Halbwertszeit für den Protonenzerfall zu berechnen, wurde das geometrische Mittel der zwei semi-empirischen Formeln

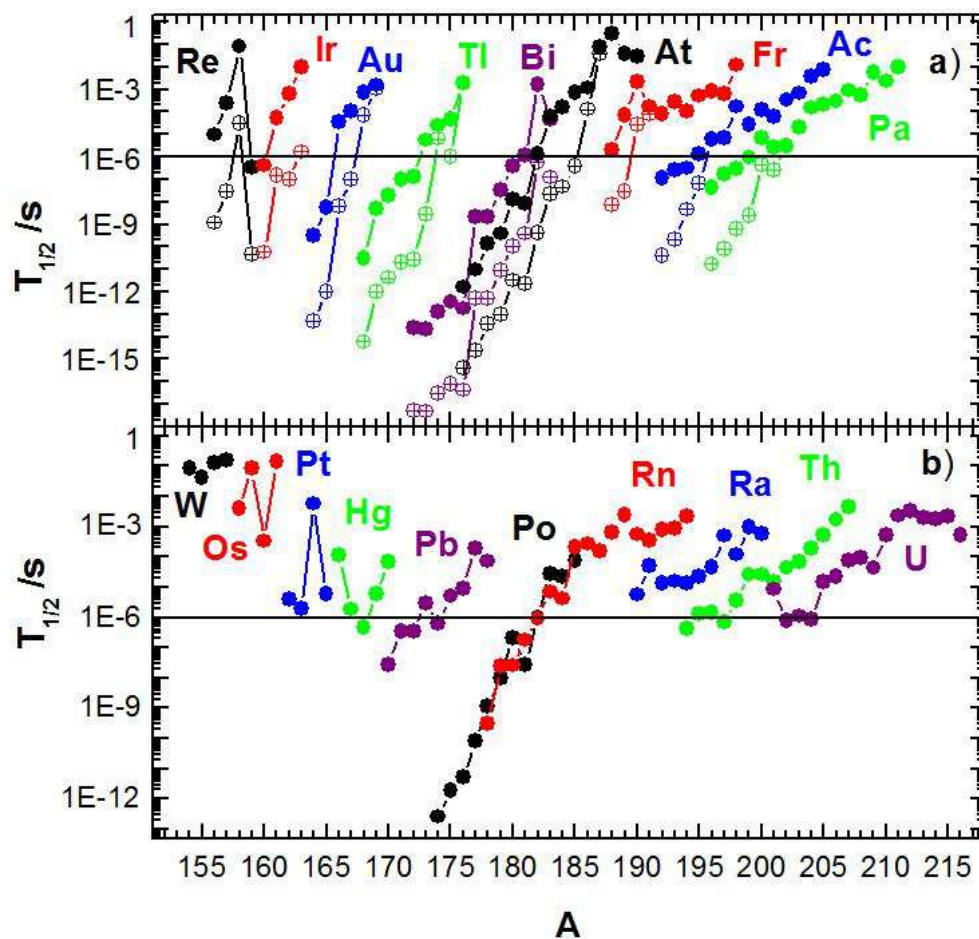


Abbildung 2: Erwartete totale Halbwertszeiten für die unbekannt neutronen-armen Isotope mit $N < 126$ und $Z = 74-92$ - (a) Isotope mit ungerader Protonenzahl: die vollen Kreise entsprechen der oberen Grenzen $T_{\frac{1}{2}}^U$ ($\Delta l = 5$) während die leeren Kreise die unteren Grenzen $T_{\frac{1}{2}}^L$ ($\Delta l = 0$) der totalen Halbwertszeiten repräsentieren; (b) Isotope mit gerader Protonenzahl

benutzt. Als Q_p -Wert wurde der arithmetische Durchschnitt von den berechneten Werten aus den nuklearen Massen von Möller-Nix und Goriely *et al.* genommen. Für die unbekanntene neutronenarmen Isotope mit ungerader Protonenzahl, $N < 126$ und $Z = 74-92$ wurden die totalen Halbwertszeiten $T_{\frac{1}{2}}$ aus den partiellen Halbwertszeiten für den Alpha-, β^+ / EC - und Protonenzerfall ermittelt. Aber da es zwei Werte für $T_{\frac{1}{2},p}$ gibt, nämlich eine untere Grenze $T_{\frac{1}{2},p}^L$ und eine obere Grenze $T_{\frac{1}{2},p}^U$, gibt es auch zwei Werte für die totale Halbwertszeit $T_{\frac{1}{2}}$, nämlich eine untere Grenze $T_{\frac{1}{2}}^L$ und eine obere Grenze $T_{\frac{1}{2}}^U$. Es konnten 41 bislang unbekanntene Isotope festgestellt werden, bei denen beide Grenzen $T_{\frac{1}{2}}^L$ und $T_{\frac{1}{2}}^U$ dem Intervall $[1 \mu\text{s}, 1 \text{s}]$ angehören (siehe Abbildung 2). Diese sind daher aus der Sicht des Zerfalls sehr wahrscheinlich am SHIP nachweisbar. In Abbildung 3 sind sie in rot, orange und gelb gefärbt.

Die Werte der Wirkungsquerschnitte für die Synthese von neuen neutronenarmen Isotopen mit $N < 126$ und $74 \leq Z \leq 92$ wurden mit Hilfe des statistischen Verdampfungscode HIVAP berechnet. Werte unter 1 pb wurden für die Produktion von Isotopen am SHIP nicht berücksichtigt, weil dazu die Bestrahlungszeiten zu lange würden. Deshalb muß man in der Lage sein, zuverlässige Werte für die Wirkungsquerschnitte vorhersagen zu können. Dabei ist ein Fehler von einer oder zwei Größenordnungen immer noch ein sehr nützliches Ergebnis, das zu den Vorbereitungen eines Experiments notwendig ist. HIVAP berechnet die Wirkungsquerschnitte von Verdampfungsrestkernen von Fusionsreaktionen mit einem statistischen Modell. Es berücksichtigt die Emission von Neutronen, Protonen, α -Teilchen, γ -Strahlen und Spaltung. Der erste Teil ist die Berechnung des Wirkungsquerschnitt der Fusion. Die anschließende Berechnung der Verdampfung ist der zweite Teil der HIVAP Berechnung. Zuerst wurden die Ergebnisse von HIVAP getestet. Dafür wurden 70 Reaktionen studiert, von denen acht aus unseren Experimenten R263 und R266 stammen. Insgesamt waren die Vorhersagen mit diesem Code sehr zufriedenstellend: die durchschnittliche Abweichung lag bei einem Faktor kleiner als vier. 117 Reaktionen (28 verschiedene Strahlen und 24 verschiedene Targets) wurden berücksichtigt. Es ergab sich, daß damit 73 neue neutronenarme Isotope mit $N < 126$ und

$74 \leq Z \leq 92$ mit einem Wirkungsquerschnitt größer als 1 pb synthetisiert werden können: 41 durch xn Kanäle und 32 durch pxn Kanäle.

Heute haben radioaktive Ionenstrahlen (RIBs) eine schwächere Intensität als die stabilen Strahlen. In der Zukunft könnten aber diese vergleichbar werden. Dann wäre ihre Verwendung für die Herstellung von neuen Isotopen von höchstem Interesse. Deshalb wurden die möglichen Werte der Wirkungsquerschnitte von Reaktionen mit RIBs untersucht. 49 Reaktionen (11 verschiedene Strahlen und 22 verschiedene Targets) wurden berücksichtigt. Damit könnten 21 neue Isotope mit einem Wirkungsquerschnitt größer als 1 pb synthetisiert werden und 24 Isotope könnten mit höheren Wirkungsquerschnitten produziert werden als mit stabilen Strahlen.

Insgesamt könnten 65 neue neutronenarme Isotope mit $N < 126$ und $74 \leq Z \leq 92$ mit einem Wirkungsquerschnitt größer als 1 pb und mit Halbwertszeiten $1\mu s < T_{\frac{1}{2}} < 1s$ synthetisiert werden (in rot in Abbildung 3) und 9 weitere mit RIBS (in orange in Abbildung 3). Diese wären aus der Sicht des Zerfalls und der Synthese sehr wahrscheinlich am SHIP nachweisbar.

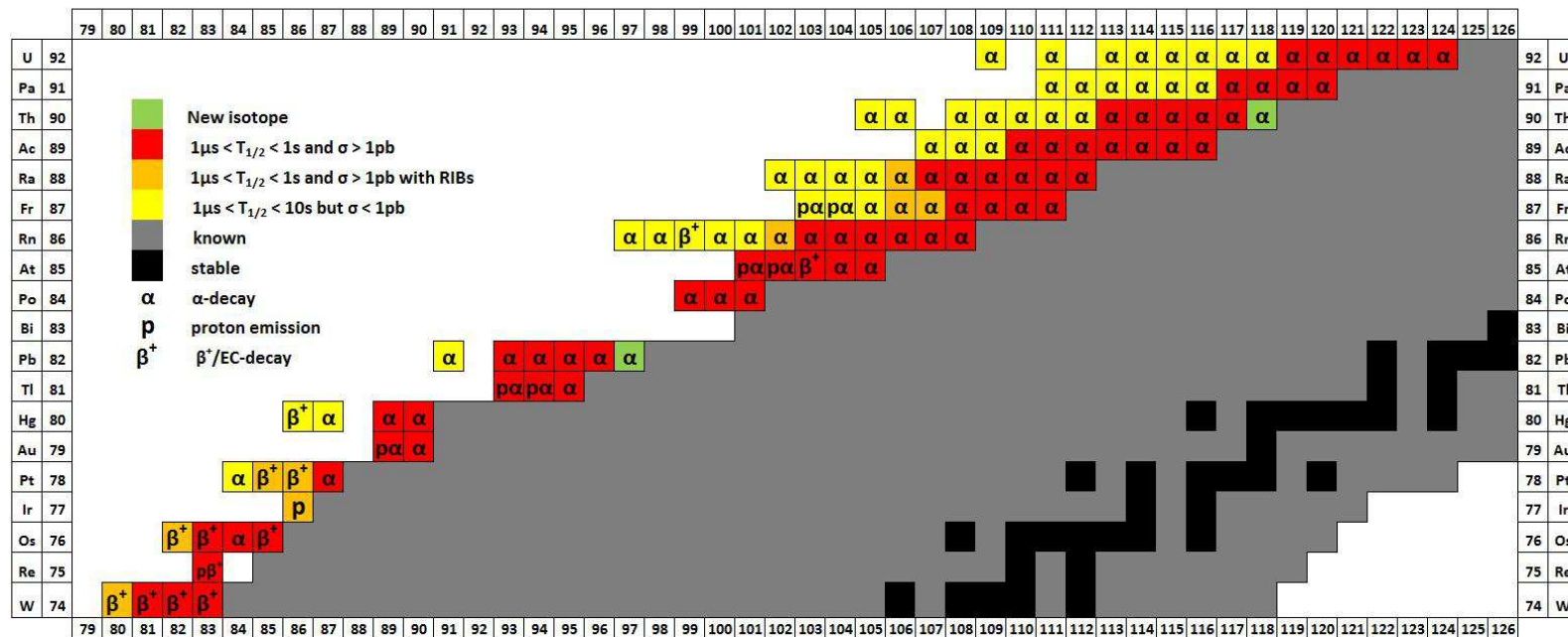


Abbildung 3: Eigenschaften der Synthese und des Zerfalls von neutronenarmen Isotopen mit $N < 126$ und $74 \leq Z \leq 92$
 Die Hauptzerfallsmodi (kleinste partielle Halbwertszeiten) sind durch Buchstaben gekennzeichnet: α , β^+ und p für α -, β^+ /EC- und Protonenzerfall. Bei Isotopen mit ungerader Protonenzahl, wenn die Hauptzerfallsmodi, die $T_{1/2}^L$ und $T_{1/2}^U$ entsprechen, verschieden sind, werden beide Zerfallsmodi angegeben. Der erste und zweite Buchstabe entsprechen der unteren bzw. oberen Grenze. Wenn die Zerfallsmodi identisch sind, wird nur ein Buchstabe verwendet. Siehe im Text die Erklärung der Farben.

To my parents and spouse.

Deutschland: Land der Möglichkeiten.

Mille viae ducunt hominem per saecula Romam. (Alanus de Insulis)

Chi addimanna nun fa errore. (Neapolitan proverb)

Acknowledgements

It is very hard to express with words on a keyboard the feelings I have towards the following people that made the completion of this thesis possible and the time I spent at GSI a great one. Nevertheless I will try to express my deepest gratitude to the following persons (the order of appearance is meaningless):

At GSI:

Professor Sigurd Hofmann allowed me to come to Germany to pursue the research, now written in this thesis. He is, in my opinion, an example for every young scientist in the world to follow. His dedication and passion for his work never stop to amaze me. His famous achievements are the culmination of a life dedicated to the nuclear physics field. Despite his busy schedule he always had time for me. One could not hope for a better Doktorvater.

Professor Andrei Andreyev helped me in many ways. He took an enormous amount of his time to teach me a lot. As a professor I am sure he will transmit to his students the same love, passion and dedication with which he accomplishes his job every day. Andrei is an immense inspiration for all those who want to become great physicists. It is a joy to joke with him after work. He is always in a good mood and it is highly contagious.

Dr. Fritz-Peter Heßberger helped me a lot whenever I needed him. He always had the right answer for any question I could imagine. He is one of the most dedicated physicists I know and his particular humor is going to be missed. His jokes made my stay here a very pleasant time. It is impossible not to stumble over his name in his field of research. He is one of the persons I am going to miss particularly. He was always in a good mood

and had some ironical jokes ready. It was always a pleasure to encounter him during the day.

Dr. Sophie Heinz was always available when I needed her help. She is the sweetest physicist I know and a fantastic colleague to work with. She loves what she does and to share it with the younger generations. She has always time for others even if it means staying much longer at work. I am sure her dedication will bare fruitful results in her complicated topic of transfer reactions as well as in waking the interest for nuclear physics in the younger generations.

Dr. Stanislav Antalic was always available to clarify the subtleties of Go4 or any other problem I encountered. He had always time for me. The answer with which he answered 99% of my questions will remain with me forever: "Yes and No." He is a very smart and funny Slovakian with whom it is always a pleasure to drink a beer.

Dr. Dieter Ackermann was always extremely friendly to me. He helped me with enthusiasm every time he could. He is a great colleague and I wish him to achieve great things in the next years in his field.

Dr. Bettina Lommel and **Dr. Birgit Kindler** were always very friendly and efficient colleagues. They are always in a contagious good mood that makes this working environment so pleasant.

Frau Engel was like her name: a real angel with me through all the application process.

Dr. Marina Litvinova and **Siggi Raiss** were the nicest secretaries one could imagine.

Future **Dr. Victor Comas** has always accompanied me from day one at the university. We arrived together to the German shores. His presence every day has of course made my stay here in Germany a little bit more Cuban. The many hours spent together make us like family.

Hans-Georg Burkhard was the best roommate I could hope for. His comments everyday allowed me to enjoy the typical friendly good mood of the people of Hessen.

Dr. Barbara Sulignano was the friendliest person at GSI. Her departure for France provoked a great sorrow in all of us at SHIP.

Dr. Gianluigi Clemente was a great friend even though he would have thrown me out of his house if I had cut the spaghetti.

To all **my friends** at GSI that made my stay a very pleasant experience.

In general I also have to thank **Germany** and the region of **Hessen** in particular that made it possible to travel 9000 km to make my PhD here. The slogan *Germany: land of opportunities* was in my case an understatement. It was a life changing and life shaping experience. In the same line of thought and not too far fetched I also owe to **GSI** the opportunity to meet **Diana**, my beloved wife who makes my life complete. For her, apart from all my love, my deepest thanks for encouraging me every day to reach for the stars.

In Cuba:

Professor Oscar Edgar Rodríguez Hoyos dedicated a lot of time to teach me not only about physics but also about life. His vision of the university was unique and he went against all the windmills to enforce it, but unlike Don Quijote he always beat the giants.

Professor Fernando Guzmán was first a great table tennis adversary, then a friend, a great professor and a wonderful rector. The Higher Institute of Applied Sciences and Technologies was his institute and he made it a wonderful place for students to first study nuclear physics and then reach out for the stars. He treated us like sons and we all hope never to disappoint him.

At FIAS:

Professor Walter Greiner helped me by accepting to be my Doktorvater for a period of time. For this I am extremely grateful.

Professor Henner Büsching was extremely helpful with the scholarship that allowed me to fulfill this work. He is an incredibly competent manager of this scholarship program that he succeeded to build up from scratch in

a few weeks. He is really passionate about what he makes and one can see it in the results.

Professor Appelshäuser also helped me with my scholarship. He was extremely friendly and explained very clearly how the whole program was structured.

Contents

List of Figures	xi
List of Tables	xiii
1 Introduction	1
2 Physical background	3
2.1 Element Synthesis: The Nuclear Fusion	3
2.2 Radioactive beams	4
2.2.1 The IF (“In-Flight”) method	5
2.2.2 The ISOL (<i>Ion-Source-On-Line</i>) method	6
2.2.3 Comparison and Outlook	6
2.3 Production Cross-sections	6
2.4 HIVAP	7
2.5 Alpha decay	8
2.5.1 Alpha-decay Q-value	8
2.5.2 Relationship between Q_α and $T_{\frac{1}{2},\alpha}$	10
2.5.3 Branching Ratios and Partial Half-lives	11
2.5.4 Hindrance factor and reduced α emission widths δ_α^2	12
2.5.4.1 Hindrance Factor	12
2.5.4.2 Reduced α Emission Widths δ_α^2	13
2.5.5 Theoretical formalism for the calculation of α -decay half-lives . .	13
2.5.6 Semiempirical formulae for the calculation of α -decay half-lives .	14
2.5.6.1 Viola and Seaborg	15
2.5.6.2 Poenaru and Rurarz	15
2.5.6.3 Royer	16

CONTENTS

2.5.6.4	Parkhomenko and Sobiczewski	16
2.6	Beta Decay	18
2.6.1	Beta decay theory	18
2.6.2	β^+ / EC -decay half-lives calculation	19
2.7	Proton Decay	19
2.7.1	Simple theory for proton emission in spherical nuclei	21
2.7.2	Semiempirical formulae	23
2.8	Masses	26
2.8.1	Finite-range droplet macroscopic model (FRDM) and folded-Yukawa single-particle microscopic model	26
2.8.2	Skyrme-Hartree-Fock-Bogoliubov mass formulae	27
3	Experimental devices and techniques	29
3.1	Ion sources, accelerator and beams	29
3.1.1	Ion sources	29
3.1.2	Accelerator	30
3.1.3	Beams	30
3.2	Targets	31
3.3	Separation	31
3.3.1	The velocity filter SHIP	31
3.3.2	Transmission of SHIP	32
3.4	Detectors	33
3.4.1	TOF detectors	33
3.4.2	Silicon detectors	34
3.4.2.1	The STOP detector	34
3.4.2.2	The STOP detector calibration	34
3.4.2.3	The BOX detector	35
3.4.2.4	The VETO detector	35
3.4.3	Germanium detector and its calibration	36
3.5	Data acquisition	36
3.5.1	Electronic system	36
3.5.2	The Go4 analysis framework	39
3.6	The correlation method	40

4	Experimental results	43
4.1	R263	43
4.1.1	Th	45
4.1.1.1	^{210}Th and ^{212}Th isotopes	45
4.1.1.2	^{209}Th isotope	48
4.1.1.3	The new isotope ^{208}Th	51
4.1.2	Ac	51
4.1.3	Ra	54
4.2	R266	56
4.2.1	Pb	56
4.2.1.1	^{181}Pb	57
4.2.1.2	^{180}Pb	57
4.2.1.3	The new isotope ^{179}Pb	58
4.2.2	^{181g}Tl and ^{177g}Au	59
4.2.3	^{174}Pt and ^{172}Pt	59
4.2.4	^{177}Hg	59
5	Half-lives	61
5.1	New parameters for semi-empirical α -decay formulae	62
5.1.1	Effect of the orbital electron screening	64
5.2	$T_{\frac{1}{2},\alpha}$	68
5.3	$T_{\frac{1}{2},\beta}$	69
5.4	$T_{\frac{1}{2},p}$	69
5.5	$T_{\frac{1}{2},2p}$	74
5.6	Total $T_{\frac{1}{2}}$	74
6	Cross-sections	81
6.1	HIVAP benchmark	81
6.2	New isotopes	82
6.2.1	Reactions	82
6.2.2	xn channels	84
6.2.3	pxn channels	84
6.2.4	α xn channels	87
6.3	Reactions with RIBs	88

CONTENTS

6.3.1	Reactions, new isotopes and higher cross-sections	89
6.3.2	Study to increase the cross-sections with RIBs for a given com- pound nucleus	91
7	Summary and Outlook	95
7.1	Summary	95
7.2	Outlook	96
	References	99

List of Figures

1	Separator für Produkte von Schwerionenreaktionen	iv
2	Erwartete totale Halbwertszeiten für die unbekanntenen neutronenarmen Isotope mit $N < 126$ und $Z = 74-92$	vii
3	Eigenschaften der Synthese und des Zerfalls von neutronenarmen Isotopen mit $N < 126$ und $74 \leq Z \leq 92$	x
2.1	ISOL and “in-flight” methods of RIB creation and post-acceleration.	5
2.2	Fit discrepancies for the $T_{\frac{1}{2},p}$ semiempirical formulae	25
2.3	Comparison of experimental and calculated microscopic energies E_{mic} for 1654 nuclei, for the macroscopic model corresponding to the finite-range droplet model	26
2.4	Differences between experimental and calculated masses as a function of the neutron number N for the HFB-17 mass model	28
3.1	The Separator for Heavy ion Reaction Products (SHIP)	32
3.2	Transmission ε_{trans} of the velocity filter SHIP	33
3.3	Block diagram of the focal plane detector	37
3.4	Data acquisition system	38
3.5	Timing Diagram	39
4.1	R263 Energy spectra	44
4.2	^{210}Th half-life	46
4.3	^{212}Th half-life	46
4.4	Th α -decay systematics	52
4.5	^{212}Th half-life	53
4.6	^{208}Ra half-life	55

LIST OF FIGURES

5.1	Connection between the energies of α -, two-proton- and proton-decay (Q_α , Q_{2p} and Q_p , respectively)	72
5.2	Expected total half-lives for the unknown neutron deficient isotopes with $N < 126$ and $Z = 74-92$	75
6.1	HIVAP benchmark	83
6.2	Comparison of σ_{xn} with $\sigma_{\alpha xn}$	88
6.3	Comparison of σ with σ_{RIB}	92
7.1	Results concerning the production and decay properties of neutron deficient isotopes with $N < 126$ and $74 \leq Z \leq 92$	97
7.2	The Author	107

List of Tables

1	Ergebnisse von Experimenten R263 und R266	v
2.1	Results obtained by Parkhomenko and Sobiczewski	17
2.2	Results obtained by Zhang <i>et al.</i>	20
4.1	Reactions used in R263	45
4.2	Th isotopes	47
4.3	^{208}Th and ^{209}Th decay chains	49
4.4	Ac and Ra isotopes	54
4.5	Reactions used in R266	55
4.6	Isotopes investigated in R266	56
4.7	α -Branching Ratios of isotopes investigated in R266	57
5.1	Known neutron deficient isotopes with $Z = 74-92$ used to test and to fit the parameters of Eqs. (2.28), (2.36) and (2.38)	63
5.2	Test of the parameters given by Parkhomenko and Sobiczewski	64
5.3	Results of the new fits	65
5.4	Parameters for the three semi-empirical α -decay formulae of Viola-Seaborg, Royer and Parkhomenko-Sobiczewski	66
5.5	Results of the new fits taking into account the orbital electron screening effect	67
5.6	Comparison of the theoretical Q_α values	68
5.7	Estimated Q_α , partial α -decay half-lives $T_{\frac{1}{2},\alpha}$, partial β^+/EC - decay half-lives $T_{\frac{1}{2},\beta}$ and total half-lives $T_{\frac{1}{2}}$ for so far unknown even- Z neutron deficient isotopes with $N < 126$ and $Z = 74-92$	70

LIST OF TABLES

5.8	Comparison of the Q_α , Q_p and Q_{2p} values calculated with the theoretical masses of Goriely <i>et al.</i>	71
5.9	Comparison of the $T_{\frac{1}{2},p}$ values	73
5.10	Estimated Q_α , Q_p , partial α -decay half-lives $T_{\frac{1}{2},\alpha}$, partial β^+/EC -decay half-lives $T_{\frac{1}{2},\beta}$, lower and upper limits for proton emission partial half-lives $T_{\frac{1}{2},p}$ and lower and upper limits for total half-lives $T_{\frac{1}{2}}$ for so far unknown odd- Z neutron deficient isotopes with $N < 126$ and $Z = 74-92$	78
6.1	Reactions calculated with HIVAP	85
6.2	New isotopes obtained through xn channels	86
6.3	New isotopes obtained through pxn channels	87
6.4	Reactions calculated with HIVAP using radioactive beams	89
6.5	New isotopes obtained with radioactive beams	90
6.6	Higher cross-sections with radioactive beams for 24 new isotopes of section 6.2	91
6.7	Beam-target combinations of the type described in Eq. 6.2 belonging to the 27 pairs of reactions calculated with HIVAP described in subsection 6.3.2	92

1

Introduction

A nucleus consists of A nucleons: Z protons, that carry each an electrical charge $+e$ and N slightly heavier, uncharged neutrons. Inside a nucleus, these particles are bound together by an attractive force: the nuclear strong force. Otherwise, the Coulomb repulsion between the positively charged protons would not permit the existence of stable matter. Of the 3600 experimentally produced isotopes, only around 300 are stable.

Nuclei are quantum-mechanical systems where the interactions between nucleons are so complex that theoretical models that try to describe their experimentally measured properties, cannot reproduce all of them for all nuclei at the same time.

These models explain particularly well the main properties of nuclei close to the stability line but struggle to do the same when one moves away towards the drip-lines for instance. It is therefore understandable that one should try to compile as much data as possible concerning these exotic nuclei that are farther from stability to improve the existing theoretical models and perhaps obtain one day a universal model able to describe all the characteristics of all nuclei. For this particular purpose, one would need to study these nuclei thoroughly, measuring all their properties. Of course, the main experimental challenge is that both, half-lives and cross-sections tend to decrease the farther these nuclei are from stability.

The scientific problem behind this thesis is the need of data of exotic neutron deficient nuclei with $N < 126$ and $74 \leq Z \leq 92$ to improve nuclear theoretical models. Furthermore, one needs to fully study these isotopes, the first step for this being, synthesizing them and detecting them.

1. INTRODUCTION

Our main objective is thus to predict which new neutron deficient isotopes with $N < 126$ and $74 \leq Z \leq 92$ can be synthesized through fusion evaporation reactions and subsequently detected and identified using recoil separators, by estimating their most probable half-life and cross-section values.

Chapter 2 provides the physical background for a better understanding of the results described in the following sections. Chapter 3 outlines the experimental devices and techniques used at SHIP to synthesize and to detect neutron-deficient isotopes. Chapter 4 deals with two experiments carried out to produce new neutron-deficient isotopes and improve the data of already known nuclides because of the necessity to have as much data in that region as possible to make more reliable half-life and cross-section predictions. Chapter 5 is about total half-life predictions of new neutron-deficient isotopes with $N < 126$ and $74 \leq Z \leq 92$ using nuclear masses from theoretical calculations and semi-empirical formulae to calculate the α -, β^+/EC -, and proton-decay partial half-life values whereas in Chapter 6 their cross-sections are estimated using the statistical evaporation code HIVAP. A summary of the major issues of this thesis and an outlook can be found at the end.

2

Physical background

The following sections in this chapter are dedicated to explain the basic physical phenomena connected with the production, decay and identification of neutron deficient nuclei with $N < 126$ and $74 \leq Z \leq 92$. They should merely serve as the apparatus to better understand the problematics of the next chapters where the analysis of the experiments is described and the interpretation of the data is put into perspective using the physical terms and ideas described here. The information that is outlined in this chapter is all based on published results from other authors.

2.1 Element Synthesis: The Nuclear Fusion

Nuclear fusion is the process by which two atomic nuclei join together to form a single heavier nucleus. It is usually accompanied by the release or absorption of energy. The excitation energy that the compound nucleus formed in this manner carries away can be expressed as:

$$E^* = Q + \frac{M}{M + m} E_p, \quad (2.1)$$

where $Q = (M + m - M_{CN})c^2$ is the reaction Q-value, E_p is the projectile's energy in the laboratory frame and M , m and M_{CN} are the masses of the target nucleus, of the projectile and of the compound nucleus, respectively. For the newly formed (or fused) compound nuclei the main de-excitation process is the emission of particles:

- neutrons (xn channels) or

2. PHYSICAL BACKGROUND

- protons and neutrons (pxn or $2pxn$ channels) or
- an α particle and neutrons (αxn channels)
- an α particle, neutrons and protons ($\alpha xnyp$ channels)

and γ rays. In this way an evaporation residue is formed.

2.2 Radioactive beams

The contents of this section are taken mainly from [1] and [2].

One of the ways to reach and to investigate the outer regions of the chart of nuclides is to create, separate and capture exotic, radioactive nuclei in traps and accumulate enough of them to then accelerate beams of these nuclides in order to study their interactions with other target nuclei. There are two main problems that one has to overcome to obtain beams with high enough yields to satisfy the needs of the experimental physicists: these nuclei are unstable and in general, the farther they are from stability, the shorter their life-times are and the lower their production cross-sections are. The first is inconvenient for the time-consuming accelerating process since one has to deliver a beam of these nuclides before they decay into another nuclear species. The second makes it necessary to separate them clearly from the other nuclides produced with similar or even much higher cross-sections if they are less exotic. One has therefore to separate and select from the many radioactive nuclei created at the same time, the required ones, in a short time. This process reduces the yields by orders of magnitude. Today the biggest disadvantage of these beams is their relatively low yield, and one interesting challenge for the physicists working in this area is to achieve beams with intensities comparable to the ones achieved with stable beams (see [1]).

Radioactive Ion Beams (RIBs) is a relatively new and promising experimental technique that allows to reach regions of the chart of nuclides that could only be reached with difficulties or not at all otherwise *i.e.* with the use of stable beams. One of these is the neutron deficient region that is studied in this work. RIBs are seen today as an important and very encouraging tool to investigate reaction mechanisms and nuclear structure in regions close to the so-called drip-lines. Many facilities are being designed and constructed to allow this purpose. There are two general approaches that can be used to produce RIBs: the “In-Flight” (IF) separation method and the

Isotope-Separator-On-Line (ISOL) method. The RIBs can be further used in secondary reactions to achieve even more exotic nuclei.

We will give a short description of these two methods.

2.2.1 The IF (“In-Flight”) method

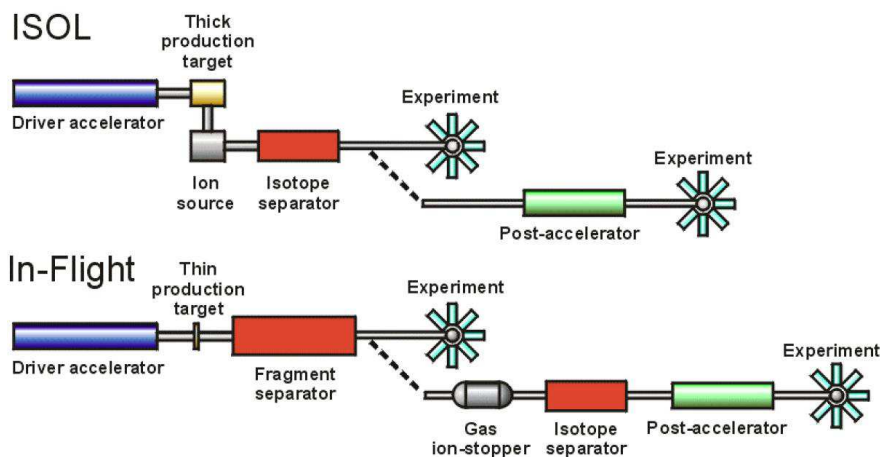


Figure 2.1: ISOL and “in-flight” methods of RIB creation and post-acceleration [1]. -

In the “in-flight” method, an intense beam of heavy ions is accelerated and fragmented on a thin target. The forward momentum of the fragmented ions is then used for mass separation or for further reactions (figure 2.1). The advantages of this method include its speed and that there is no relation with the chemical properties of the element. On the other hand, according to Cornell [1] two disadvantages are:

- Beams with bad ion optical qualities and need of carefully designed mass separators with high acceptance.
- Beam intensities are generally lower than that of the light-ion beams used for the ISOL method.

IF facilities exist and are in use in several laboratories in the world: GSI (Germany), GANIL (France), Dubna (Russia), RIKEN (Japan) and MSU (USA).

2. PHYSICAL BACKGROUND

2.2.2 The ISOL (*Ion-Source-On-Line*) method

In the ISOL method, a high-intensity primary beam of light particles induces spallation, fusion evaporation, fission or fragmentation reactions on a thick target, which is usually kept at high temperatures to facilitate the diffusion and effusion of reaction products into an ion source for ionization and extraction. The subsequent use of a mass separator allows the newly created exotic nuclides to be used for experiments at low energy or to be accelerated by a second accelerator (figure 2.1). A noticeable feature of this method is that by using very high intensities of driver beams of high-energy protons or reactor neutrons, very exotic nuclides with extremely low production cross-sections can still be obtained in a considerable amount. However, the two main disadvantages of this method are that some isotopes have half-lives which are too short for enough nuclei to survive this process and that the dependence on the chemical properties of the produced elements makes it difficult to extract some of them from the target, or to ionize sufficient numbers (see [1]).

ISOL facilities exist and are in use in laboratories worldwide spread: Louvain-la-Neuve (Belgium), Jyväskylä (Finland), REX-ISOLDE CERN (Switzerland), SPIRAL-GANIL (France), Oak-Ridge (USA) and ISAC TRIUMF (Canada).

2.2.3 Comparison and Outlook

As mentioned before, the advantages of one method are basically the disadvantages of the other. One has to insist on the following fact: the intensities reached with RIBs are not yet comparable to the ones achieved with stable beams. But, nevertheless, they remain a good alternative to investigate the unexplored, more exotic regions of the chart of nuclides. In the future, the RIBs facilities will combine the principles of the two aforementioned methods. By doing this, physicists will avoid, for example, the long delay of the ISOL technique by stopping the reaction products in a noble gas filled chamber and by guiding the ions using electrical fields and extracting them through an RF cooler (see [1]).

2.3 Production Cross-sections

The formation of an Evaporation Residue, can be treated in three main phases [3]:

- Two nuclei amalgamate to form a single common shape. Low energy surface vibrations and the transfer of a few nucleons occur.
- A spherical or nearly spherical compound nucleus is formed.
- The survival of the excited compound nucleus while evaporating neutrons and emitting γ -rays (competes with fission) *i.e.* the formation of an evaporation residue.

The evaporation residue cross-section can be evaluated as follows [4]:

$$\sigma_{er}(E) = \sum_{l=0}^{\infty} (2l+1) \sigma_l^{fus}(E, l) W_{sur}(E, l), \quad (2.2)$$

where the entrance channel effects are included in the partial fusion cross-section $\sigma_l^{fus}(E)$ defined by the expressions:

$$\sigma_l^{fus}(E) = \sigma_l^{capture}(E, l) P_{CN}(E, l), \quad (2.3)$$

$$\sigma_l^{capture}(E) = \frac{\lambda^2}{4\pi} p_l^{capture}(E), \quad (2.4)$$

Here λ is the de Broglie wavelength of the entrance channel, $P_{CN}(E, l)$ is a factor taking into account the decrease of the fusion probability due to re-separation of the dinuclear system before fusion, $p_l^{capture}(E)$ is the capture probability which depends on the collision dynamics and determines the amount of partial waves leading to capture and $W_{sur}(E, l)$ is survival probability of the compound nucleus for a given angular momentum l .

2.4 HIVAP

HIVAP [5] is a standard statistical evaporation code. It calculates out the cross-sections of evaporation residues of fusion reactions using a statistical model. It considers the emission of neutrons, protons, α -particles, γ -rays and fission. The first part of the calculation is the fusion cross-section calculation. The effect of deformation and the

2. PHYSICAL BACKGROUND

fluctuations of the fusion barrier are taken into account. Due to the fusion model used, the angular momentum and excitation energy distributions of the compound nuclei is unequivocally determined. This is the starting point for the subsequent evaporation calculation which is the second part of the HIVAP calculation. Here the population of the daughter nuclei is calculated taking into account the level densities of both mother and daughter nuclei, the transmission coefficients for each decay channel, the ground-state masses, the particle-separation energies, the ground-state shell effects, the fission barriers and the γ -strengths. A more detailed description of the calculations can be found in [6].

2.5 Alpha decay

This section is mainly taken from [3] and [7].

A specific decay mode, especially for heavy nuclei is α -decay. This process can be expressed by the following equation:



where X and X' represent the mother and daughter nuclei and α is the nucleus of a ${}^4\text{He}$ atom. The α decay is from the energetic point of view favorable because the total mass of the end products is smaller than the mass of the initial nucleus *i.e.* the Q-value of the decay is positive.

2.5.1 Alpha-decay Q-value

The Q_α -value for the α decay can be calculated using atomic masses, either known experimentally or calculated using a nuclear model:

$$Q_\alpha = (M_m - M_d - M_{He})c^2 \quad (2.6)$$

where M_m , M_d and M_{He} are the atomic masses of the mother and daughter nuclei and the ${}^4\text{He}$ atom, respectively.

The Q_α -value is divided between the total kinetic energy of the decay fragments which is the sum of the kinetic energies of the α particle, E_α and the daughter nucleus, E_d and the excitation energy of the daughter nucleus E_d^* , unless it is left in the ground-state in which case $E_d^* = 0$:

$$Q_\alpha = E_\alpha + E_d + E_d^* \quad \text{or} \quad (2.7)$$

$$Q_\alpha = E_\alpha + E_d \quad \text{if} \quad E_d^* = 0 \quad (2.8)$$

In the case of a decay to the ground-state of the daughter nucleus, if the conservation of linear momentum is considered, the total kinetic energy of the system has to be divided between the decay products inversely proportionally to their masses. Therefore the Q_α value is obtained from the experimentally measured α -particle energy E_α as

$$Q_\alpha = E_\alpha + E_d = E_\alpha \left(1 + \frac{M_{He}}{M_d} \right) \approx E_\alpha \left(1 + \frac{4}{A_d} \right) \quad (2.9)$$

where A_d is the mass number of the daughter nucleus (see [7]).

This Q_α value doesn't take into consideration, however, the electron cloud that surrounds the daughter nucleus. In fact, its value is somewhat smaller than what would be obtained if dealing with nuclei deprived of their electrons. The α -particle loses namely some energy while crossing this electron cloud. This orbital screening correction E_{sc} for α decay [8, 9] can be expressed as:

$$E_{sc} = 65.3 \cdot Z^{7/5} - 80 \cdot Z^{2/5} \quad [eV] \quad (2.10)$$

where Z is the proton number of the daughter nucleus. Therefore the Q_α^{bare} value of a nucleus without electrons can be deduced from the measured α -particle energy (see [7]) as stated in:

$$Q_\alpha^{bare} \approx E_\alpha \left(1 + \frac{4}{A_d} \right) + E_{sc} \quad (2.11)$$

2. PHYSICAL BACKGROUND

The α -particle must carry away an angular momentum l in the range $|I_i - I_f| \leq l \leq (I_i + I_f)$ and the parity π follows the selection rule $\pi_f = \pi_i(-1)^l$.

2.5.2 Relationship between Q_α and $T_{\frac{1}{2},\alpha}$

Geiger and Nuttall [10] noticed in 1911 that in the α decay there is a dependence (Geiger-Nuttall rule) between the decay energy and the half-life: the higher the decay energy, the shorter the half-life. Taagepera and Nurmia [11] were even able to fit this smooth dependence (especially for even-even nuclei) with this semi-empirical formula:

$$\log T_{\frac{1}{2},\alpha} = 1.61 \left(Z \cdot E_\alpha^{-\frac{1}{2}} - Z^{\frac{2}{3}} \right) - 28.9 \quad (2.12)$$

In the equation, $T_{\frac{1}{2},\alpha}$ is given in years, Z is the atomic number of the daughter nucleus and E_α is the kinetic energy of the α particle in MeV.

Equation (2.12) shows the very sensitive relation between the α -decay energy and the half-life. A small change in the α -decay energy corresponds to a much larger change in half-life, related to the atomic number and the decay energy.

In the late 1920's, to explain this characteristic of α decay, Gamow [12] and Gurney and Condon [13] developed a quantum theory where the α -particles tunnel through the Coulomb barrier. The α particles have a smaller energy than the Coulomb barrier. Their wavefunction is therefore exponentially attenuated as they pass through it and the emission probability is thus a very sensitive function of their energy. This is why we are confronted to a huge range of experimental half-lives.

According to this theory, a preformed α particle knocks, with frequency ω , against the walls of the spherical potential barrier $V(r)$ caused by the Coulomb interaction. In classical physics, it could not penetrate the potential barrier. However in quantum mechanics the α -particle tunnels through the potential barrier with the penetration probability P . Using the WKB-integral (Wentzel-Kramers-Brillouin) over the classically forbidden region of the potential one can estimate this factor:

$$P = e^{-G} = \exp \left[-2\sqrt{2\mu/\hbar^2} \int_{R_i}^{R_o} [V(r) - Q_\alpha^{bare}]^{\frac{1}{2}} dr \right] \quad (2.13)$$

where G is the Gamov factor, R_i and R_o are the classical turning points, $V(r)$ is the Coulomb barrier and μ is the reduced mass which is defined as:

$$\mu = \frac{M_{He}M_d}{M_{He} + M_d} \approx \frac{4 \cdot A_d}{4 + A_d} \cdot m_u \quad (2.14)$$

where m_u is the atomic mass unit.

The α -decay constant λ_α^{calc} is the product of the frequency ω and the probability P :

$$\lambda_\alpha^{calc} = \frac{\ln 2}{T_{\frac{1}{2},\alpha}^{calc}} = \omega P \quad [s^{-1}] \quad (2.15)$$

The term ω can be calculated as a fraction of the internal α -particle velocity and the nuclear radius, giving

$$\omega = v_{in}/R \quad (2.16)$$

From the aforementioned assumptions, one can deduce that the relation between $T_{\frac{1}{2},\alpha}$ and Q_α is:

$$\log T_{\frac{1}{2},\alpha} = A + \frac{B}{\sqrt{Q_\alpha}} \quad (2.17)$$

where A is a constant and B depends on Z . But this is the Geiger-Nuttall law of α -decay, because $\lambda_\alpha = \ln 2/T_{\frac{1}{2},\alpha}$.

2.5.3 Branching Ratios and Partial Half-lives

When decay schemes involve various decay modes, they can be quite complex. In that case λ is equal to the sum of all partial decay constants λ_i for all individual decay modes:

$$\lambda = \sum_i \lambda_i \quad i = \alpha, \beta^+, \beta^-, EC, SF, \dots \quad (2.18)$$

2. PHYSICAL BACKGROUND

The branching ratio can be defined as:

$$b_i = \frac{\lambda_i}{\lambda}, \quad (2.19)$$

and the partial half-life:

$$T_{\frac{1}{2},i} = \frac{\ln 2}{\lambda_i}. \quad (2.20)$$

It should be noted, however, that the partial half-life cannot be measured directly: for a specific nuclide, only the total half-life can be measured experimentally.

2.5.4 Hindrance factor and reduced α emission widths δ_α^2

2.5.4.1 Hindrance Factor

The hindrance factor HF expresses the differences between the calculated and the measured α -decay half-lives. It reflects the structural differences between the initial and the final states in mother and daughter nuclei, respectively:

$$HF = \frac{T_{\frac{1}{2}}^{exp}}{T_{\frac{1}{2}}^{calc}} \quad (2.21)$$

In general these hindrances for odd A nuclides are divided into 5 classes [14]:

- “ $1 < HF < 4$: the transition is called a favored transition. In such decays, the emitted α particle is assembled from two low lying pairs of nucleons in the parent nucleus, leaving an odd nucleon in its initial orbital. To form an α particle within a nucleus, two protons and two neutrons must come together with their spins coupled to zero and with zero orbital angular momentum relative to the center of mass of the α particle. These four nucleons are likely to come from the highest occupied levels of the nucleus. In odd A nuclei, because of the odd particle and the difficulty of getting a “partner” for it, one pair of nucleons is drawn from a

lower lying level, causing often the daughter nucleus to be formed in an excited state.

- $4 < HF < 10$: there is a mixing or favorable overlap between the initial and final nuclear states involved in the transition.
- $10 < HF < 100$: the spin projections of the initial and final states are parallel, but the wave function overlap is not favorable.
- $100 < HF < 1000$: transitions with a change in parity but with projections of initial and final states being parallel.
- $1000 < HF$: indicate that the transition involves a parity change and a spin flip, that is, the spin projections of the initial and final states are antiparallel, which requires substantial reorganization of the nucleons in the parent when the α particle is emitted.”

2.5.4.2 Reduced α Emission Widths δ_α^2

The reduced α -emission width δ_α^2 is given by:

$$\delta_\alpha^2 = \frac{\lambda_\alpha^{exp} \cdot h}{P} \quad (2.22)$$

where λ_α^{exp} is the experimental alpha-decay constant, h is Planck’s constant and P the penetration probability calculated according to the method of Rasmussen [15]. It should be noted that both the hindrance factor and the reduced width express the measured speed of the α -decay compared to the theoretically calculated value. Comparing equations (2.15), (2.21) and (2.22) one can observe that they are inversely proportional to each other.

2.5.5 Theoretical formalism for the calculation of α -decay half-lives

Using the formalism of Rasmussen [15], the edge of the potential barrier at the surface of the daughter nucleus is smoothed by the superposition of the real part of the α -nuclear potential derived by Igo [16] from the optical-model analysis and the Coulomb potential. The centrifugal potential caused by the orbital angular momentum

2. PHYSICAL BACKGROUND

l of the emitted α -particle is also considered. The barrier penetration probability P can be written as follows:

$$P = \exp \left[-2\sqrt{2\mu/\hbar^2} \int_{R_i}^{R_o} \left[V(r) + \frac{2Ze^2}{4\pi\epsilon_0 r} + \frac{\hbar^2}{2\mu r^2} l(l+1) - Q_\alpha^{bare} \right]^{\frac{1}{2}} dr \right] \quad (2.23)$$

with the potential derived by Igo:

$$V(r) = -1100 \cdot \exp \left[-\frac{r - 1.17 \cdot A^{\frac{1}{3}}}{0.574} \right] \quad (2.24)$$

where A and Z represent the mass and atomic numbers of the daughter nucleus and μ is the reduced mass given in equation (2.14). The penetration probability P is obtained by numerical calculation of the integral between the inner and outer classical turning points, see [7].

2.5.6 Semiempirical formulae for the calculation of α -decay half-lives

Several semiempirical approaches are used for the theoretical half-life value evaluation.

For the evaluation of these results we will define some magnitudes: $\bar{\delta}$ is the average of absolute values of discrepancies,

$$\bar{\delta} = \frac{1}{N} \sum_{k=1}^N \left| \log_{10} \left(T_{\frac{1}{2},\alpha,k}^{calc} / T_{\frac{1}{2},\alpha,k}^{exp} \right) \right| \quad (2.25)$$

$$\bar{f} = 10^{\bar{\delta}}, \quad (2.26)$$

and rms is the root-mean-square value of these discrepancies:

$$rms = \left[\frac{1}{N} \sum_{k=1}^N \log_{10}^2 \left(T_{\frac{1}{2},\alpha,k}^{calc} / T_{\frac{1}{2},\alpha,k}^{exp} \right) \right]^{\frac{1}{2}} \quad (2.27)$$

2.5.6.1 Viola and Seaborg

In 1966, Viola and Seaborg [17] proposed the use of a 7-parameter formula:

$$\log_{10} T_{\frac{1}{2},\alpha}^{VS}(Z, N) = (aZ + b)Q_{\alpha}^{-\frac{1}{2}} + (cZ + d) + h_i \quad (2.28)$$

where Z is proton number, N is neutron number and $Q_{\alpha}(Z,N)$ is the α -decay energy of a parent nucleus. The quantities a, b, c, d and h_i are adjustable parameters; h_i (originally denoted by $\langle \log F_i \rangle$), $i = p, n, pn$, are the average hindrance factors for o-e (*i.e.* odd-proton), e-o (*i.e.* odd-neutron) and o-o (*i.e.* odd-proton and odd-neutron) nuclei, respectively. For e-e nuclei, $h_i = 0$.

One can adjust the four parameters a, b, c, d to experimental values of the half-lives $T_{\frac{1}{2},\alpha}^{exp}$ (taken in seconds) with the use of experimental values of Q_{α}^{exp} (taken in MeV) for even-even nuclei for which both these data exist.

Then, keeping these four values of a, b, c, d fixed, an adjustment of the three other parameters h_p, h_n, h_{pn} to $T_{\frac{1}{2},\alpha}^{exp}$ with the use of Q_{α}^{exp} for odd-even, even-odd and odd-odd nuclei, respectively, is possible.

2.5.6.2 Poenaru and Rurarz

In 1980 Poenaru *et al.* [18] derived a semiempirical relationship on the ground of the fission theory of alpha decay and three years later, Rurarz [19] improved the values of some coefficients:

$$\log_{10} T_{\frac{1}{2},\alpha}^{PR}(Z, N) = (B_1 + B_2y + B_3z + B_4y^2 + B_5yz + B_6z^2) \frac{K_s}{\ln 10} - 20.446 \quad [s] \quad (2.29)$$

with

$$K_s = 2.52956 Z_d \sqrt{\frac{A_d}{AQ_{\alpha}}} (\arccos \sqrt{x} - \sqrt{x(1-x)}); \quad Q_{\alpha} = E_{\alpha} \frac{A}{A_d} \quad [MeV] \quad (2.30)$$

where

$$x = 0.4253 Q_{\alpha} \frac{1.5874 + A_d^{\frac{1}{3}}}{Z_d}; \quad A_d = A - 4; \quad Z_d = Z - 2 \quad (2.31)$$

$$y = (N - N_i)(N_{i+1} - N_i); \quad N_i \leq N \leq N_{i+1}; \quad N_i = \dots, 51, 83, 127, 185, \dots \quad (2.32)$$

2. PHYSICAL BACKGROUND

$$z = (Z - Z_i)(Z_{i+1} - Z_i); \quad Z_i \leq Z \leq Z_{i+1}; \quad Z_i = \dots, 51, 83, 115, 121, \dots \quad (2.33)$$

$$B_1 = 0.988662; \quad B_2 = 0.016314; \quad B_3 = 0.020433 \quad (2.34)$$

$$B_4 = 0.027896; \quad B_5 = B_6 = -0.003033 \quad (2.35)$$

2.5.6.3 Royer

In 2000, Royer [20] proposed a 12-parameter formula:

$$\log_{10} T_{\frac{1}{2},\alpha}^R(Z, N) = aZQ_\alpha^{-\frac{1}{2}} + bZ^{\frac{1}{2}}A^{\frac{1}{6}} + c \quad (2.36)$$

where Z and A are proton and mass numbers of a parent nucleus, respectively, and a , b , c are adjustable parameters. All three parameters are adjusted separately for each class of nuclei: ee, oe, eo and oo. Thus, this gives altogether 12 parameters.

An adjustment of the parameters to experimental values $T_{\frac{1}{2},\alpha}^{exp}$ with the use of experimental values Q_α^{exp} , both taken the same as in adjustment of the Viola-Seaborg parameters (see subsection 2.5.6.1), is necessary.

2.5.6.4 Parkhomenko and Sobiczewski

This section is mainly a summary of a published paper by Parkhomenko and Sobiczewski [21].

In 2005 Parkhomenko and Sobiczewski [21] checked the values of the Viola-Seaborg parameters fitted for elements with $84 \leq Z \leq 110$, Eq. (2.28). They realized that the value of the parameter b was too small compared to the values of aZ for such large Z . They suggested a 3-parameter formula

$$\log_{10} T_{\frac{1}{2},\alpha}^{PS}(Z, N) = aZQ_\alpha^{-\frac{1}{2}} + bZ + c \quad (2.37)$$

which might not be much worse (for e-e nuclei) than the 4-parameter one of Eq. (2.28). Indeed obtained results were even slightly better. The parameters are shown in table 2.1.

The authors argued that in the case of odd- A and o-o nuclei, structure of the ground states (g.s.) of the parent and the daughter nuclei are, in general, different.

Table 2.1: Results obtained by Parkhomenko and Sobiczewski [21] - The first column represents the class of nuclei, N the number of nuclei that were used for adjustment of the parameters of each class, $\bar{\delta}$ is the average of absolute values of discrepancies, rms is the root-mean-square value of these discrepancies, $\bar{f} = 10^{\bar{\delta}}$, n_p is the number of adjustable parameters for each class, \bar{E}_i is 0 for e-e nuclei, \bar{E}_p for o-e nuclei, \bar{E}_n for e-o nuclei and $\bar{E}_p + \bar{E}_n$ for o-o nuclei. The last three columns give the parameters a, b and c of equations (2.37) and (2.38).

Nuclei	N	$\bar{\delta}$	rms	\bar{f}	n_p	\bar{E}_i [MeV]	a	b	c
e-e	61	0.128	0.165	1.34	3	0	1.5372	-0.1607	-36.573
o-e	45	0.318	0.407	2.08	1	0.113			
e-o	55	0.508	0.602	3.22	1	0.171			
o-o	40	0.603	0.724	4.01	0	0.284			

This causes a hindrance of the transition between these states (see subsection 2.5.4). A parent nucleus prefers to decay from its g.s. to such an excited state of its daughter which has the same (or similar) structure. When the excitation energy of such a state is unknown, it is straightforward to treat it as an adjustable parameter. Thus, the formula (2.37), generalized to describe also odd-A and o-o nuclei, takes the form

$$\log_{10} T_{\frac{1}{2},\alpha}^{PS}(Z, N) = aZ(Q_\alpha - \bar{E}_i)^{-\frac{1}{2}} + bZ + c \quad (2.38)$$

where $\bar{E}_i = 0$ for e-e nuclei, $\bar{E}_i = \bar{E}_p$ (average excitation energy of proton one-quasiparticle state to which α decay goes) for o-e nuclei, $\bar{E}_i = \bar{E}_n$ (average excitation energy of neutron one-quasiparticle state to which α decay goes) for e-o nuclei and $\bar{E}_i = \bar{E}_{pn}$ (average excitation energy of one-proton and one-neutron quasiparticle state) for o-o nuclei. To minimize the number of adjustable parameters, they put the average excitation energy \bar{E}_{pn} of o-o nuclei as equal to the sum of the average energies of o-e (\bar{E}_p) and e-o (\bar{E}_n) nuclei, *i.e.*

$$\bar{E}_{pn} = \bar{E}_p + \bar{E}_n \quad (2.39)$$

2. PHYSICAL BACKGROUND

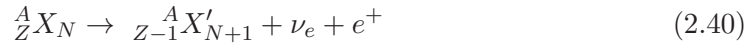
This way, they could obtain a formula ((2.38)) with only 5 adjustable parameters to describe all four classes of nuclei. With the 3-parameters a, b, c (fitted to data for e-e nuclei) kept fixed, adjustment of the two parameters \overline{E}_p and \overline{E}_n to $T_{\frac{1}{2},\alpha}^{exp}$ with the use of Q_{α}^{exp} for o-e and e-o nuclei, respectively, is achieved. \overline{E}_{pn} is obtained by Eq. (2.39).

2.6 Beta Decay

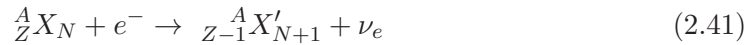
2.6.1 Beta decay theory

Beta decay occurs in nuclei with too many or too few neutrons to be stable. For neutron deficient isotopes, β^+ - and EC decay are very important decay modes, while in neutron-rich isotopes the same is true for β^- -decay. In 1930 Pauli predicted the existence of a new neutral particle, the neutrino, in order to explain the continuous spectrum of β -decay. In 1956 it was detected for the first time while Lee and Yang suggested that parity might not be conserved during this decay mode [22]. A result confirmed experimentally by Wu one year later [23], awarding them immediately the Nobel prize.

Neutron deficient isotopes can decay converting a proton into a neutron via β^+ -decay:



or via electron-capture (EC) decay:



Beta transitions are classified as allowed or forbidden according to their spin and parity changes, $\Delta J = J_i - J_f$ and $\Delta\pi = \pi_i \cdot \pi_f$, respectively:

- Allowed Transitions: $\Delta\pi = +1$ and $\Delta J = 0$ or ± 1 .
- n-times Forbidden Transitions: $\Delta\pi = (-1)^n$, $\Delta J = n, n + 1$ (exception: 1st-forbidden transition which may have $\Delta J = 0$)

n is the order of forbiddenness of the transition. With increasing order, the transitions become slower.

Therefore:

- 1st-forbidden transitions ($n=1$): $\Delta\pi = -1$ and $\Delta J = 0, \pm 1, \pm 2$.
- 2nd-forbidden transitions ($n=2$): $\Delta\pi = +1$ and $\Delta J = \pm 2, \pm 3$.
- 3rd-, 4th, ..., -forbidden transitions ($n = 3, 4, \dots$): $\Delta\pi = -1$ and $\Delta J = \pm 3, \pm 4, \Delta\pi = +1$ and $\Delta J = \pm 4, \pm 5, \dots$, respectively.

2.6.2 β^+/EC -decay half-lives calculation

In 1997 Möller *et al.* published partial half-lives for β^+/EC -decay [24]. For their calculations they used the masses they published two years earlier [25]. The formalism used by Möller *et al.* to calculate Gamow-Teller β -strength functions involves adding pairing and Gamow-Teller residual interactions to the folded-Yukawa single-particle Hamiltonian and solving the resulting Schrödinger equation in the quasi particle random phase approximation (QRPA).

In 2007 Zhang *et al.* [26] determined a semi-empirical formula to predict β^+/EC -decay partial half-lives. They found an exponential law between the experimental half-lives of β^+/EC -decays with the same order and the proton and mass numbers. It is written in the following form:

$$\log_{10} T_{\frac{1}{2},\beta}(Z, N) = (c_1 Z + c_2)N + c_3 Z + c_4 \quad (2.42)$$

The parameters of this formula shown in table 2.2 were obtained by fitting experimental data of β^+/EC -decay.

2.7 Proton Decay

Isotopes of uneven elements that are very neutron deficient can decay not only by α - or β^+/EC -decay but also by proton emission. We have to consider this possibility when trying to determine their total half-life.

A nucleus can emit a proton in the following way:

2. PHYSICAL BACKGROUND

Table 2.2: Results obtained by Zhang *et al.* [26] - The first column represents the order of the β^+/EC -decay transition from ground state to ground state, rms is the root-mean-square value of these discrepancies, $\bar{f} = 10^{\bar{\delta}}$, n_p is the number of adjustable parameters for each class, \bar{E}_i is 0 for e-e nuclei, \bar{E}_p for o-e nuclei, \bar{E}_n for e-o nuclei and $\bar{E}_p + \bar{E}_n$ for o-o nuclei. The last three columns give the parameters a, b and c of equations (2.37) and (2.38).

Order	c ₁	c ₂	c ₃	c ₄			rms
				e-o, o-e	o-o	e-e	
Allowed	-0.00179	0.4233	-0.3405	-0.6443	-1.7089	-0.2132	0.47
1 st Forbid.	-0.00127	0.3992	-0.4183	3.8215	3.7969	4.0364	0.35
2 nd Forbid.	-0.00162	0.3980	-0.3286	-0.1618	-0.4854	0.0267	0.35

$${}^A_Z X_N \rightarrow {}^{A-1}_{Z-1} X'_N + p \quad (2.43)$$

For spontaneous proton emission, just as for α -decay, the reaction value Q_p must be positive. This condition defines the limit of proton unbound nuclei *i.e.* the proton drip line.

The Q_p -value can be calculated using the atomic masses of the mother (M_m) and the daughter nuclei (M_d) and the masses of the elementary particles m_i , as

$$Q_p = (M_m - M_d - m_p - m_e)c^2 \quad (2.44)$$

Conservation of linear momentum requires that the total kinetic energy be divided between the two products in inverse proportion to their masses:

$$Q_p = E_p + E_d \quad (2.45)$$

$$E_p = Q_p \frac{M_d}{M_d + m_p} \quad (2.46)$$

and using eq. (2.46)

$$E_d = Q_p \frac{m_p}{M_d + m_p} = \frac{E_p m_p}{M_d} \quad (2.47)$$

Observing equation (2.23) one can notice that compared to α -particles, protons experience approximately:

- a factor of two lower Coulomb barrier
- a factor of four higher angular momentum barrier

This last feature makes the half-life of the proton emission extremely sensitive to the angular momentum l of the emitted proton. When measuring experimental values it is thus possible to receive direct spectroscopic information on the ordering and structure of the proton orbitals involved in the decay.

During the proton emission, the angular momentum of the emitted proton must be in the range $|I_i - I_f| \pm \frac{1}{2} \leq l \leq (I_i + I_f) \pm \frac{1}{2}$ and the parity π follows the selection rule $\pi_i = \pi_f (-1)^l$.

According to Dong *et al.* [27], to study the half-lives of spherical proton emitters, this decay mode can be treated not only within the framework of the WKB barrier penetration model (simple quantum tunneling effect through a potential barrier) but also other approaches have been used such as the distorted-wave Born approximation [28], the coupled-channels approach [29–32], the density-dependent M3Y (DDM3Y) effective interaction [33, 34], the effective interaction of Jeukenne, Lejeune, and Mahaux (JLM)[34], and the unified fission model [35].

2.7.1 Simple theory for proton emission in spherical nuclei

This section is taken from [7, 36, 37].

The knocking frequency f at which the proton knocks on the potential barrier and tries to penetrate it can be reliably estimated using the equation:

$$f = \frac{\sqrt{2}\pi^2 \hbar^2}{m^{3/2} R_c^3 (zZe^2/4\pi\epsilon_0 R_c - Q_p^{bare})} \quad [s^{-1}] \quad (2.48)$$

2. PHYSICAL BACKGROUND

The theoretical decay constant λ_{calc} is calculated using the potential barrier penetration probability P in the following way:

$$\lambda_{calc} = f \cdot P \quad (2.49)$$

The potential barrier between the proton and the daughter nucleus consists of the superposition of the nuclear $V_{jl}(r)$, the Coulomb $V_C(r)$ and the centrifugal potential $V_l(r)$. The real part of the optical model potential given by Becchetti and Greenlees [37] was used for the nuclear potential $V_{jl}(r)$ [36]. The parameterizations of the nuclear potential and the formulae used for the Coulomb and centrifugal potentials are presented in equations (2.50)–(2.57) [37].

$$V_{jl}(r) = -V_R f(r, R_R, a_R) + V_{SO} \lambda_\pi^2 \bar{\sigma} \cdot \bar{l} (1/r)(d/dr)[f(r, R_{SO}, A_{SO})] \quad (2.50)$$

$$V_R = 54.0 - 0.32 \cdot E_p + 0.4Z/A^{1/3} + 24.0(N - Z)/A \quad [MeV] \quad (2.51)$$

$$V_C(r) = \frac{zZe^2}{4\pi\epsilon_0 r} \left(3 - \frac{r^2}{R_c^2}\right) \quad for \quad r \leq R_c \quad (2.52)$$

$$V_C(r) = \frac{zZe^2}{4\pi\epsilon_0 r} \quad for \quad r > R_c \quad (2.53)$$

$$V_l(r) = l(l+1) \frac{\hbar^2}{2\mu r^2} \quad (2.54)$$

$$\bar{\sigma} \cdot \bar{l} = l \quad for \quad j = l + \frac{1}{2} \quad (2.55)$$

$$\bar{\sigma} \cdot \bar{l} = -(l+1) \quad for \quad j = l - \frac{1}{2} > 0 \quad (2.56)$$

$$f(r, R, a) = \frac{1}{1 + \exp[(r - R)/a]} \quad (2.57)$$

- $\bar{\sigma} \cdot \bar{l}$ = scalar product of the intrinsic and orbital angular momentum operators

- j, l = total and orbital angular momentum quantum numbers of the emitted particle (angular momentum transfer)
- z, Z = charge of proton and daughter nucleus
- A, N = mass and neutron numbers of daughter nucleus
- $R_R = 1.17 \cdot A^{1/3}$ [fm], $a_R = 0.75$ [fm], $R_c = 1.21 \cdot A^{1/3}$ fm
- $R_{SO} = 1.01 \cdot A^{1/3}$ [fm], $a_{SO} = 0.75$ [fm], $V_{SO} = 6.2$ MeV
- μ = reduced mass $\approx \frac{m_p \cdot A}{m_p/m_u + A}$
- $m_u = 931.501$ [MeV/c²], $m_p = 938.211$ MeV/c²
- λ_π^2 = pion Compton wavelength squared ≈ 2.0 fm²

In analogy with the α decay (WKB method) the penetration probability P is obtained by integrating over the potential barrier between the classical turning points R_i and R_o ,

$$P = \exp \left[-2 \sqrt{2\mu/\hbar^2} \int_{R_i}^{R_o} [V_{jl}(r) + V_C(r) + V_l(r) - Q_p^{bare}]^{\frac{1}{2}} dr \right] \quad (2.58)$$

In reference [38] a review of more sophisticated and recent approaches and theories on proton radioactivity is given.

2.7.2 Semiempirical formulae

This section is a summary of a published article [27].

In 2009, two semiempirical formulae for the calculation of the proton emission half-life *i.e.* (2.59) and (2.60) similar to the ones proposed for α decay by Viola-Seaborg (Eq. (2.28)) and Royer (Eq. (2.36)), respectively, were presented by Dong, Zhang and Royer [27]:

$$\log_{10}[T_{\frac{1}{2},p}^{DV}(s)] = (aZ + b)Q_p^{-\frac{1}{2}} + c + c_0 \frac{l(l+1)}{\sqrt{(A-1)(Z-1)A^{-\frac{2}{3}}}} \quad (2.59)$$

2. PHYSICAL BACKGROUND

$$\log_{10}[T_{\frac{1}{2},p}^{DR}(s)] = a + bA^{\frac{1}{6}}\sqrt{Z} + cZQ_p^{-\frac{1}{2}} + c_0 \frac{l(l+1)}{\sqrt{(A-1)(Z-1)A^{-\frac{2}{3}}}} \quad (2.60)$$

where Z and A are charge and mass numbers of the parent nucleus, respectively, and Q_p the proton decay energy in MeV.

In these two formulae, one can appreciate that the first terms are similar to the ones in Eq (2.28) and Eq. (2.36), respectively. The last added term $c_0 \frac{l(l+1)}{\sqrt{(A-1)(Z-1)A^{-\frac{2}{3}}}}$ is the contribution to the partial half-life $T_{\frac{1}{2},p}$ of the centrifugal barrier energy given in Eq. (2.54) that reduces the tunneling probability and hence increases the half-life. This addition was based on a similar formula for α decay [39, 40] to take into account the influence of angular momentum transfer.

Performing a least squares fit to the half-lives of the first 25 spherical proton emitters available in [27], they obtained a set of parameters for formulae (2.59) and (2.60). Their values are:

$$a = 0.3437, b = 4.9628, c = -31.1253 \text{ and } c_0 = 2.5950 \quad (2.61)$$

with $\bar{\delta}$ (average of absolute values of discrepancies) = 0.153 and

$$a = -23.0632, b = -0.4225, c = 0.4170 \text{ and } c_0 = 2.5989 \quad (2.62)$$

with $\bar{\delta} = 0.183$, respectively.

Additionally, they obtained a set of parameters for half-lives of deformed proton emitters by employing a least squares fit to data, which included 11 nuclei ($Z = 53-67$) that could be found in [27] or [29]. These parameters are:

$$a = 0.3637, b = 4.6467, c = -30.9299 \text{ and } c_0 = 2.6244 \quad (2.63)$$

with $\bar{\delta} = 0.323$ and

$$a = -23.9341, b = -0.3936, c = 0.4385 \text{ and } c_0 = 2.6167 \quad (2.64)$$

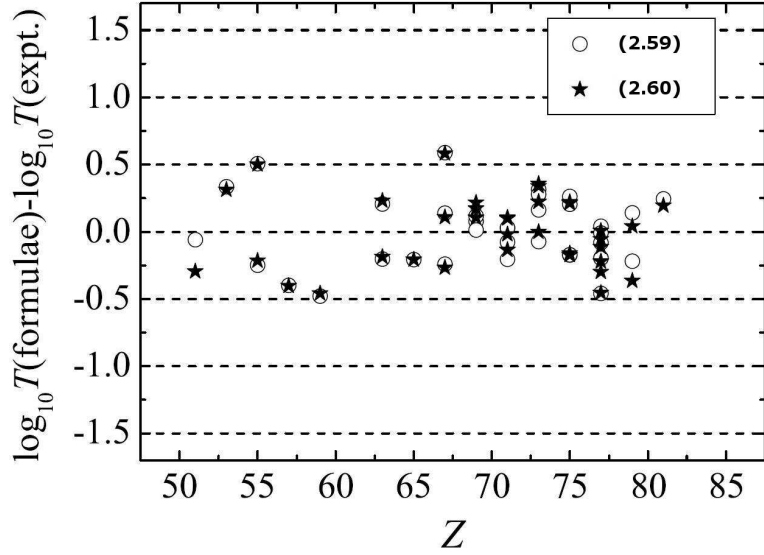


Figure 2.2: Fit discrepancies for the $T_{\frac{1}{2},p}$ semiempirical formulae - Deviation between the formulae (2.59) and (2.60) and the experimental logarithm of half-lives for proton emission. The figure is taken from [27].

with $\bar{\delta} = 0.316$, respectively.

In Dong, Zhang and Royer's approach the half-lives increase by 3–4 orders of magnitude when the angular momentum transfer Δl varies from zero to five. This means that the partial half-life of proton emission is quite sensitive to the angular momentum l carried away by the emitted proton. Many proton emitters have been recently observed in experiments because the ensuing higher centrifugal barriers significantly prolong their half-lives to a large extent. On the other hand, this elevated sensitivity helps to determine the l value when the half-life $T_{\frac{1}{2},p}$ and the Q_p value are experimentally measured. In doing so, one can extract some useful information about nuclear structure.

According to the authors, the two formulae (2.59) and (2.60) can confirm each other and better results will be obtained in the future, but already, the experimental proton emission half-lives of most nuclei could be predicted within a factor of less than two as can be seen in figure 2.2. Some larger deviations (within a factor of three) were attributed to the shell effects not being taken into account and the odd-A nuclei not being distinguished from odd-odd nuclei. Finally the authors concede that the large

2. PHYSICAL BACKGROUND

dependences on both Q_p and Δl on the $T_{\frac{1}{2},p}$ calculation imply that it is quite difficult to predict the half-life of proton emission for unknown nuclei since the Q_p value can not be obtained with a good accuracy and since the uncertainty on the Δl value is large.

2.8 Masses

In many studies the model error is defined by the root-mean-square (rms) deviation, which is given by:

$$rms = \left[\frac{1}{n} \sum_{i=1}^n (M_{exp}^i - M_{th}^i)^2 \right]^{\frac{1}{2}} \quad (2.65)$$

2.8.1 Finite-range droplet macroscopic model (FRDM) and folded-Yukawa single-particle microscopic model

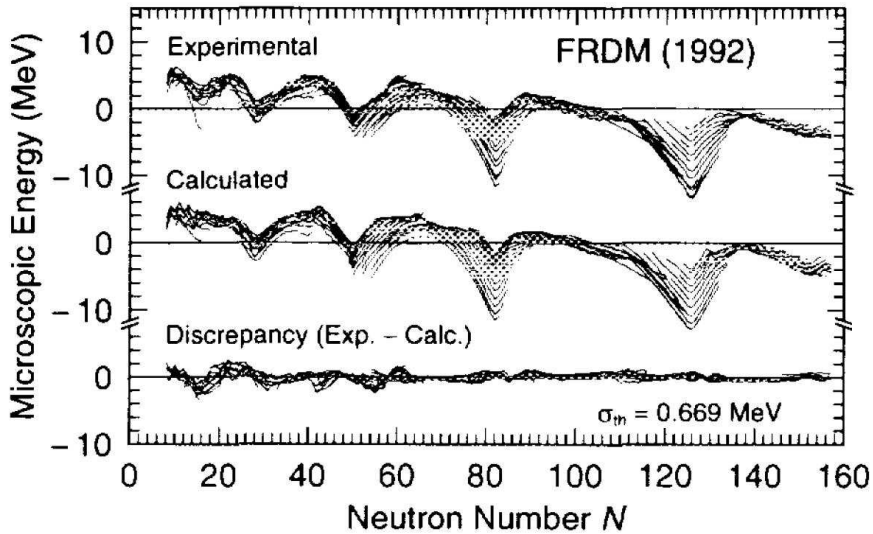


Figure 2.3: Comparison of experimental and calculated microscopic energies E_{mic} for 1654 nuclei, for the macroscopic model corresponding to the finite-range droplet model - The bottom part shows the differences between these two quantities which is equivalent to the difference between measured and calculated ground-state masses. There are almost no systematic errors remaining for nuclei with $N \geq 65$, for which region the error is only 0.448 MeV. The lines are drawn through isotopes chains. The figure and the caption are taken from [25].

In 1995 Möller and Nix [25] tabulated the masses and other parameters of 8979 nuclei from ^{16}O to $A = 339$. Their calculations were based on the finite-range droplet macroscopic model (FRDM) and the folded-Yukawa single-particle microscopic model. The authors further explained that the results were obtained using the Lipkin-Nogami pairing model, minimization of the ground-state energy with respect to additional shape degrees of freedom and an eighth-order Strutinsky shell correction. Figure 2.3 shows the result of such a mass calculation. The authors plotted in the top part the differences between measured masses and the spherical macroscopic FRDM contributions against the neutron number N , with isotopes of a particular element connected by a line. These experimental microscopic corrections should be compared with the calculated microscopic corrections plotted in the middle part of the figure. When the macroscopic and microscopic parts of the mass calculation are combined and subtracted from the measured masses, the deviations in the bottom part of the figure remain (see [25]). The trends of the error in the heavy region suggest that this mass model should be quite reliable for nuclei beyond the current end of the periodic system. The error of the mass model is 0.669 MeV for the entire region of nuclei considered, but is only 0.448 MeV for the region $N \geq 65$ [25].

2.8.2 Skyrme-Hartree-Fock-Bogoliubov mass formulae

In 2009, Goriely *et al.* [41] published microscopic mass tables based on their latest model: HFB-17. It used the Hartree-Fock-Bogoliubov method with Skyrme and contact-pairing forces, together with phenomenological Wigner terms and correction terms for the spurious collective energy. The authors further explained that model parameters were fitted on the 2149 measured masses of nuclei with N and $Z \geq 8$ given in the 2003 AME [42], requiring that the model reproduced several properties of uniform asymmetric nuclear matter determined by microscopic calculations with realistic nucleon-nucleon potentials. This HFB-17 mass model, by treating the pairing more realistically than in any of their earlier models achieved an rms deviation on the 2149 measured masses of nuclei with N and $Z \geq 8$ of only 0.581 MeV (see [41]). The deviations between the experimental data and the HFB-17 predictions are shown graphically in fig. 2.4.

2. PHYSICAL BACKGROUND

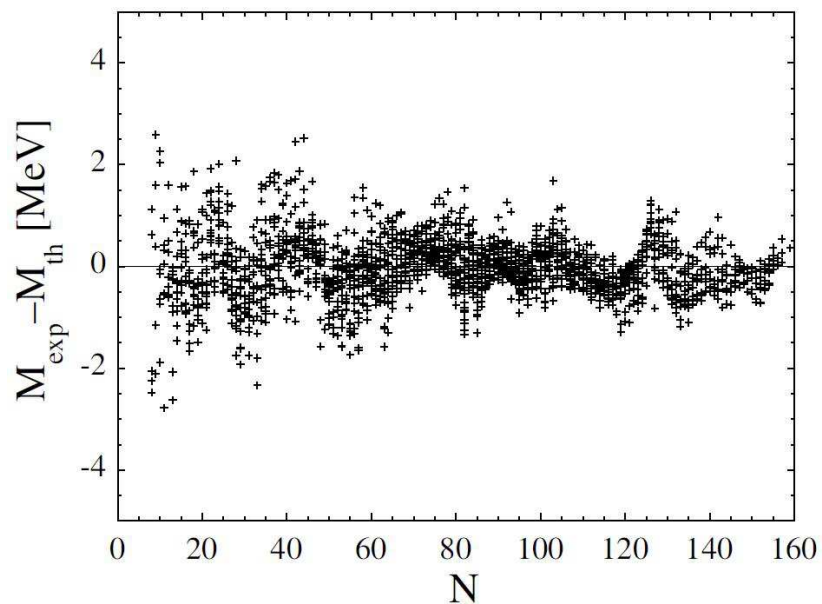


Figure 2.4: Differences between experimental and calculated masses as a function of the neutron number N for the HFB-17 mass model - The rms and mean (data-theory) values of these deviations on the 2149 measured masses of nuclei with N and $Z \geq 8$ are 0.581 MeV and -0.019 MeV, respectively. The figure and the caption are taken from [41].

3

Experimental devices and techniques

In the following chapter we will discuss the experimental devices and techniques we used to synthesize, detect and identify neutron-deficient isotopes. The information that is outlined in this chapter is all based on published results from other authors. To avoid paraphrase, quotation marks are often used.

3.1 Ion sources, accelerator and beams

The two main experiments for synthesis of neutron-deficient isotopes in complete-fusion reactions were carried out at GSI in 2008 during two experimental runs, R263 and R266:

- R263: ^{64}Ni ions from an ECR (electron cyclotron resonance) source on enriched ^{144}Sm targets
- R266: ^{40}Ca ions from a Penning (PIG) source on enriched $^{147,150,152}\text{Sm}$ targets

Both beams were accelerated by the UNILAC (Universal Linear Accelerator).

3.1.1 Ion sources

Spädtke explains that for the Penning (PIG) source, “the highest level of experience is available at GSI. The source is either operated with the desired isotope in gaseous form, or if this is not available, sputter technique is applied. Thus most of

3. EXPERIMENTAL DEVICES AND TECHNIQUES

the elements are available. In some cases special treatment of the material used as sputter electrode is necessary” [43]. According to Hofmann and Münzenberg [44] some years ago “the facilities for experiments at low projectile energies were upgraded. A new high-charge injector was built, including a 14-GHz- ECR (electron cyclotron resonance) CAPRICE-type ion source [45]. The ion source is followed by a radio-frequency quadrupole and an interdigital H-structure accelerator that provide a beam energy of 1.4 MeV/u (MeV per mass unit u) for direct injection into the Alvarez section of the UNILAC [46]. The advantages, compared with the previously used Penning ion source are:

- Low consumption of material ($\approx 0.2 - 4$ mg/h).
- Intense and stable projectile currents.
- A high-quality beam of low emittance, halo free and of well-defined energy.

The high beam quality is a result of the high ionic charge state attained (10^+ in the case of ^{70}Zn [47]). This charge state is maintained throughout the acceleration process. An increase by stripping of electrons is unnecessary. The reduction of projectile background behind the SHIP is partially due to the increased beam quality.”

3.1.2 Accelerator

The SHIP, later described in subsection 3.3.1, is placed at the central beam line of the UNILAC at GSI Helmholtzzentrum für Schwerionenforschung in Darmstadt, Germany. According to Hofmann and Münzenberg [44], “this accelerator is able to deliver beams for all stable elements up to uranium with a relatively high intensity. For example, the following values could be obtained at the target: $3.0\text{ p}\mu\text{A}$ for $^{40}\text{Ar}^{8+}$, $1.2\text{ p}\mu\text{A}$ for $^{58}\text{Fe}^{8+}$, and $0.4\text{ p}\mu\text{A}$ for $^{82}\text{Se}^{12+}$ ($1\text{ p}\mu\text{A} = 6.24 \cdot 10^{12}$ particles/s). The beam energy can be varied practically continuously by using a set of single resonators. The relative accuracy of the beam energy is ± 0.003 MeV/u. The absolute energies are accurate to ± 0.01 MeV/u.”

3.1.3 Beams

Pulsed (5 ms beam on/15 ms beam off) ^{64}Ni and ^{40}Ca beams with a typical intensity of 500 pA were provided by the UNILAC.

The relevant beam energies and targets used are given in table 4.1 and 4.5.

3.2 Targets

Eight target segments of a specific Sm isotope were mounted on a target wheel rotating synchronously with the UNILAC macropulsing.

The targets were prepared from isotopically enriched material of $^{152}\text{SmF}_3$, $^{150}\text{SmF}_3$, $^{147}\text{SmF}_3$ and $^{144}\text{SmF}_3$ with an enrichment of 98.4%, 95.6%, 96.4% and 96.4%, respectively. Samarium fluoride layers with a thickness in the range of 327–546 $\mu\text{g}/\text{cm}^2$ were evaporated on carbon foils of 40 $\mu\text{g}/\text{cm}^2$ and covered with a layer of 10 $\mu\text{g}/\text{cm}^2$ of carbon in order to improve the radiative cooling and to reduce material losses by sputtering [48].

A movable carbon stripper foil with a thickness of 40–60 $\mu\text{g}/\text{cm}^2$ is mounted behind the target. This foil is used for charge equilibration of the reaction products.

3.3 Separation

Neutron-deficient isotopes have low production cross-sections and very short half-lives. It is thus necessary to use a fast and efficient separation method of the evaporation residues (ERs) from the primary beam and products of transfer reactions.

3.3.1 The velocity filter SHIP

In our experiments on synthesis and investigation of very neutron deficient isotopes with $N < 126$ and $74 \leq Z \leq 92$ the velocity filter SHIP was used (figure 3.1). It is designed to separate ERs from the projectiles and target like nuclei on the basis of their velocity differences.

SHIP is made out of two velocity filters where the electric and magnetic fields are separated. Each filter is a combination of one electrostatic deflector and two magnetic dipoles. The first filter stage is preceded by a quadrupole triplet that collects and focuses the recoiling fusion products and followed by a velocity slit. The reaction products at this stage are already separated from the primary beam. The second filter stage works with inverted senses of deflection for all fields. Only the particles moving with the correct velocity are allowed to pass through the separator. The target is

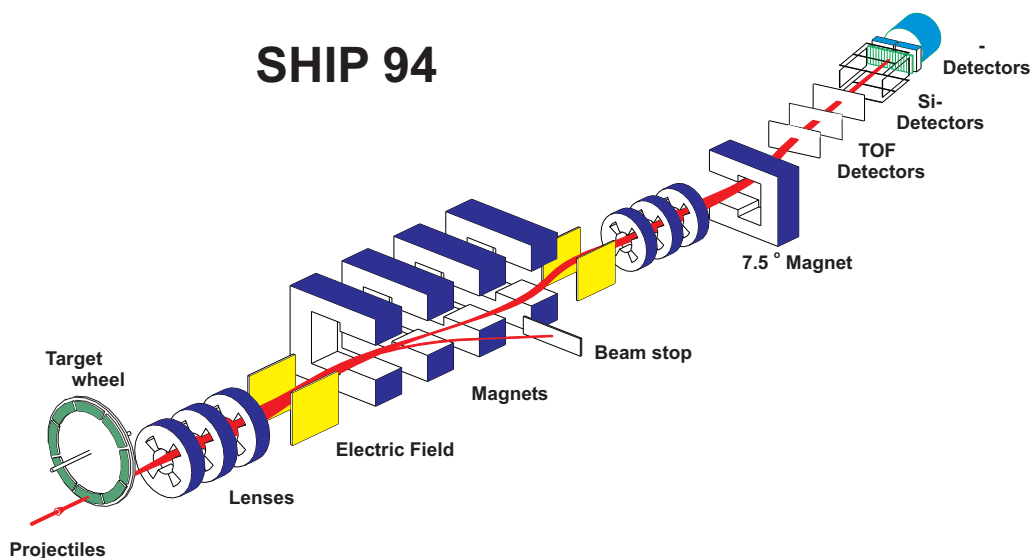


Figure 3.1: The Separator for Heavy ion Reaction Products (SHIP) [49] -

placed close to the first triplet resulting in almost 100 % probability (for the symmetric combination projectile–target) of recoils being caught. The last quadrupole triplet focuses the separated ERs on the STOP detector in the focal plane of the separator. Deflected projectiles are stopped in the beam stop (a water-cooled copper plate) which also serves as a Faraday cup for measuring the beam current (see [3, 49, 50]).

The background consisting of scattered projectiles and target like nuclei was reduced by a factor of 10 – 50 by installing a 7.5° deflection magnet (see figure 3.1). The total background suppression of the separator integrated over the whole energy spectrum is $10^{10} - 10^{11}$ [50]. The separator accepts ions in a velocity interval of $\pm 5\%$ and a charge state of the products up to $\pm 10\%$ around the mean value [49].

The flight time of the reaction products considered here through SHIP is $\approx 1.3\mu\text{s}$.

3.3.2 Transmission of SHIP

As can be seen in figure 3.2, the transmission ε_{trans} of the SHIP for ER depends strongly on the mass ratio of the beam and target nuclei. The highest transmission rate is obtained for ERs from reactions with inverse kinematics. If the masses of the projectile and target nuclei differ greatly, the transmission decreases significantly.

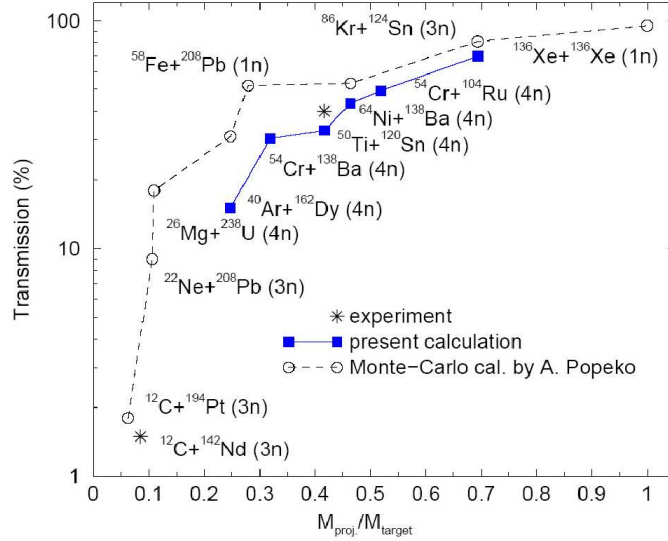


Figure 3.2: Transmission ε_{trans} of the velocity filter SHIP - Squares represent the results of the simulations of M.Mazzocco et al. [51], the stars are experimental values and circles refer to previous calculations done by A.Popeko [52]. The figure and the caption are taken from [53].

3.4 Detectors

The detector system of SHIP is shown in figure 3.1. It is composed of three time-of-flight detectors (TOF), eight identical 16-strip silicon wafers (one to stop the ions, six backward detectors and another one is used as a veto detector) and a clover-type four-crystal germanium detector.

3.4.1 TOF detectors

After the 7.5° deflection magnet three secondary time-of-flight electron foil detectors are mounted 15 cm apart from each other, see figure 3.1 [54]. Each detector consists of: one foil of $32 \mu\text{g}/\text{cm}^2$ of carbon and $20 \mu\text{g}/\text{cm}^2$ of MgO and a vertical metallic grid placed a few millimeters apart.

These detectors have a time resolution of ≈ 700 ps. When a heavy ion passes through a carbon-MgO foil the emitted electrons are accelerated by a 4 kV potential between the foils and the grids. These electrons are then bent by the use of a perpendicular magnetic field onto a microchannel plate (MCP) to amplify them further. The foils have a transmission of 100 % (see [53]).

3. EXPERIMENTAL DEVICES AND TECHNIQUES

Measuring the deposited kinetic energy of a particle in the STOP detector and its speed thanks to the time-of-flight detectors it is possible to have a rough estimate of the particles's mass. For example in the case of ^{283}Cn , the mean atomic mass number determined was $A = 286 \pm 10$ [55].

The efficiency of the TOF detector system is $\approx 99.8\%$ [53]. Therefore in anti-coincidence with the STOP detector spectra with little background can be obtained.

3.4.2 Silicon detectors

SHIP was built using silicon semiconductor detectors cooled to $-10\text{ }^\circ\text{C}$ to study the decay properties of heavy and super-heavy nuclei that decay mainly through α -, β -decay and/or fission. Their half-lives range from microseconds to hours. The energy calibration remained stable for the entire duration of our experimental runs. Foils can be put in front of the STOP detector to suppress part of the low energetic background or/and to reduce the implantation energy of the Evaporation Residues, see figure 3.1.

3.4.2.1 The STOP detector

According to the author of this thesis [56], after separation by the velocity filter SHIP, the evaporation residues are implanted in a $300\text{ }\mu\text{m}$ thick, $35 \times 80\text{ mm}^2$ 16-strip position-sensitive silicon detector (PSSD) mounted at the focal plane of SHIP [44], where their subsequent particle decays were measured. Each strip is position sensitive in the vertical direction with a resolution of $\approx 0.4\text{ mm}$ (FWHM) between the implanted ER and succeeding decay products. For correlations, one needs to take ≈ 2.5 FWHM. For that reason, the stop detector is equivalent to ≈ 560 single detectors (35×16 strips), each with an active area of $5 \times 1\text{ mm}^2$, see figure 3.1.

An α -particle with a range R emitted from an implanted Evaporation Residue in the STOP detector at a depth d will be detected by the detector with an efficiency *i.e.* a probability $e_d = (d + R)/(2R)$ as long as $d \leq R$. Typical values for nuclei produced here are $d \approx (4-11)\text{ }\mu\text{m}$ and $R \approx (35-65)\text{ }\mu\text{m}$, and hence $e_d \approx 0.53-0.66$.

3.4.2.2 The STOP detector calibration

The α -energy calibration of the STOP detector was performed internally by using the known α lines of isotopes that all have an uncertainty of $\approx 5\text{ keV}$ [56]. These isotopes

were produced either directly in different evaporation channels of the studied reactions or were the decay products of directly-produced nuclei. In this way, problems with energy losses due to the detector's dead layer in the case of an external calibration source were avoided. The broad energy range of $\approx 5800\text{--}7500$ keV and a small energy uncertainty for the majority of the α lines used for the calibration allowed us to make a reliable calibration extrapolation into the α -energy region of $7800\text{--}8200$ keV, relevant for the Th isotopes studied in our work [56]. A typical α -energy resolution of each strip of the STOP detector was ≈ 25 keV (FWHM) in the energy interval $6000\text{--}8200$ keV. Since α emission is the dominant decay mode of most of the nuclei produced in the considered reactions, the identification of nuclides was based on the observation of genetically correlated α -decay chains [56].

3.4.2.3 The BOX detector

This section is taken from a published article by the author of this thesis [56].

Upstream the STOP detector, six silicon detectors of similar shape (BOX detector) are mounted in an open box geometry, see figure 3.1. They were used to measure the energies of α particles escaping from the STOP detector in the backward direction in a solid angle of 80 % of 2π . In these backward detectors, neighboring strips are connected galvanically so that 28 energy sensitive segments are formed. The direction of an α particle or a fission fragment that escapes the STOP detector can be roughly retraced. By adding up the energy deposition in the STOP detector and BOX detector, the full energy of the escaping α -particles could be recovered, though with a somewhat reduced energy resolution. A typical α -energy resolution for the sum signal was ≈ 70 keV (FWHM), which was in most cases sufficient to unambiguously distinguish the decays of interest. These detectors were calibrated using the same isotopes mentioned in the previous subsection [56].

3.4.2.4 The VETO detector

The veto detector is placed behind the stop detector, see figure 3.1. The task of this detector is to reject, in coincidence with the stop detector, the signals coming from the particles which pass through the stop detector and are not recognized by the TOF system (mainly high energy protons and α -particles).

3. EXPERIMENTAL DEVICES AND TECHNIQUES

3.4.3 Germanium detector and its calibration

Behind the STOP detector a fourfold segmented Clover detector was installed for prompt and delayed α - γ or α -X-ray coincidence measurements within a time window of $\Delta T(\alpha\text{-}\gamma) \leq 5 \mu\text{s}$ to study excited levels in daughter nuclei [56]. The registration probability of an α - γ coincidence is 14 % in the energy interval [100 keV,300 keV] [50, 57].

The calibration of this detector was performed using ^{152}Eu and ^{133}Ba sources. One can calibrate a wide range of γ energies: from several tens of keV up to 1.5 MeV. The energy uncertainty is usually better than 1 keV.

3.5 Data acquisition

3.5.1 Electronic system

This sections is taken from [53].

The electronic scheme of the STOP and BOX detectors is shown in figure 3.3. A charge sensitive preamplifier is connected at the ends of each strip. To obtain the total energy deposited by a particle, the signals from each end are collected and added together. The energies of the different implanted particles span over a very large range. Therefore two amplification channels are used. In the figure they are marked as H (High energy range of 320 MeV, low amplification) and L (Low energy range of 16 MeV, high amplification). For every strip three signals are obtained: a total energy and two position signals. The 16 strips are divided into two groups of 8 even-numbered and odd-numbered strips. After their amplification each signal is multiplexed and processed by the ADCs. After detection of a signal in any one of the eight even or odd strips, during $25 \mu\text{s}$ no further signal can be processed (data acquisition dead time) in these eight strips (see [53]).

Sulignano [53] describes further that “output from the 8-channel multiplexers (mixer) is inhibited by the trigger signal supplied by the pattern trigger (PT), which is used also for the identification of the strip number. In this way, the mixer processes signals from single strips at a time in order to avoid noise and off-set summing from the other seven strips. For the processing of the ADC signals, an ADC multiplexer (AMUX) based data acquisition system is used. This AMUX system (NIM based)

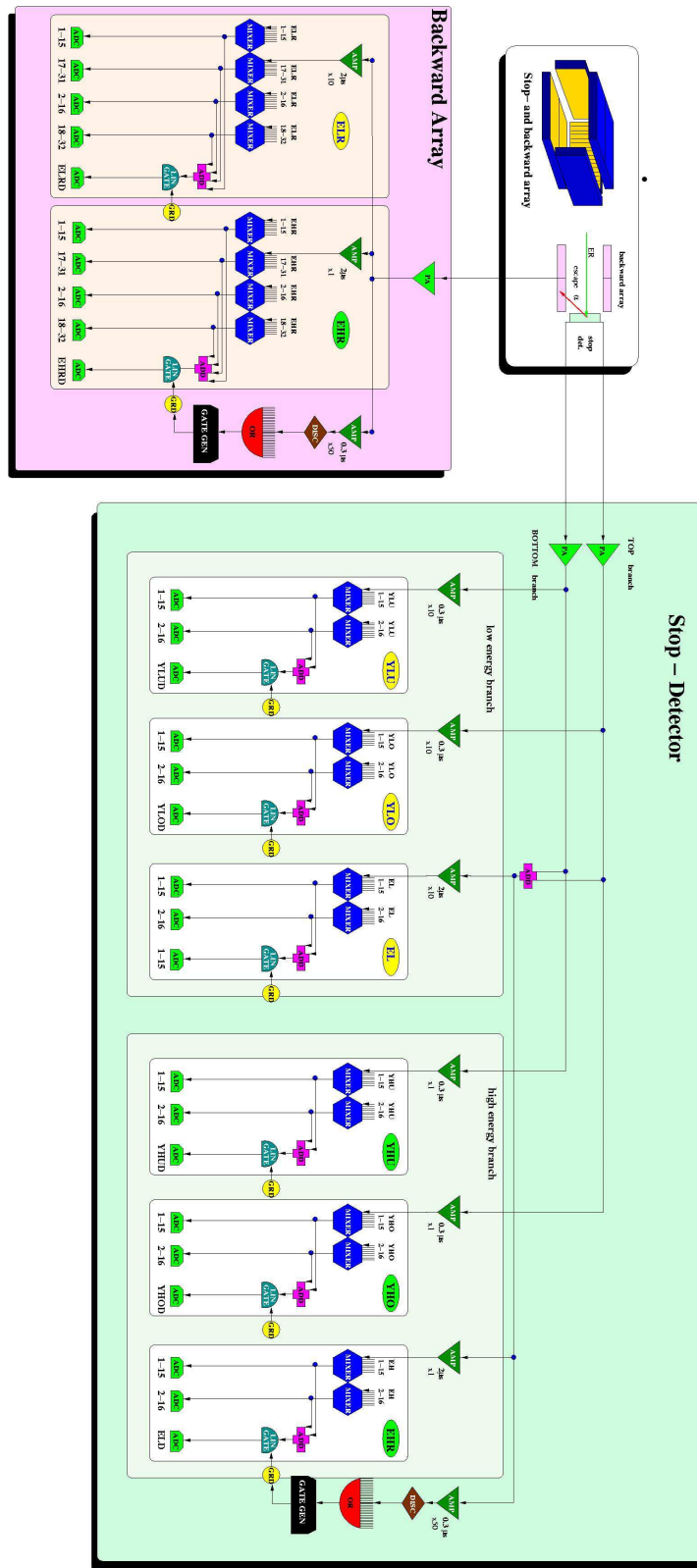


Figure 3.3: Block diagram of the focal plane detector - Block diagram of the focal plane detector (STOP and BOX detectors) with associated electronics. The figure and the caption are taken from [50].

3. EXPERIMENTAL DEVICES AND TECHNIQUES

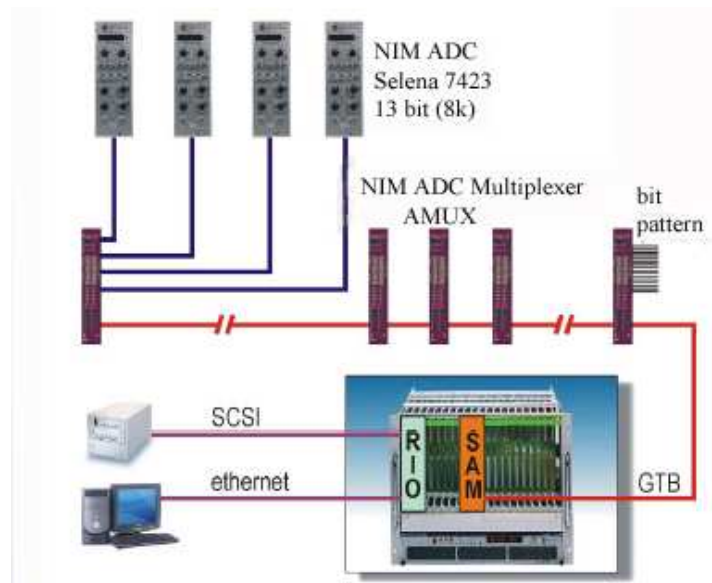


Figure 3.4: Data acquisition system - Example of the connection of the data acquisition system. Four ADCs are connected to one AMUX. These modules are connected to a SAM3 module through GTBM. Each AMUX contains a 16 bit pattern unit. It is possible to connect to one port of the two inputs of a SAM3 up to 15 AMUX modules, so in total 30 AMUX modules and 120 ADCs can be read out by one SAM3. Finally, the events are read out by the DAQ processor which prepares the data for mass storage and online analysis. The ADC multiplexers have been developed for SHIP by the electronics group of GSI [58, 59]. The figure and the caption are taken from [53].

was developed by Hoffmann et al. [58, 59]. The AMUX module has the property to readout and control 4 spectroscopy ADCs. Nine AMUX modules are chained on the GTB (GeraeTe Bus). GTB is a differential bus used for list mode data transfer between a control and readout module (SAM) and the AMUX modules. The SAM module serves for event building and communication with the DAQ CPU. The trigger bus connects all AMUX modules with the control port of the SAM and synchronizes the system of SAM and AMUX modules (see figure 3.4). The first firing ADC triggers the coincidence time. All ADC signals that fall into the coincidence interval are accepted. At the end of the coincidence time, the pattern registers (each AMUX contains a 16 bit pattern register) are clocked and the conversion time of the ADCs starts. The end of the conversion time triggers an interrupt on the SAM, which starts the readout (see figure 3.5). The data are buffered in an event queue with a length of 400 events on the AMUX modules. The readout of the events to the SAM is done asynchronously by sending a readout signal from the SAM to the AMUX modules via the GTB. The SAM is then read out with a VME processor (RIO) running an MBS (Multi Branch System [30]) data acquisition system developed by the GSI electronics group.”

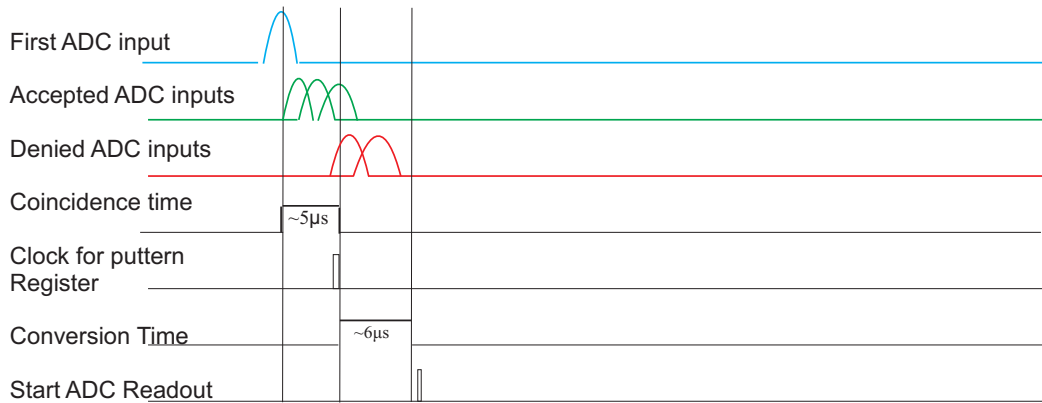


Figure 3.5: Timing Diagram - Timing diagram for an AMUX readout cycle. The figure and the caption are taken from [53].

3.5.2 The Go4 analysis framework

The Analysis Framework used to process and analyze the experimental data presented in this work (see Chapter 4) is Go4 [60] (GSI Object Oriented On-line Offline). It is based on the ROOT [61] system of CERN. According to Streicher [3] Go4

3. EXPERIMENTAL DEVICES AND TECHNIQUES

was designed “as an on-line monitoring and off-line analysis framework with the specific requirements of the low and medium energy nuclear and atomic physics experiments. The analysis itself can be run in remote GUI (Graphical User Interface) controlled mode or in batch mode from the command line, which is about 30 % faster. The analysis framework provides the syntax to organize the analysis in steps which can be controlled from the GUI with each step having its own inputs, outputs and processing classes. The Go4 GUI includes a browser and a tree viewer which can be used without analysis to process standard ROOT files. The Go4 has been developed on Linux.”

3.6 The correlation method

The position sensitivity of the silicon strip detectors gives us the possibility to use the time, position and energy correlation method. This method represents a very useful tool for the identification of neutron deficient isotopes which have, in general, a very low production rate.

The Evaporation Residues are implanted directly into the silicon STOP detector. There, exact information on their horizontal and vertical positions, their detection time and their energy can be obtained. The same is true for their decay products (α -particles, fission fragments, electrons...). This is what makes it possible to assign decay products to their parents. It is the basic principle of the correlation method. Not only can one assign a daughter nucleus to its mother, but whole chains of several decays can be reconstructed and assigned to the correct implanted Evaporation Residue. A famous use of this technique has been the synthesis of new elements, where the correct assignation of decay products to unknown new nuclei is crucial [62]. When one deals with isotopes in the chains whose decay properties (half-life and decay energy) are known, the correlations are easier to make. It is more difficult when a new isotope or a new state of an isotope is analyzed. The measured positions of the decay products and the implanted evaporation residues are the same because the ranges of the emitted α -particles ($\approx 40\text{-}60 \mu\text{m}$) and of the recoiled daughter nucleus ($\approx 10 \mu\text{m}$) are small compared with the detector resolution ($\approx 400 \mu\text{m}$). In the analysis with Go4 (see 3.5.2), variable time and position windows for the “ER–Decay Product” and/or “Decay Product–Decay Product” pairs are used to obtain the possible correlations. Choosing a too large interval of time or position leads to the inclusion of random correlations

depending on the implantation rate of the current experiment. In fact, the intensity of the beam has to be chosen in order to guarantee that the average time measured between events recorded in the same “pixel” of the stop detector is long compared with the half-life of the decay product one wants to detect and analyze. The high segmentation of the STOP detector helps to minimize random correlations: each strip is 5 mm wide and has a vertical position resolution of $\approx 400 \mu\text{m}$ FWHM (see above subsection 3.4.2.1). The short-lived nature of the nuclei in our region of interest ($N < 126$ and $Z = 74\text{--}92$) helps to reduce the number of random correlations.

3. EXPERIMENTAL DEVICES AND TECHNIQUES

4

Experimental results

Our two main experiments were R263 and R266.

4.1 R263

For R263, some of the results presented here were published in 2010 by the author of this thesis [56]. The new neutron-deficient isotope ^{208}Th was produced in the complete-fusion reaction $^{64}\text{Ni} + ^{147}\text{Sm} \rightarrow ^{208}\text{Th} + 3\text{n}$. Evaporation residues were separated in-flight by the velocity filter SHIP and subsequently identified on the basis of energy-, position- and time-correlated α -decay chains. The measured α -decay energy and half-life value of ^{208}Th are 8044(30) keV and $1.7_{-0.6}^{+1.7}$ ms, respectively. Improved data on the α decay of $^{209,210,212}\text{Th}$, $^{208g,208m,209}\text{Ac}$ and ^{208}Ra were obtained using complete fusion reactions of ^{64}Ni with $^{147,150,152}\text{Sm}$ targets.

Two beam energies of 288(1) and 294(1) MeV at the beginning of the target were used in our experiments (see table 4.1). These energies corresponded to the expected maxima of production cross-sections of fusion evaporation channels of our interest, as calculated with the HIVAP statistical model code [5].

The errors of the half-life values and production cross-sections were determined by the procedure described in [63].

4. EXPERIMENTAL RESULTS

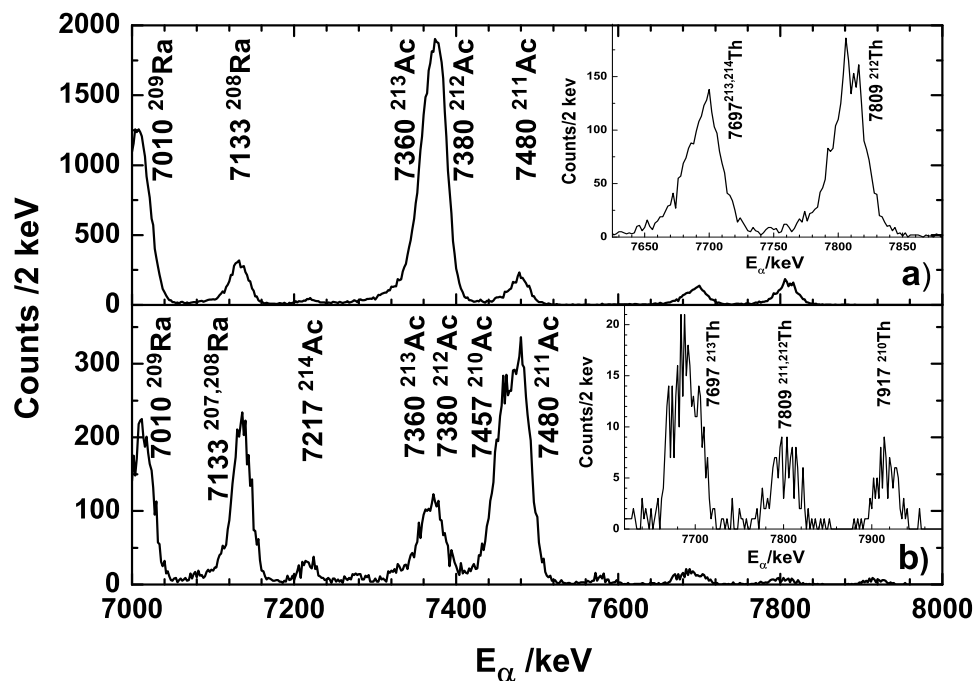


Figure 4.1: R263 Energy spectra - Energy spectra of the α decays in the PSSD, collected between the beam pulses in the reactions $^{64}\text{Ni}(288 \text{ MeV}) + ^{152}\text{Sm} \rightarrow ^{212}\text{Th} + 4\text{n}$ (a) and $^{64}\text{Ni}(294 \text{ MeV}) + ^{150}\text{Sm} \rightarrow ^{210}\text{Th} + 4\text{n}$ (b). Some peaks are labeled with the α -decay energy (in keV) and the isotope to which the α decay belongs. In the broader double peaks of $^{210,211}\text{Ac}$, $^{212,213}\text{Ac}$, $^{207,208}\text{Ra}$, $^{211,212}\text{Th}$ and $^{213,214}\text{Th}$ we just included earlier reported literature values to guide the reader.

Table 4.1: Reactions used in R263 - Beam energies E_{lab} at the beginning of the target, number of observed correlated events N and production cross-sections σ .

Isotope	Reaction	E_{lab} /MeV	N	σ /pb
^{212}Th	$^{64}\text{Ni} + ^{152}\text{Sm} \rightarrow ^{212}\text{Th} + 4\text{n}$	288	1430	34000(900)
^{210}Th	$^{64}\text{Ni} + ^{150}\text{Sm} \rightarrow ^{210}\text{Th} + 4\text{n}$	294	165	1590(130)
^{209}Th	$^{64}\text{Ni} + ^{147}\text{Sm} \rightarrow ^{209}\text{Th} + 2\text{n}$	288	4	29_{-15}^{+22}
^{208}Th	$^{64}\text{Ni} + ^{147}\text{Sm} \rightarrow ^{208}\text{Th} + 3\text{n}$	288	3	22_{-13}^{+20}
	$^{64}\text{Ni} + ^{147}\text{Sm} \rightarrow ^{208}\text{Th} + 3\text{n}$	294	1	95_{-79}^{+219}
^{209}Ac	$^{64}\text{Ni} + ^{150}\text{Sm} \rightarrow ^{209}\text{Ac} + \text{p}4\text{n}$	294	77	1080(140)
	$^{64}\text{Ni} + ^{147}\text{Sm} \rightarrow ^{209}\text{Ac} + \text{p}1\text{n}$	288	31	330(70)
^{208m}Ac	$^{64}\text{Ni} + ^{150}\text{Sm} \rightarrow ^{208m}\text{Ac} + \text{p}5\text{n}$	294	1	14_{-12}^{+32}
	$^{64}\text{Ni} + ^{147}\text{Sm} \rightarrow ^{208m}\text{Ac} + \text{p}2\text{n}$	288	13	140(50)
^{208g}Ac	$^{64}\text{Ni} + ^{150}\text{Sm} \rightarrow ^{208g}\text{Ac} + \text{p}5\text{n}$	294	4	56_{-30}^{+40}
	$^{64}\text{Ni} + ^{147}\text{Sm} \rightarrow ^{208g}\text{Ac} + \text{p}2\text{n}$	288	47	500(80)
^{208}Ra	$^{212}\text{Th} \rightarrow ^{208}\text{Ra} + \alpha$		–	–

4.1.1 Th

4.1.1.1 ^{210}Th and ^{212}Th isotopes

The energy spectra of α decays, measured in the PSSD in pauses between beam pulses (*beam off* time interval) for the reactions $^{64}\text{Ni}(288 \text{ MeV}) + ^{152}\text{Sm} \rightarrow ^{212}\text{Th} + 4\text{n}$ and $^{64}\text{Ni}(294 \text{ MeV}) + ^{150}\text{Sm} \rightarrow ^{210}\text{Th} + 4\text{n}$ are shown in figs. 4.1a and 4.1b, respectively. The main peaks in the spectra are due to α decays of the $^{210,211,212,213,214}\text{Ac}$ and $^{207,208,209}\text{Ra}$ isotopes produced by pxn and αxn evaporation channels, respectively, whereas the Th isotopes were all produced by xn channels. Several pairs of isotopes in this region have quite similar energies ($^{210,211}\text{Ac}$, $^{212,213}\text{Ac}$, $^{207,208}\text{Ra}$, $^{211,212}\text{Th}$ and $^{213,214}\text{Th}$), which leads to two α decays combined in one broader peak. However, in most cases, due to the proper choice of the beam energy, only one of the isotopes within each pair was dominantly produced, while the contribution of the second decay was usually negligible (see also below). The presence of ^{213}Th and $^{213,214}\text{Ac}$ in fig. 4.1b is explained by a small admixture of the heavier $^{152,154}\text{Sm}$ isotopes in the ^{150}Sm target, as these Th and Ac isotopes are not expected to be produced at this beam energy on the ^{150}Sm target.

4. EXPERIMENTAL RESULTS

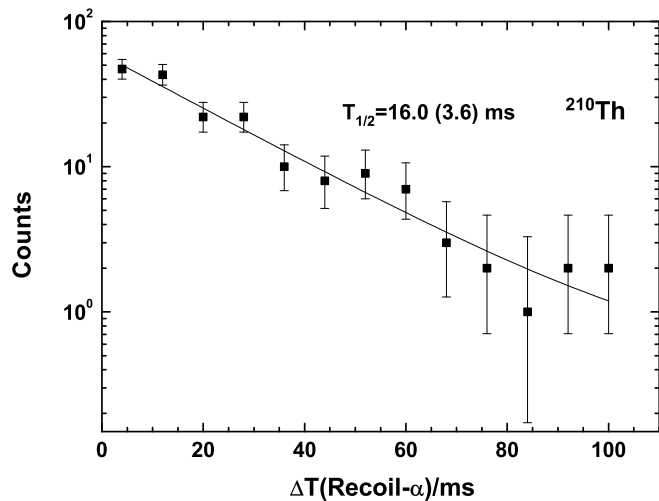


Figure 4.2: ^{210}Th half-life - ER- α time distribution of the ^{210}Th α decays from fig. 4.1b. The continuous solid line shows the result of an exponential decay fit with a constant background.

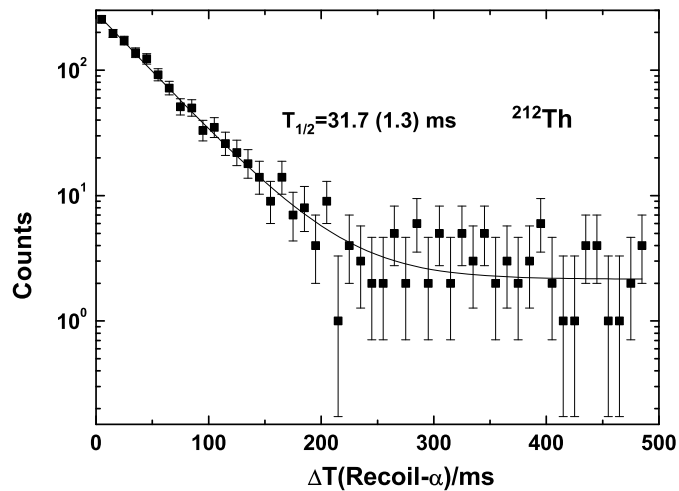


Figure 4.3: ^{212}Th half-life - ER- α time distribution of the ^{212}Th α decays from fig. 4.1a. The continuous solid line shows the result of an exponential decay fit with a constant background.

The ERs- α correlation analysis was performed for known α decays of ^{212}Th and ^{210}Th in the α -energy intervals of $E_\alpha(^{212}\text{Th}) = (7.76\text{--}7.86)$ MeV and $E_\alpha(^{210}\text{Th}) = (7.87\text{--}7.97)$ MeV, respectively. ER- α time windows of 500 ms and 120 ms were used for ^{212}Th and ^{210}Th , respectively. In total, 1430 (^{212}Th) and 165 (^{210}Th) correlated ER- α chains were found. From the respective time distributions between the recoil implantation and subsequent α decays more precise half-life values of 16.0(3.6) ms for ^{210}Th and 31.7(1.3) ms for ^{212}Th were deduced (fig. 4.2 and fig. 4.3). Improved α -decay energy values for these isotopes were also obtained: $E_\alpha(^{210}\text{Th}) = 7917(6)$ keV and $E_\alpha(^{212}\text{Th}) = 7809(5)$ keV (table 4.2). The measured cross-sections are given in table 4.1.

Table 4.2: Th isotopes - α -particle energies, half-lives and reduced α -widths of parent activities measured in the present work and compared with earlier measurements. The half-lives calculated with the semi-empirical formula from [21] are given in the last column.

Nuclei	E_α /keV	$T_{1/2}$ /ms	δ_α^2 /keV	E_α /keV	$T_{1/2}$ /ms	Ref.	$T_{1/2}$ /ms
	Present work			Literature			[21]
^{212}Th	7809(5)	31.7(1.3)	56(3)	7802(10)	30^{+20}_{-10}	[64]	10
^{210}Th	7917(6)	16.0(3.6)	55(13)	7899(17)	9^{+17}_{-4}	[65]	4.6
^{209}Th	8123(25)	$2.5^{+1.7a}_{-0.7}$	87^{+61}_{-29}	8080(50)	$3.8^{+6.9}_{-1.5}$	[66]	3.5
^{208}Th	8044(30)	$1.7^{+1.7}_{-0.6}$	229^{+234}_{-94}	–	–	–	1.9

^a including the 2 events from [66]. With our 4 events only: $T_{1/2} = 1.9^{+1.9}_{-0.7}$ ms (see table 4.3 and Section 4.1.1.2).

A possible contribution of α decays of ^{211}Th , which could be weakly produced in the 5n- evaporation channel of the $^{64}\text{Ni} + ^{152}\text{Sm} \rightarrow ^{216}\text{Th}^*$ reaction, to the α -decay peak of ^{212}Th had to be carefully considered in fig. 4.1a. This is because the reported α -decay energy (7.792(14) MeV) and half-life value (37^{+28}_{-11} ms) of ^{211}Th [65] are comparable to those of ^{212}Th , thus based on decay properties alone a clear separation of both isotopes is not possible. However, with the proper choice of the beam energy in our study, which corresponded to the dominant evaporation channels with four nucleons (^{212}Ac and ^{212}Th), the contribution of ^{211}Th (5n channel) is small. This is confirmed by the comparison of the intensities of the ^{212}Ac (p3n channel) and of ^{211}Ac (p4n channel) in fig. 4.1a, which shows that the production of the channel with evaporation of five nucleons was indeed lower by a factor of ten at the beam energy of 288 MeV.

4. EXPERIMENTAL RESULTS

4.1.1.2 ^{209}Th isotope

In a previous study, only two ^{209}Th α -decay events were reported, from which an energy of 8080(50) keV and a half-life value of $3.8_{-1.5}^{+6.9}$ ms were determined [66].

We produced the isotope ^{209}Th in the reaction $^{64}\text{Ni} + ^{147}\text{Sm} \rightarrow ^{209}\text{Th} + 2\text{n}$, see table 4.1. To achieve an unambiguous identification of ^{209}Th , produced with a rather low cross-section value, we searched for decay chains consisting of four consecutive α decays, starting from the recoil implantation in the PSSD (ER- $\alpha_1(^{209}\text{Th})$ - $\alpha_2(^{205}\text{Ra})$ - $\alpha_3(^{201}\text{Rn})$ - $\alpha_4(^{197}\text{Po})$ correlation analysis).

A time window of $\Delta(\text{ER}-\alpha) \leq 20$ ms and an energy interval of $E_{\alpha_1} = 7.8\text{--}8.3$ MeV were used to search for the α decays of ^{209}Th . To find the subsequent members of the correlation chains, time windows and energy intervals corresponding to the decay properties of the descendants of ^{209}Th , i.e. the isotopes ^{205}Ra , ^{201}Rn and ^{197}Po were used, which are shown in table 3. In our search for long lived isotopes such as ^{197m}Po in our correlated decay chains we had to evaluate the probability of a chance coincidence. The probabilities of occurrence of such an event with an energy in the 6335–6415 keV interval (^{197m}Po) due to the α decay of two different evaporation residues (implanted at the same position) within 30s, 60s and 90s are of only 4.3%, 8.3% and 12.3%, respectively. Four chains were assigned to the decay of the ^{209}Th isotope (table 4.3).

Based on these events, a decay energy of 8123(25) keV and a half-life of $1.9_{-0.7}^{+1.9}$ ms were deduced, which agree with previously reported values [66] but are more precise, see table 4.2.

It is important to note here that despite the limited accuracy of ± 30 keV, the energies of the $\alpha_2 - \alpha_4$ members of the observed decay chains of ^{209}Th rather agree with the reported α -decay energies of ^{205m}Ra (7370(20) keV [67]), ^{201m}Rn (6773(2) keV [68]) and ^{197m}Po [69], than with the α -decay energies of ^{205g}Ra (7340(20) keV [67]), ^{201g}Rn (6725(2) keV [68]) and ^{197g}Po [69]. In particular, the deduced α -decay energy of ^{197}Po in our experiment (6384(30) keV) is in agreement with the tabulated value of 6383(3) keV for ^{197m}Po [69], rather than with the tabulated value of 6282(4) keV for ^{197g}Po [69]. This suggests that the observed decays chains of ^{209}Th are of the type ER- $\alpha_1(^{209}\text{Th})$ - $\alpha_2(^{205m}\text{Ra})$ - $\alpha_3(^{201m}\text{Rn})$ - $\alpha_4(^{197m}\text{Po})$. This is in agreement with the previous study [66] who also observed ^{197m}Po as α_4 decay in the two chains measured (see below for more details).

Table 4.3: ^{208}Th and ^{209}Th decay chains - Energies deposited in the stop detector (or sum energies from stop and box detectors) and time intervals between $\text{ER}-\alpha_1$ and $\alpha_x-\alpha_{x+1}$ for our ^{208}Th and ^{209}Th decay chains. Mean α -particle energies and partial α -decay half-lives of parent activities measured in the present chains and compared with earlier measurements are given.

Event #	^{209}Th		^{205m}Ra		^{201m}Rn		^{197m}Po	
	E_{α_1}/keV	$\Delta t/\text{ms}$	E_{α_2}/keV	$\Delta t/\text{ms}$	E_{α_3}/keV	$\Delta t/\text{s}$	E_{α_4}/keV	$\Delta t/\text{s}$
1	8099	4.2	7392	124	6728 ^b	11.3	6379	28.67
2	8135	1.7	7366	92.4	6758 ^b	2.98	–	–
3	8136	1.1	7365 ^b	64.9	6787	0.767	–	–
4	8136 ^b	4.0	7392 ^b	112	3779 ^a	3.65	6389	13.01
		$T_{1/2}/\text{ms}$		$T_{1/2}/\text{ms}$		$T_{1/2}/\text{s}$		$T_{1/2}/\text{s}$
1,2,3,4 ^c	8123(25)	$1.9_{-0.7}^{+1.9}$	7379(30)	68_{-23}^{+68}	6787(30)	$3.24_{-1.08}^{+3.24}$	6384(30)	$14.45_{-4.9}^{+14.45}$
Lit.	8080(50)[66]	$3.8_{-1.5}^{+6.9}$ [66]	7370(20)[67]	170_{-40}^{+60} [67]	6773(2)[68]	3.8(1)[68]	6383(3)[69]	25.8(1)[70]
	^{208}Th		^{204}Ra		^{200}Rn		^{196}Po	
	E_{α_1}/keV	$\Delta t/\text{ms}$	E_{α_2}/keV	$\Delta t/\text{ms}$	E_{α_3}/keV	$\Delta t/\text{s}$	E_{α_4}/keV	$\Delta t/\text{s}$
5	8018	6.1	7485	58.6	6849 ^b	0.980	–	–
6	8070	0.7	7481	38.0	547 ^a	6.65	6536 ^b	9.68
7	7975 ^b	1.9	7495	24.1	6914	0.571	6522	5.00
8	7893 ^b	0.9	7475	132	1644 ^a	0.064	6522	3.05
		$T_{1/2}/\text{ms}$		$T_{1/2}/\text{ms}$		$T_{1/2}/\text{s}$		$T_{1/2}/\text{s}$
5,6,7,8 ^c	8044(30)	$1.7_{-0.6}^{+1.7}$	7484(25)	44_{-15}^{+44}	6914(30)	$1.4_{-0.5}^{+1.4}$	6522(25)	$4.1_{-1.5}^{+5.6}$
Lit.	–	–	7486(8)[71]	57_{-5}^{+11} [71]	6903(3)[69]	1.03(5)[70]	6521(3)[69]	5.56(12)[70]

^a escaped alpha, measured only in the PSSD, no coincident signal in the box detectors was observed

^b decay energy is reconstructed by adding up the energy deposition in the PSSD and in the box detectors

^c escaped (^a) and reconstructed (^b) events were only considered for the half-life calculations due to their worse energy resolution.

4. EXPERIMENTAL RESULTS

By using both the four decay time intervals $\Delta T(\text{ER-}\alpha_1)$ from our study and the two reported time intervals $\Delta T(\text{ER-}\alpha_1)$ for ^{209}Th from [66], we deduced the half-life value of $2.5_{-0.7}^{+1.7}$ ms for this isotope, provided in table 4.2. Due to an inferior α energy resolution of 98 keV (FWHM) for the 6.779 MeV α particles in [66], we did not use those two events to deduce the α -decay energy of ^{209}Th based on all six events.

As mentioned above, our data indicate that the observed α decays of ^{209}Th feed, most probably, the isomeric state in ^{205}Ra . This isomeric state has a tentative spin-parity assignment of $I^\pi=(13/2^+)$, based on systematics in neighboring odd-A nuclei and on the unhindered α decay into the presumable $I^\pi=(13/2^+)$ isomer in ^{201}Rn [68, 72].

The reduced α -decay width of $\delta_\alpha^2(^{209}\text{Th})=87_{-29}^{+61}$ keV can be deduced for the 8123(25) keV decay using the Rasmussen approach for $\Delta L=0$ transitions [73]. This value is comparable to the reduced α -width of 55(13) keV for the neighboring isotope ^{210}Th , which suggests that the 8123 keV decay of ^{209}Th is unhindered and connects states with the same spin and parity in the parent ^{209}Th and daughter ^{205}Ra nuclei. Therefore, based on the tentative spin-parity assignment of $I^\pi=(13/2^+)$ for ^{205m}Ra , a tentative spin-parity assignment of $I^\pi=(13/2^+)$ could also be done for the state in ^{209}Th that decays by emission of 8123 keV α -particles.

This inference would also be in agreement with the well-known fact that in the complete-fusion reactions with heavy-ions, the high-spin states have a preferential population in comparison with the low-spin states. Despite this, based on our data alone we cannot draw any definitive conclusion with regard to whether the observed state in ^{209}Th is the ground or excited state. However it is known for lighter even Z nuclei (Ra,Rn,Po) that the excitation energy of the $13/2^+$ states decreases gradually with decreasing neutron number. Since $13/2^+$ was assigned to an isomeric state at 1118 keV in ^{213}Th [74] and as for lighter even-Z nuclei (Ra, Rn, Po) the decrease of the excitation energy of the $13/2^+$ states from N=123 to N=119 is lower than 730 keV, it is rather unlikely that the $I=13/2^+$ state would become the ground state already in ^{209}Th .

As can be seen from figs. 4.4a and 4.4b, our $T_{\frac{1}{2},\alpha}$ and Q_α values for ^{209}Th extend smoothly the respective systematics for the Th isotopes. However, the $Q_\alpha(^{208}\text{Th})$ value is slightly lower than that for ^{209}Th , and thus, does not follow this trend. This could possibly be explained as due to the above-proposed scenario of the decay from the $I=13/2^+$ isomer in ^{209}Th . Another tentative scenario which could be suggested here

is the influence of the (predicted) deformation [25] setting in the lightest Th isotopes, from ^{212}Th on. However, we prefer not to draw any definitive inference in this case.

4.1.1.3 The new isotope ^{208}Th

The new isotope ^{208}Th isotope was produced at two beam energies in the reaction $^{64}\text{Ni} + ^{147}\text{Sm} \rightarrow ^{208}\text{Th} + 3\text{n}$, see table 4.1. Similarly to ^{209}Th , a search for decay chains with four consecutive α decays, starting from the recoil implantation in the PSSD was performed.

Four decay chains, shown in table 3, were found. The decay properties of the last three members of these chains are in good agreement with the published values of the descendants of ^{208}Th i.e. the isotopes ^{204}Ra , ^{200}Rn and ^{196}Po . An α -decay energy of 8044(30) keV and a half-life of $1.7_{-0.6}^{+1.7}$ ms were deduced for ^{208}Th . The energy was deduced based on only the two events with the full energy deposition of the α_1 decay in the PSSD. For half-life determination, all four events were used.

The systematics of reduced widths (δ_α^2) for even-even Po, Rn, Ra and Th isotopes with $118 \leq N \leq 132$ is shown in fig. 4.4c. Their comparison in this region of neutron numbers shows the smooth increase of values with the increase of atomic number along the isotone lines. This is a feature generally accepted for the alpha decay process. Note also the kink at $N=126$ in reduced widths of all these elements, which is due to the neutron shell closure.

The reduced α -decay width of $\delta_\alpha^2(^{208}\text{Th}) = 229_{-94}^{+234}$ keV was deduced for the 8044(30) keV decay using the Rasmussen approach for $\Delta L=0$ transitions [15]. Within its large uncertainty, this value continues the smoothly-increasing trend of the reduced α widths of the even-even isotopes $^{210-216}\text{Th}$.

Calculations using the phenomenological formula found in Ref. [21] reproduce the α -decay half-life values fairly well, both for even-A $^{208-232}\text{Th}$ and odd-A $^{209-229}\text{Th}$ isotopes, see fig. 4.5. The calculated values for $^{208,209,210,212}\text{Th}$ isotopes are also given in table 4.2.

4.1.2 Ac

In previous studies, several authors reported half-life and α -decay energy values for ^{209}Ac , ^{208m}Ac and ^{208g}Ac isotopes [66, 75–78], see table 4.4. The ERs- α correlation

4. EXPERIMENTAL RESULTS

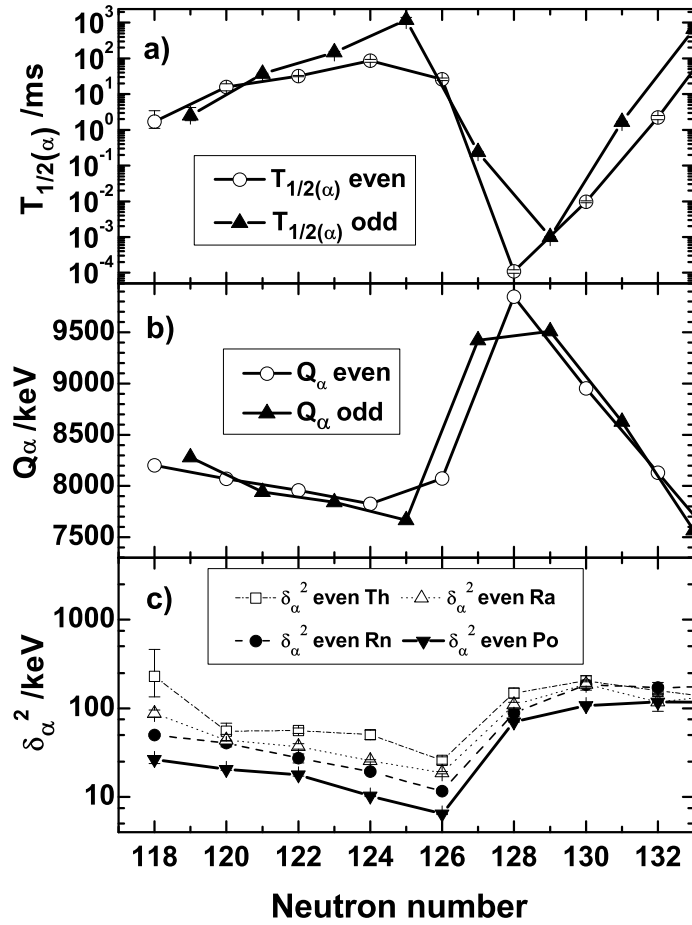


Figure 4.4: Th α -decay systematics - α -decay systematics for the $118 \leq N \leq 132$ Th isotopes: (a) partial $T_{1/2,\alpha}$ values; (b) Q_α -decay energies. For ^{209}Th , the value could be that of an isomeric state; (c) reduced α -widths for the even Th, Ra, Rn and Po isotopes.

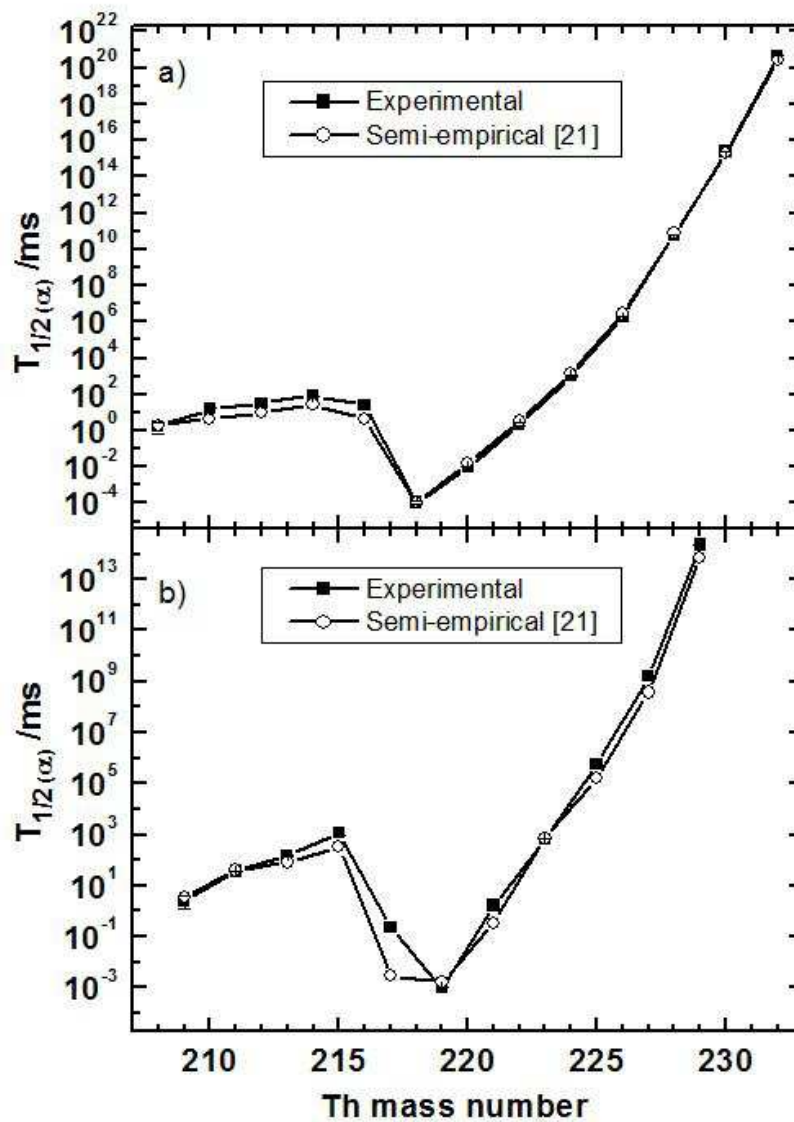


Figure 4.5: ^{212}Th half-life - Experimental and semi-empirically calculated [21] partial $T_{\frac{1}{2},\alpha}$ values for the even $^{208-232}\text{Th}$ (a) and odd $^{209-229}\text{Th}$ (b) isotopes.

4. EXPERIMENTAL RESULTS

analysis was performed for known α decays of ^{209}Ac , ^{208m}Ac and ^{208g}Ac in the α -energy intervals of $E_\alpha(^{209}\text{Ac}) = (7.53\text{--}7.63)$ MeV, $E_\alpha(^{208m}\text{Ac}) = (7.70\text{--}7.80)$ MeV and $E_\alpha(^{208g}\text{Ac}) = (7.53\text{--}7.63)$ MeV, respectively. ER- α time windows of 1 s, 500 ms and 1 s were used for ^{209}Ac , ^{208m}Ac and ^{208g}Ac , respectively. In total, 108 (^{209}Ac), 14 (^{208m}Ac) and 51 (^{208g}Ac) correlated ER- α chains were found. From the respective time distributions between the recoil implantation and subsequent α decays improved half-life values of 77_{-7}^{+8} ms for ^{209}Ac , $23.6_{-5.0}^{+8.6}$ ms for ^{208m}Ac and 100_{-12}^{+16} ms for ^{208g}Ac were deduced. Improved α -decay energy values for these isotopes were also obtained: $E_\alpha(^{209}\text{Ac}) = 7580(10)$ keV, $E_\alpha(^{208m}\text{Ac}) = 7747(10)$ keV and $E_\alpha(^{208g}\text{Ac}) = 7566(10)$ keV (table 4.4). The measured cross-sections are given in table 4.1.

Table 4.4: Ac and Ra isotopes - α -particle energies and half-lives of parent activities measured in the present work and compared with earlier measurements. The half-lives calculated with the semi-empirical formula given in [21] are listed in the last column.

Nuclei	E_α /keV	$T_{1/2}$ /ms	E_α /keV	$T_{1/2}$ /ms	Ref.	$T_{1/2}$ /ms
	Present work		Literature			[21]
^{209}Ac	7580(10)	77_{-7}^{+8}	7582(50) ^a	92(11) ^a	[69, 70]	50
^{208m}Ac	7747(10)	$23.6_{-5.0}^{+8.6}$	7747(14) ^b	28(7) ^c	[69, 70]	50
^{208g}Ac	7566(10)	100_{-12}^{+16}	7581(50) ^c	97(16) ^c	[69, 70]	210
^{208}Ra	7133(5)	1110(45)	7133(5)	1300(200)	[79]	280

^a E_α and $T_{1/2}$ averaged from references [66, 75–78] and [66, 76–78], resp.

^b average from references [66, 75, 77].

^c E_α and $T_{1/2}$ averaged from references [66, 77], resp.

4.1.3 Ra

A correlation analysis of the type $\alpha_1\text{--}\alpha_2$ with an 8 s time window was performed for $^{212}\text{Th}\text{--}^{208}\text{Ra}$ chains. Based on this analysis, a half-life value of 1110(45) ms was deduced for ^{208}Ra (fig. 4.6) and an α branching ratio of 87(3) % was derived for the first time. The previous reported values for the half-life and for the EC/ β^+ branching, the latter based on systematics, were of 1.3(2) s and 5 % [70], respectively.

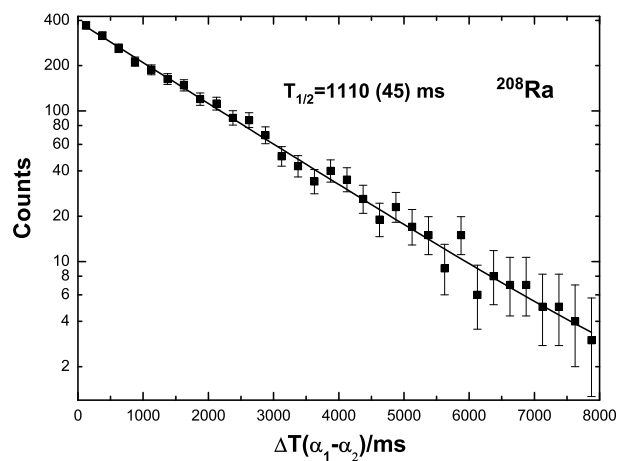


Figure 4.6: ^{208}Ra half-life - α_1 - α_2 time distribution of the ^{212}Th - ^{208}Ra α decays. The continuous solid line shows the result of an exponential decay fit.

Table 4.5: Reactions used in R266 - Beam energies E_{lab} at the beginning of the target, number of observed correlated events N and production cross-sections σ .

Isotope	Reaction	E_{lab} /MeV	N	σ /pb
^{181}Pb	$^{40}\text{Ca} + ^{144}\text{Sm} \rightarrow ^{181}\text{Pb} + 3n$	196	700	19000(700)
^{180}Pb	$^{40}\text{Ca} + ^{144}\text{Sm} \rightarrow ^{180}\text{Pb} + 4n$	209-212	100	1600(160)
^{179}Pb	$^{40}\text{Ca} + ^{144}\text{Sm} \rightarrow ^{179}\text{Pb} + 5n$	232	12	140(40)
^{181g}Tl	$^{40}\text{Ca} + ^{144}\text{Sm} \rightarrow ^{181g}\text{Tl} + p2n$	196	a	a
^{177}Hg	$^{181}\text{Pb} \rightarrow ^{177}\text{Hg} + \alpha$	—	—	—
^{177g}Au	$^{181g}\text{Tl} \rightarrow ^{177g}\text{Au} + \alpha$	—	—	—
^{174}Pt	$^{178}\text{Hg}^b \rightarrow ^{174}\text{Pt} + \alpha$	—	—	—
^{172}Pt	$^{176}\text{Hg}^c \rightarrow ^{172}\text{Pt} + \alpha$	—	—	—

^a Due to a long half-life, it was not possible to determine an exact number.

^b Produced directly in the reaction $^{40}\text{Ca} + ^{144}\text{Sm} \rightarrow ^{178}\text{Hg} + \alpha 2n$.

^c Descendant of ^{180}Pb produced in the second reaction listed.

4. EXPERIMENTAL RESULTS

4.2 R266

The results from R266 were published in 2009 and 2010 in four articles [80–83] of which the author of this thesis was a co-author. He participated actively in the preparation and the execution of the experiments as well as in the analysis of the results.

The new neutron-deficient isotope ^{179}Pb was produced in the complete-fusion reaction $^{40}\text{Ca} + ^{144}\text{Sm} \rightarrow ^{179}\text{Pb} + 5\text{n}$. The measured α -decay energy and half-life value of ^{179}Pb are 7350(20) keV and $3.5_{-0.8}^{+1.4}$ ms, respectively. Improved data on the α decay of $^{180,181}\text{Pb}$, ^{181g}Tl , ^{177g}Au , $^{174,172}\text{Pt}$ and ^{177}Hg were also obtained. In the following subsections a summary of these results will be given. Further details are given in the papers [80–83].

4.2.1 Pb

Table 4.6: Isotopes investigated in R266 - α -particle energies, half-lives and reduced α -widths of parent activities measured in the present work and compared with earlier measurements. The half-lives calculated with the semi-empirical formula given in [21] are listed in the last column.

Nuclei	Present work			Literature			[21]
	E_α /keV	$T_{1/2}$ /ms	δ_α^2 /keV	E_α /keV	$T_{1/2}$ /ms	Ref.	$T_{1/2}$ /ms
^{181}Pb	7016(15)	36(2)	37(4)	7044(15)	50_{-30}^{+40}	[84]	7.6
				7065(20)	45(20)	[85]	
^{180}Pb	7254(10)	4.2(5)	54(8)	7230(40)	4_{-2}^{+4}	[86]	0.34
				7250(15)	4.5(11)	[87]	
^{179}Pb	7350(20)	$3.5_{-0.8}^{+1.4}$	33_{-10}^{+14}	–	–	–	0.57
^{181g}Tl	6181(7)	^a	<18	6180	3400(600)	[88]	2400
				6186(10)	3200(300)	[89]	
^{177g}Au	6161(7)	1530(70)	29(5)	6156(6)	1462(32)	[90]	350
				6154(10)	–	[91]	

^a Due to the high implantation rate of ERs, no half-life value could be deduced.

Table 4.7: α -Branching Ratios of isotopes investigated in R266 - Improved or for the first time measured α -branching ratios b_α in R266.

Isotope	b_α /%	b_α /%	Ref.
	Present work	Literature	
^{177}Hg	100(5)	85	[92, 93]
^{177g}Au	40(6)	–	–
^{174}Pt	67(2)	67(6)	[91]
^{172}Pt	97(3)	94(12)	[94]
		94^{+6}_{-32}	[95]

4.2.1.1 ^{181}Pb

The reaction used to produce ^{181}Pb isotopes was $^{40}\text{Ca} + ^{144}\text{Sm} \rightarrow ^{181}\text{Pb} + 3n$ at a beam energy of 196(1) MeV in front of the target, see also table 4.5. The ERs- α correlation analysis was performed on the basis of the known alpha decay energies of ^{181}Pb in the α -energy interval of $E_\alpha = (6.9\text{--}7.15)$ MeV. An ER- α time window of 500 ms was used. In total, approximately 700 correlated ER- α chains were found. Their belonging to ^{181}Pb was further evidenced by the presence of α - α correlations of these α decays with the known α decays of the daughter ^{177}Hg and granddaughter ^{173}Pt nuclides. Indeed, the measured data compare well with the tabulated values for these two nuclides. From the respective time distributions between the recoil implantation and subsequent α decays an improved half-life value of 36(2) ms was deduced for ^{181}Pb . An improved α -decay energy value for this isotope was also obtained: $E_\alpha = 7016(15)$ keV (table 4.6). For the full ^{181}Pb and ^{177}Hg decay schemes see figure 2 in [80]. There, the 7016-keV α decay is interpreted as being due to the fine structure α decay of ^{181}Pb feeding the known $9/2^-$ excited state at 77 keV in ^{177}Hg [96]. As shown in Ref. [96], this state deexcites directly to the proposed $7/2^-$ ground state of ^{177}Hg by a presumed M1 77-keV transition.

4.2.1.2 ^{180}Pb

The reaction used to produce ^{180}Pb isotopes was $^{40}\text{Ca} + ^{144}\text{Sm} \rightarrow ^{180}\text{Pb} + 4n$ at beam energies of 209–212(1) MeV in front of the target [80], see table 4.5. In the past, two half-life and α -decay energy values agreeing within the error bars were reported in the literature for ^{180}Pb (see table 4.6). The ERs- α correlation analysis was performed

4. EXPERIMENTAL RESULTS

respecting the known α -decay energies of ^{180}Pb in the interval $E_\alpha = (7.2\text{--}7.3)$ MeV. An ER- α time window of 500 ms was used. In total, approximately 100 α -decay events of ^{180}Pb were detected. They could convincingly be identified based on their correlations with well-known α decays of daughter ^{176}Hg and granddaughter ^{172}Pt nuclides. Indeed, the measured data compare well with the tabulated values for these two nuclides. More precise values of $E_\alpha = 7254(10)$ keV and $T_{\frac{1}{2}} = 4.2(5)$ ms for ^{180}Pb were determined (see the comparison of all known data in table 4.6). Also, a more precise reduced-width value of 54(8) keV was calculated for the 7254-keV decay. This value is in good agreement with the range of $\delta_\alpha^2 = 40\text{--}70$ keV typical for unhindered $0^+ \rightarrow 0^+$ α decays of even-even isotopes in this region of the chart of the nuclides.

4.2.1.3 The new isotope ^{179}Pb

The reaction used to produce ^{179}Pb was $^{40}\text{Ca} + ^{144}\text{Sm} \rightarrow ^{179}\text{Pb} + 5n$ at a beam energy of 232(1) MeV in front of the target, see table 4.5. The new isotope ^{179}Pb was identified by α - α correlations of its α decays with the α decays of its known daughter and grand-daughter products ^{175}Hg and ^{171}Pt , respectively. Both the decay energies and half-life values for these two isotopes match well the tabulated values. In total, 12 α -decay events of ^{179}Pb were detected. From the respective time distance distributions between the recoil implantation and subsequent α decays a half-life value of $T_{\frac{1}{2}}(^{179}\text{Pb}) = 3.5_{-0.8}^{+1.4}$ ms was deduced by using the data for all these 12 correlated events. An α -decay energy value for this isotope was also estimated: $E_\alpha = 7350(20)$ keV (table 4.6). A decay scheme of ^{179}Pb is presented in figure 4 in [83]. There, the 7350-keV α decay is interpreted as being due to α -decay fine structure of ^{179}Pb feeding the known excited state at 80 keV in ^{175}Hg [97]. As shown in Ref. [97], this low-lying, presumed $9/2^-$ state, deexcites directly to the proposed $7/2^-$ ground state of ^{175}Hg by an 80-keV M1 transition. The situation is similar to the one for the ^{181}Pb isotope (see 4.2.1.1).

The calculated reduced α -decay width, $\delta_\alpha^2(7350 \text{ keV}) = 33_{-10}^{+14}$ keV is similar to the value of 54(8) keV for the neighboring even-even isotope ^{180}Pb described in 4.2.1.2. This suggests that the 7350 keV decay of ^{179}Pb is unhindered. Therefore, $I^\pi = 9/2^-$ was assigned as the ground state of ^{179}Pb .

4.2.2 ^{181g}Tl and ^{177g}Au

During R266, approximately 3000 $\alpha_1(6181\text{ keV})\text{--}\alpha_2(6161\text{ keV})$ correlated events due to the decay chain $^{181g}\text{Tl} \rightarrow ^{177g}\text{Au}$ of the $1/2^+$ ground state of ^{181g}Tl were observed [82]. The measured α -decay energies of ^{181g}Tl and of ^{177g}Au and the half-life value of ^{177g}Au are in good agreement with the previously known values, see table 4.6 where E_α of ^{181g}Tl is actually even improved. But, due to the high implantation rate of ERs, no half-life value could be deduced for this long-lived isotope. The measured α -decay data is shown together with the literature data from Refs. [88–91] in table 4.6. By using the α - α correlation analysis, the previously unknown α -branching ratio $b_\alpha(^{177g}\text{Au}) = 40(6)\%$ was deduced, see table 4.7.

4.2.3 ^{174}Pt and ^{172}Pt

By using the ER- α_1 - α_2 correlation analysis with the longer ER- α_1 time condition suitable for the ≈ 270 -ms isotope ^{178}Hg [98, 99], approximately 10^4 correlated ^{178}Hg - ^{174}Pt events were collected [82]. An α -decay branching ratio of $b_\alpha(^{174}\text{Pt}) = 67(2)\%$ was deduced, which is in good agreement with, but more precise than the value of $b_\alpha = 67(6)\%$ from [91], see table 4.7. However, both values differ from the value of $b_\alpha = 83(5)\%$ reported earlier [93].

From a comparison of the intensity of the ER- $\alpha_1(^{176}\text{Hg})$ correlations with that of the ER- $\alpha_1(^{176}\text{Hg})\text{--}\alpha_2(^{172}\text{Pt})$ correlations, an α -decay branching ratio of $b_\alpha = 97(3)\%$ was deduced for ^{172}Pt [83]. This value is consistent with but is more precise than the values of $b_\alpha = 94_{-32}^{+6}\%$ from Ref. [95] and $b_\alpha = 94(12)\%$ from Ref. [94], see table 4.7.

4.2.4 ^{177}Hg

From the comparison of the number of $\alpha_1(6990\text{--}7100\text{ keV})$ decays of ^{181}Pb and the number of $\alpha_1(^{181}\text{Pb}, 6990\text{--}7100\text{ keV})\text{--}\alpha_2(^{177}\text{Hg}, 6582\text{ keV})$ correlated decays, an α -branching ratio of $b_\alpha = 100\%$ was deduced for ^{177}Hg with a precision of 5%, which is determined by the statistical uncertainty [80]. This value is larger and more precise than the previously reported estimate of $b_\alpha \approx 85\%$ (see Refs. [93, 100] and table 4.7).

4. EXPERIMENTAL RESULTS

5

Half-lives

As mentioned in the introduction, to investigate the properties and the structure of a specific nuclide, synthesis is not sufficient. One has to separate it from the other produced isotopes, detect it and identify it by assigning unequivocally its N and Z numbers. At SHIP for example, isotopes with half-lives between $1 \mu\text{s}$ and 1s can be separated, detected and identified by using the system based on 100 MHz XIA Pixie-16 modules and developed for the experiments at the HRIBF, Oak Ridge [101, 102]. This data acquisition system can be connected parallel to the existing SHIP electronics as it was done for the first observation of $2p$ radioactivity of ^{45}Fe at the GSI FRS [103]. For longer half-lives, the background is usually so high that a direct identification is very complicated. For shorter ones, the isotopes will decay before their implantation into the stop detector if they were synthesized by the nuclear reaction process or their electronic signals might be lost in the dead time of the data acquisition system. It is important to mention that for the mere identification of a particular nucleus, the presence of α - α correlations is sufficient even if the half-life value of the synthesized nucleus cannot be determined. So even if the half-lives lie outside the aforementioned range an identification could be possible without determination of the half-life. We proceeded to estimate the half-lives of so far unknown neutron deficient isotopes with $N < 126$ and $74 \leq Z \leq 92$ in order to see if their detection and direct identification at SHIP is possible. For this purpose we had to estimate as accurately as possible the expected α -, β^+ / EC -decay and proton emission (for odd- Z isotopes) partial half-lives since those are the dominant decay modes of these isotopes. The utility of the results obtained in Chapter 4 will be shown in the next section.

5.1 New parameters for semi-empirical α -decay formulae

In order to estimate the α -decay half-lives of the unknown neutron deficient isotopes we used the semi-empirical formulae of Viola-Seaborg, Royer and Parkhomenko-Sobiczewski ((2.28), (2.36) and (2.38), respectively). These contain some parameters that depend on the nuclei used for the fit. For more accurate results one should use parameters that were obtained by fitting nuclei that are as close as possible to the region where predictions are done. Following this line of thought and in a first approach, we used the three aforementioned formulae with the parameters that Parkhomenko and Sobiczewski [21] had obtained by fitting nuclei with proton number $Z = 84\text{--}111$ to test their predictive power on the 137 known neutron deficient isotopes with $Z = 74\text{--}92$ of table 5.1. Twelve of these were studied in more detail in Chapter 4 and are marked in red. The results of these calculations are shown in table 5.2. To obtain more reliable results, we then tried to improve these parameters to better predict the α -decay half-lives of unknown neutron deficient isotopes with $N < 126$ and $Z = 74\text{--}92$. For this purpose we fitted these three formulae using the same isotopes of table 5.1 we had just used to test the parameters from [21]. The parameters obtained with our new fits are given in table 5.4 and the results obtained with them are shown in table 5.3.

It is evident that the values of $\bar{\delta}$ (Eq. (2.25)) and hence of \bar{f} (Eq. (2.26)) are much higher i.e. worse in table 5.2 than in table 5.3. This could be expected since the parameters corresponding to the latter table were obtained by using the same known isotopes with which the parameters corresponding to the former table were tested while being obtained by Parkhomenko and Sobiczewski for isotopes lying in another region. These results illustrate how sensitive the parameters of these semi-empirical α -decay formulae are to the variations of the atomic number Z . To put it differently, the parameters obtained by Parkhomenko and Sobiczewski in Ref. [21] with slightly heavier nuclei can be improved for the prediction of so far unknown isotopes with $N < 126$ and $Z = 74\text{--}92$. Of these three formulae, Royer's is the most stable to the variation of Z and Parkhomenko-Sobiczewski's formula is the least stable one with the strongest changes between tables 5.2 and 5.3. As mentioned in section 2.5.2, the relationship between Q_α and $T_{\frac{1}{2},\alpha}$ is very sensitive. It was therefore extremely useful to have the improved values of the twelve isotopes marked in red in table 5.1 especially of the two new isotopes because they are closer to the ones whose half-lives we want to predict.

5.1 New parameters for semi-empirical α -decay formulae

Table 5.1: Known neutron deficient isotopes with $Z = 74-92$ used to test and to fit the parameters of Eqs. (2.28), (2.36) and (2.38) - These 137 nuclei were used to test the parameters given in [21] for the three semi-empirical α -decay formulae of Viola-Seaborg, Royer and Parkhomenko-Sobiczewski. The results are shown in table 5.2. These nuclei were also used to fit these formulae obtaining new parameter values that are given in table 5.4 while the results of the fits can be found in table 5.3. These nuclei are separated in four classes since the parameters of these semi-empirical formulae are adjusted separately for each class of nuclei: even-even, even-odd, odd-even and odd-odd. The 12 isotopes whose values were improved in Chapter 4 are marked in red.

Type	Nuclei												
e-e	^{158}W	^{160}W	^{162}W	^{162}Os	^{164}Os	^{166}Os	^{168}Os	^{166}Pt	^{168}Pt	^{170}Pt	^{172}Pt	^{174}Pt	
	^{176}Pt	^{174}Hg	^{176}Hg	^{178}Hg	^{180}Hg	^{182}Hg	^{180}Pb	^{182}Pb	^{184}Pb	^{186}Pb	^{188}Pb	^{190}Po	
	^{192}Po	^{194}Po	^{196}Po	^{198}Po	^{200}Po	^{206}Po	^{208}Po	^{198}Rn	^{200}Rn	^{202}Rn	^{204}Rn	^{206}Rn	
	^{208}Rn	^{210}Rn	^{202}Ra	^{204}Ra	^{206}Ra	^{208}Ra	^{210}Ra	^{212}Ra	^{210}Th	^{212}Th	^{214}Th		
e-o	^{159}W	^{161}W	^{163}Os	^{165}Os	^{169}Os	^{167}Pt	^{169}Pt	^{171}Pt	^{173}Pt	^{175}Pt	^{173}Hg	^{175}Hg	
	^{177}Hg	^{181}Hg	^{183}Hg	^{179}Pb	^{181}Pb	^{189}Po	^{191}Po	^{193}Po	^{195}Po	^{197}Po	^{209}Po	^{195}Rn	
	^{197}Rn	^{199}Rn	^{201}Rn	^{203}Rn	^{205}Rn	^{207}Rn	^{209}Rn	^{211}Rn	^{203}Ra	^{205}Ra	^{207}Ra	^{209}Ra	
	^{211}Ra	^{211}Th	^{213}Th										
o-e	^{163}Re	^{167}Ir	^{169}Ir	^{173}Au	^{177}Au	^{179}Au	^{177}Tl	^{179}Tl	^{193}At	^{195}At	^{197}At	^{199}At	
	^{201}At	^{203}At	^{205}At	^{207}At	^{199}Fr	^{201}Fr	^{203}Fr	^{205}Fr	^{207}Fr	^{209}Fr	^{211}Fr	^{207}Ac	
	^{209}Ac	^{211}Ac	^{213}Ac	^{213}Pa	^{215}Pa								
o-o	^{162}Re	^{166}Ir	^{168}Ir	^{170}Au	^{172}Au	^{174}Au	^{196}At	^{198}At	^{200}At	^{202}At	^{200}Fr	^{202}Fr	
	^{204}Fr	^{206}Fr	^{208}Fr	^{210}Fr	^{206}Ac	^{208}Ac	^{210}Ac	^{212}Ac	^{212}Pa	^{214}Pa			

5. HALF-LIVES

The results shown in table 5.3 are good (low values of $\bar{\delta}$ and \bar{f}) and quite similar for all three formulae. Nevertheless, the ones obtained with the formula of Parkhomenko-Sobiczewski are slightly better than the other ones. We also give the results for the geometric mean $\bar{T}_{\frac{1}{2},\alpha}$ of the half-lives obtained with the three other formulae (cf. equation (5.1)). They are as good as the ones obtained with the formula of Parkhomenko-Sobiczewski (same mean value of \bar{f}) but with a lower mean value of rms. This is why we chose to use $\bar{T}_{\frac{1}{2},\alpha}$ to estimate α -decay partial half-lives of neutron deficient isotopes with $N < 126$ and $Z = 74-92$ (c.f. section 5.2).

$$\bar{T}_{\frac{1}{2},\alpha} = \sqrt[3]{T_{\frac{1}{2},\alpha}^{VS} \cdot T_{\frac{1}{2},\alpha}^R \cdot T_{\frac{1}{2},\alpha}^{PS}} \quad (5.1)$$

Table 5.2: Test of the parameters given by Parkhomenko and Sobiczewski [21]

- The test results were obtained for the three different semi-empirical α -decay formulae of Viola-Seaborg, Royer and Parkhomenko-Sobiczewski using the reported parameters from [21] and the reported experimental values of both half-life and Q_α of the known neutron deficient isotopes of table 5.1. The orbital electron screening effect was not taken into account. The first column represents the class of nuclei, N the number of nuclei (with experimentally measured both half-life and Q_α) that were used to test the parameters of each class, $\bar{\delta}$ is the average of absolute values of discrepancies, rms is the root-mean-square value of these discrepancies and $\bar{f} = 10^{\bar{\delta}}$.

Nuclei	N	Viola-Seaborg			Royer			Park.-Sob.		
		$\bar{\delta}$	rms	\bar{f}	$\bar{\delta}$	rms	\bar{f}	$\bar{\delta}$	rms	\bar{f}
e-e	47	0.882	0.910	7.63	0.552	0.593	3.56	0.942	0.975	8.74
o-e	29	0.478	0.546	3.01	0.433	0.494	2.71	0.956	1.001	9.03
e-o	39	0.430	0.503	2.69	0.180	0.224	1.51	1.104	1.149	12.69
o-o	22	0.209	0.258	1.62	0.165	0.202	1.46	1.066	1.105	11.65

5.1.1 Effect of the orbital electron screening

As mentioned in section 2.5.1 the measured kinetic energy of an α particle outside an atom is smaller than its energy when it penetrates the Coulomb barrier because of the orbital electron screening effect (c.f. Eq. (2.11)). This energy is small (in the order

5.1 New parameters for semi-empirical α -decay formulae

Table 5.3: Results of the new fits - These results were obtained from the fitting procedure of the three semi-empirical α -decay formulae of Viola-Seaborg, Royer and Parkhomenko-Sobiczewski where the new parameters given in table 5.4 were determined. The reported experimental values of both half-life and Q_α of the known neutron deficient isotopes of table 5.1 were used for the fitting procedure. The orbital electron screening effect was not taken into account. The first column represents the class of nuclei, N the number of nuclei (with experimentally measured both half-life and Q_α) that were used for adjustment of the parameters of each class, $\bar{\delta}$ is the average of absolute values of discrepancies, rms is the root-mean-square value of these discrepancies and $\bar{f} = 10^{\bar{\delta}}$. The three last columns correspond to the geometric mean $\bar{T}_{\frac{1}{2},\alpha}$ of the half-lives obtained with the three other formulae (cf. equation (5.1)).

Nuclei	N	Viola-Seaborg			Royer			Park.-Sob.			$\sqrt[3]{T_{\frac{1}{2},\alpha}^{VS} \cdot T_{\frac{1}{2},\alpha}^R \cdot T_{\frac{1}{2},\alpha}^{PS}}$		
		$\bar{\delta}$	rms	\bar{f}	$\bar{\delta}$	rms	\bar{f}	$\bar{\delta}$	rms	\bar{f}	$\bar{\delta}$	rms	\bar{f}
e-e	47	0.115	0.137	1.30	0.126	0.153	1.34	0.124	0.151	1.33	0.119	0.119	1.31
o-e	29	0.131	0.159	1.35	0.116	0.140	1.31	0.122	0.144	1.32	0.123	0.123	1.33
e-o	39	0.161	0.199	1.45	0.171	0.211	1.48	0.165	0.209	1.46	0.161	0.161	1.45
o-o	22	0.124	0.142	1.33	0.114	0.127	1.30	0.105	0.132	1.27	0.112	0.112	1.29

of 26–36 keV) for the nuclei with $Z = 74$ –92 and its effect on $T_{\frac{1}{2},\alpha}$ is also not very impressive but still significant.

It was thus necessary to study the influence of this effect on the changes of not only the parameter values of the three semi-empirical α -decay formulae but also and most importantly on the quality of the predicted $T_{\frac{1}{2},\alpha}$ values. The obtained new parameters are given in table 5.4. A comparison of the latter with the parameters obtained without the consideration of this effect shows that they are almost not affected by the consideration of the orbital electron screening effect, their values remaining almost the same. The results concerning the quality of the predicted $T_{\frac{1}{2},\alpha}$ values are given in table 5.5. There, comparing with the results shown in table 5.3, one can observe that there is no improvement due to the inclusion of this effect. We therefore decided not to take it further into account.

5. HALF-LIVES

Table 5.4: Parameters for the three semi-empirical α -decay formulae of Viola-Seaborg, Royer and Parkhomenko-Sobiczewski obtained with fits using existing neutron deficient isotopes with $Z = 74\text{--}92$ of table 5.1 taking and not taking into account the orbital electron screening effect - For the three formulae of Viola-Seaborg, Royer and Parkhomenko-Sobiczewski their 7, 12 and 5 parameters are given, respectively.

Formulae	Parameters						
V.-S.	a	b	c	d	h_p	h_n	h_{pn}
	2.3360	-61.772	-0.49829	-9.3438	0.12494	0.17659	0.26982
Royer	a	b	c	a	b	c	
		e-e			o-e		
	1.6659	-1.1229	-28.581	1.6832	-1.2054	-27.191	
		e-o			o-o		
	1.6866	-1.2055	-27.253	1.7072	-1.2256	-27.355	
P.-S.	a	b	c	\bar{E}_p	\bar{E}_n		
	1.6012	-0.21322	-33.342	0.03055	0.04852		
V.-S. w/ screening	a	b	c	d	h_p	h_n	h_{pn}
	2.3541	-62.334	-0.50119	-9.3472	0.12490	0.17685	0.27003
Royer w/ screening	a	b	c	a	b	c	
		e-e			o-e		
	1.6781	-1.1280	-28.737	1.6952	-1.2101	-27.352	
		e-o			o-o		
	1.6991	-1.2110	-27.409	1.7189	-1.2303	-27.504	
P.-S. w/ screening	a	b	c	\bar{E}_p	\bar{E}_n		
	1.6126	-0.21415	-33.512	0.03042	0.04851		

Table 5.5: Results of the new fits taking into account the orbital electron screening effect - These results were obtained from the fitting procedure of the three semi-empirical α -decay formulae of Viola-Seaborg, Royer and Parkhomenko-Sobiczewski where the new parameters given in table 5.4 were determined. The reported experimental values of both half-life and Q_α of the known neutron deficient isotopes of table 5.1 were used for the fitting procedure taking into account the orbital electron screening effect. The first column represents the class of nuclei, N the number of nuclei (with experimentally measured both half-life and Q_α) that were used for adjustment of the parameters of each class considering the orbital electron screening energy, $\bar{\delta}$ is the average of absolute values of discrepancies, rms is the root-mean-square value of these discrepancies and $\bar{f} = 10^{\bar{\delta}}$

Nuclei	N	Viola-Seaborg			Royer			Park.-Sob.		
		$\bar{\delta}$	rms	\bar{f}	$\bar{\delta}$	rms	\bar{f}	$\bar{\delta}$	rms	\bar{f}
e-e	47	0.116	0.138	1.30	0.127	0.154	1.34	0.125	0.152	1.33
o-e	29	0.132	0.160	1.35	0.117	0.140	1.31	0.158	0.190	1.44
e-o	39	0.161	0.199	1.45	0.172	0.212	1.48	0.205	0.242	1.60
o-o	22	0.124	0.142	1.33	0.114	0.127	1.30	0.170	0.194	1.48

5. HALF-LIVES

5.2 $T_{\frac{1}{2},\alpha}$

As mentioned in section 5.1, for the determination of the partial α -decay half-life $T_{\frac{1}{2},\alpha}$ of the unknown neutron deficient isotopes, the geometric mean $\overline{T}_{\frac{1}{2},\alpha}$ of the half-lives obtained with the three semi-empirical α -decay formulae of Viola-Seaborg (Eq. (2.28)), Royer (Eq. (2.36)) and Parkhomenko-Sobiczewski (Eqs. (2.38) and (2.39)) is used (cf. equation (5.1)). We used the parameters given in the upper part of table 5.4.

Table 5.6: Comparison of the theoretical Q_α values - The experimental Q_α values of the 137 isotopes of table 5.1 are compared with the Q_α values Q_α^{MN} , Q_α^G , calculated with the theoretical masses of Möller and Nix (cf. section 2.8.1) and Goriely *et al.* (cf. section 2.8.2), respectively, and their arithmetic mean \overline{Q}_α (equation (5.2)). $\overline{\delta}$ is the average of absolute values of discrepancies, rms is the root-mean-square value of these discrepancies and $\overline{f} = 10^{\overline{\delta}}$.

N	Q_α^{MN}			Q_α^G			\overline{Q}_α		
	$\overline{\delta}$	rms	\overline{f}	$\overline{\delta}$	rms	\overline{f}	$\overline{\delta}$	rms	\overline{f}
137	1.32E-2	1.65E-2	1.031	1.65E-2	2.62E-2	1.039	1.01E-2	1.44E-2	1.024

We studied how well the Q_α values Q_α^{MN} , Q_α^G , calculated using equation (2.6) and the theoretical masses of Möller and Nix (cf. section 2.8.1) and Goriely *et al.* (cf. section 2.8.2), respectively, and their arithmetic mean \overline{Q}_α (equation (5.2)) reproduced the experimental Q_α values of the 137 isotopes given in table 5.1. The outcome of this comparison is shown in table 5.6. The results obtained with the arithmetic mean of Q_α^{MN} and Q_α^G are slightly better than the others. This is why \overline{Q}_α was used for the half-life calculation with the three aforementioned semi-empirical α -decay formulae.

$$\overline{Q}_\alpha = \frac{Q_\alpha^{MN} + Q_\alpha^G}{2} \quad (5.2)$$

In cases where only one mass value was theoretically reported, the Q_α value was either taken as Q_α^{MN} or as Q_α^G .

The estimated values of $T_{\frac{1}{2},\alpha}$ for all the so far unknown neutron deficient isotopes with $N < 126$ and $Z = 74-92$ for which at least one mass value was theoretically

calculated by Möller and Nix or Goriely *et al.* are reported in table 5.7 for even-Z isotopes and in table 5.10 for odd-Z isotopes.

5.3 $T_{\frac{1}{2},\beta}$

As mentioned in section 2.6, Möller *et al.* published β^+/EC -decay partial half-lives $T_{\frac{1}{2},\beta}$ for many so far unknown neutron deficient isotopes with $N < 126$ and $Z = 74-92$. These values are shown in tables 5.7 and 5.10 and can be recognized because they have no superscript. For all the other isotopes of the tables for which no value was published by the aforementioned authors, the β^+/EC -decay partial half-lives were calculated using (2.42) with the parameters shown in table 2.2. For the determination of the order of the transition “n”, the calculated values by Goriely *et al.* [41] of the angular momentum and the parity of the ground states were used. These predicted β^+/EC -decay partial half-lives $T_{\frac{1}{2},\beta}$ are shown in tables 5.7 and 5.10 while the order of the transition is shown as the superscript of these values: an “A” when the transition is allowed, or a number to indicate their order of forbiddenness. In the rare cases where $n > 2$ the calculated parameters for $n = 2$ were used.

5.4 $T_{\frac{1}{2},p}$

For the discussion on proton emission partial half-lives $T_{\frac{1}{2},p}$, let us consider table 5.8 and figure 5.1. In the table, the lightest isotope of each element of tables 5.7 and 5.10 is shown with its Q_α , Q_p and Q_{2p} values calculated with the theoretical masses of Goriely *et al.* In this region of interest, the lightest isotope of any element is also the one with the highest value of Q_p and Q_{2p} . In the figure, curves that represent equal decay rates between the different decay modes are plotted as function of the decay energies of the different decay modes.

For even-Z isotopes, taking into consideration the upper curves of the main section of figure 5.1, one can observe that the Q_p values shown in table 5.8 are too small in comparison with the Q_α values to prevail in the competition for the predominant decay mode. The most significative example of this feature is that of the largest value of Q_p (1.7 MeV for ^{201}U). For this value, the corresponding Q_α value for an equal decay rate according to figure 5.1 would be around 8 MeV, which is 1.5 MeV below the

5. HALF-LIVES

Table 5.7: Estimated Q_α , partial α -decay half-lives $T_{\frac{1}{2},\alpha}$, partial β^+/EC -decay half-lives $T_{\frac{1}{2},\beta}$ and total half-lives $T_{\frac{1}{2}}$ for so far unknown even- Z neutron deficient isotopes with $N < 126$ and $Z = 74-92$ - The isotopes marked with an asterisk and a “ - ” are those whose $T_{\frac{1}{2}}$ values belong to the intervals $[1\mu\text{s},1\text{s}]$ and $[0.1\mu\text{s},1\mu\text{s}]$, respectively. The ones marked with a “ - ” are thus up to one order of magnitude too small to fit in the asterisk category. All isotopes with $T_{\frac{1}{2},\beta} < T_{\frac{1}{2},\alpha}$ are colored in red. The partial β^+/EC -decay half-lives that were not taken from [24] but calculated according to [26] are marked with superscripts: an “ A ” when the transition is allowed, or a number to indicate their order of forbiddenness.

Z	A	Q_α	$T_{\frac{1}{2},\alpha}/\text{s}$	$T_{\frac{1}{2},\beta}/\text{s}$	$T_{\frac{1}{2}}/\text{s}$	Z	A	Q_α	$T_{\frac{1}{2},\alpha}/\text{s}$	$T_{\frac{1}{2},\beta}/\text{s}$	$T_{\frac{1}{2}}/\text{s}$	Z	A	Q_α	$T_{\frac{1}{2},\alpha}/\text{s}$	$T_{\frac{1}{2},\beta}/\text{s}$	$T_{\frac{1}{2}}/\text{s}$
74	154*	4.05	5.3E9	8.2E-2	8.2E-2	182 ⁻	8.85	9.6E-7	1.8E-1	9.6E-7	195*	9.59	1.3E-6	1.2E-4 ¹	1.3E-6		
	155*	4.38	5.8E7	4.2E-2	4.2E-2	183*	8.36	2.8E-5	2.5E-1	2.8E-5	196*	9.53	1.4E-6	1.5E-3 ⁴	1.4E-6		
	156*	3.82	2.5E11	1.3E-1	1.3E-1	184*	8.34	2.2E-5	4.3E-1	2.2E-5	197 ⁻	9.68	7.3E-7	1.8E-3 ⁴	7.3E-7		
	157*	5.94	5.0E-1	2.1E-1	1.5E-1	185*	8.20	7.8E-5	3.7E-1	7.8E-5	198*	9.36	3.6E-6	1.2E-1	3.6E-6		
76	158*	4.50	7.4E7	3.9E-3 ²	3.9E-3	86 182 ⁻	9.12	9.3E-7	2.3E-4 ^A	9.2E-7	199*	9.07	2.6E-5	1.3E-1	2.6E-5		
	159*	5.04	8.8E4	8.5E-2	8.5E-2	183*	8.83	7.1E-6	4.7E-4 ²	7.0E-6	200*	9.03	2.6E-5	3.0E-1	2.6E-5		
	160*	6.99	3.3E-4	1.3E-1	3.3E-4	184*	8.86	4.2E-6	3.0E-4 ¹	4.2E-6	201*	9.14	1.6E-5	2.8E-1	1.6E-5		
	161*	6.13	7.3E-1	1.7E-1	1.4E-1	185*	8.17	5.2E-4	3.6E-4 ¹	2.1E-4	202*	8.94	4.3E-5	3.9E-1	4.3E-5		
78	162*	7.88	4.0E-6	1.6E-3 ²	4.0E-6	186*	8.21	2.7E-4	9.8E-2	2.7E-4	203*	8.90	7.1E-5	4.8E-1	7.1E-5		
	163*	6.18	3.7E0	2.0E-3 ²	2.0E-3	187*	8.34	1.5E-4	9.6E-2	1.5E-4	204*	8.71	1.9E-4	6.5E-1	1.9E-4		
	164*	6.19	2.0E0	5.7E-3 ²	5.7E-3	188*	8.08	6.6E-4	1.6E-1	6.5E-4	205*	8.60	5.2E-4	7.6E-1	5.2E-4		
	165*	7.42	1.3E-4	1.1E-1	1.3E-4	189*	7.94	2.4E-3	2.0E-1	2.4E-3	206*	8.38	1.7E-3	1.1E0	1.7E-3		
80	166*	7.47	3.7E-4	1.5E-4 ¹	1.1E-4	190*	8.10	5.5E-4	3.0E-1	5.5E-4	207*	8.29	4.4E-3	1.2E0	4.3E-3		
	167*	8.31	1.9E-6	8.0E-4 ²	1.9E-6	191*	8.20	3.7E-4	2.6E-1	3.6E-4	92 201*	9.49	8.9E-6	1.3E-4 ¹	8.4E-6		
	168 ⁻	8.48	4.6E-7	2.3E-3 ²	4.6E-7	192*	8.04	8.2E-4	5.4E-1	8.1E-4	202 ⁻	9.87	7.6E-7	8.1E-4 ^A	7.6E-7		
	169*	8.12	6.1E-6	2.7E-3 ²	6.1E-6	193*	8.07	8.8E-4	5.3E-1	8.7E-4	203*	9.85	1.1E-6	1.1E-1 ¹	1.1E-6		
	170*	7.70	6.8E-5	1.2E-1	6.8E-5	194*	7.89	2.2E-3	1.3E0	2.2E-3	204 ⁻	9.84	8.5E-7	1.6E-1 ^A	8.5E-7		
82	170	9.24	2.8E-8	2.6E-4 ³	2.8E-8	88 190*	9.05	5.7E-6	3.5E-4 ¹	5.6E-6	205*	9.39	1.5E-5	2.4E-1 ¹	1.5E-5		
	171 ⁻	8.84	3.6E-7	3.1E-4 ³	3.6E-7	191*	8.72	6.0E-5	4.1E-4 ¹	5.2E-5	206*	9.28	2.2E-5	3.4E-1 ^A	2.2E-5		
	172 ⁻	8.78	3.6E-7	8.8E-4 ³	3.6E-7	192*	8.91	1.3E-5	1.1E-1	1.3E-5	207*	9.12	7.7E-5	3.7E-1 ¹	7.7E-5		
	173*	8.48	3.0E-6	1.1E-3 ³	3.0E-6	193*	8.92	1.6E-5	9.7E-2	1.6E-5	208*	9.05	9.4E-5	5.6E-1 ^A	9.4E-5		
	174 ⁻	8.68	6.2E-7	3.0E-3 ³	6.2E-7	194*	8.89	1.4E-5	2.1E-1	1.4E-5	209*	9.21	4.3E-5	4.0E-1 ¹	4.3E-5		
	175*	8.39	5.1E-6	8.2E-2	5.1E-6	195*	8.86	2.2E-5	2.3E-1	2.2E-5	210*	8.78	5.2E-4	6.8E-1 ^A	5.2E-4		
	176*	8.24	9.0E-6	1.4E-1	9.0E-6	196*	8.70	4.5E-5	3.1E-1	4.5E-5	211*	8.60	2.3E-3	6.0E-1 ¹	2.3E-3		
	177*	7.84	1.9E-4	1.4E-1	1.9E-4	197*	8.38	5.0E-4	2.4E-1	5.0E-4	212*	8.51	3.3E-3	9.2E-1 ^A	3.3E-3		
	178*	7.92	7.3E-5	2.8E-1	7.3E-5	198*	8.54	1.2E-4	7.2E-1	1.2E-4	213*	8.62	1.9E-3	1.4E0 ¹	1.9E-3		
84	179	9.74	9.7E-9	1.3E-3 ²	9.7E-9	199*	8.29	9.4E-4	8.7E-1	9.4E-4	214*	8.59	1.8E-3	2.8E0 ^A	1.8E-3		
	180 ⁻	9.12	2.1E-7	9.6E-4 ¹	2.1E-7	200*	8.31	5.9E-4	1.1E0	5.9E-4	215*	8.61	2.1E-3	1.7E0 ¹	2.1E-3		
	181	9.53	2.8E-8	9.2E-2	2.8E-8	90 194 ⁻	9.74	4.3E-7	1.0E-4 ¹	4.3E-7	216*	8.77	5.2E-4	4.1E0 ^A	5.2E-4		

Table 5.8: Comparison of the Q_α , Q_p and Q_{2p} values calculated with the theoretical masses of Goriely *et al.* - Only the lightest isotope of each element of tables 5.7 and 5.10 is shown.

Even-Z Isotopes					Odd-Z Isotopes				
Z	A	Q_α	Q_p	Q_{2p}	Z	A	Q_α	Q_p	Q_{2p}
74	154	4.19	< 0	1.25	75	156	5.19	1.88	1.28
76	158	4.50	< 0	1.41	77	160	5.51	2.25	1.81
78	162	7.88	0.32	1.98	79	164	7.13	3.20	2.82
80	166	7.47	0.47	3.26	81	168	8.80	3.69	4.49
82	170	9.24	1.12	4.02	83	172	10.8	5.62	6.38
84	179	9.74	0.91	3.52	85	176	10.5	4.55	6.09
86	182	9.12	1.27	4.27	87	188	9.16	2.26	2.42
88	190	9.05	1.13	3.15	89	192	9.32	2.86	3.87
90	194	9.74	1.23	3.91	91	196	9.80	3.07	3.94
92	201	9.49	1.70	2.88					

predicted Q_α value for this isotope. This difference corresponds roughly to 4–6 orders of magnitude in half-lives. For the other isotopes of table 5.8 and for all the other isotopes of table 5.7, the difference is even bigger because the Q_p values decrease much faster than the Q_α values. So we decided not to take further into consideration the possibility of proton emission decay for the even-Z neutron deficient isotopes of table 5.7.

For odd-Z isotopes, as was discussed in subsection 2.7.2 and can be observed in figure 2.2 very good results in the estimation of the proton emission partial half-life $T_{\frac{1}{2},p}$ were obtained by Dong, Zhang and Royer [27] with the two semiempirical formulae given in Eqs. (2.59) and (2.60). We studied how well the $T_{\frac{1}{2},p}$ values $T_{\frac{1}{2},p}^{DV}$ (cf. Eq. (2.61)), $T_{\frac{1}{2},p}^{DR}$ (cf. Eq. (2.62)) and their geometric mean $\overline{T}_{\frac{1}{2},p}$ (equation (5.3)) reproduced the experimental $T_{\frac{1}{2},p}$ values of the 13 spherical proton emitters with $Z = 75$ –81 of table I in [27]. The outcome of this comparison is shown in table 5.9. The results obtained with $\overline{T}_{\frac{1}{2},p}$ are as good as the ones obtained with $T_{\frac{1}{2},p}^{DV}$ and even slightly better than the ones obtained with $T_{\frac{1}{2},p}^{DR}$. We therefore chose the geometrical means of the results obtained with each formula using the respective parameters given

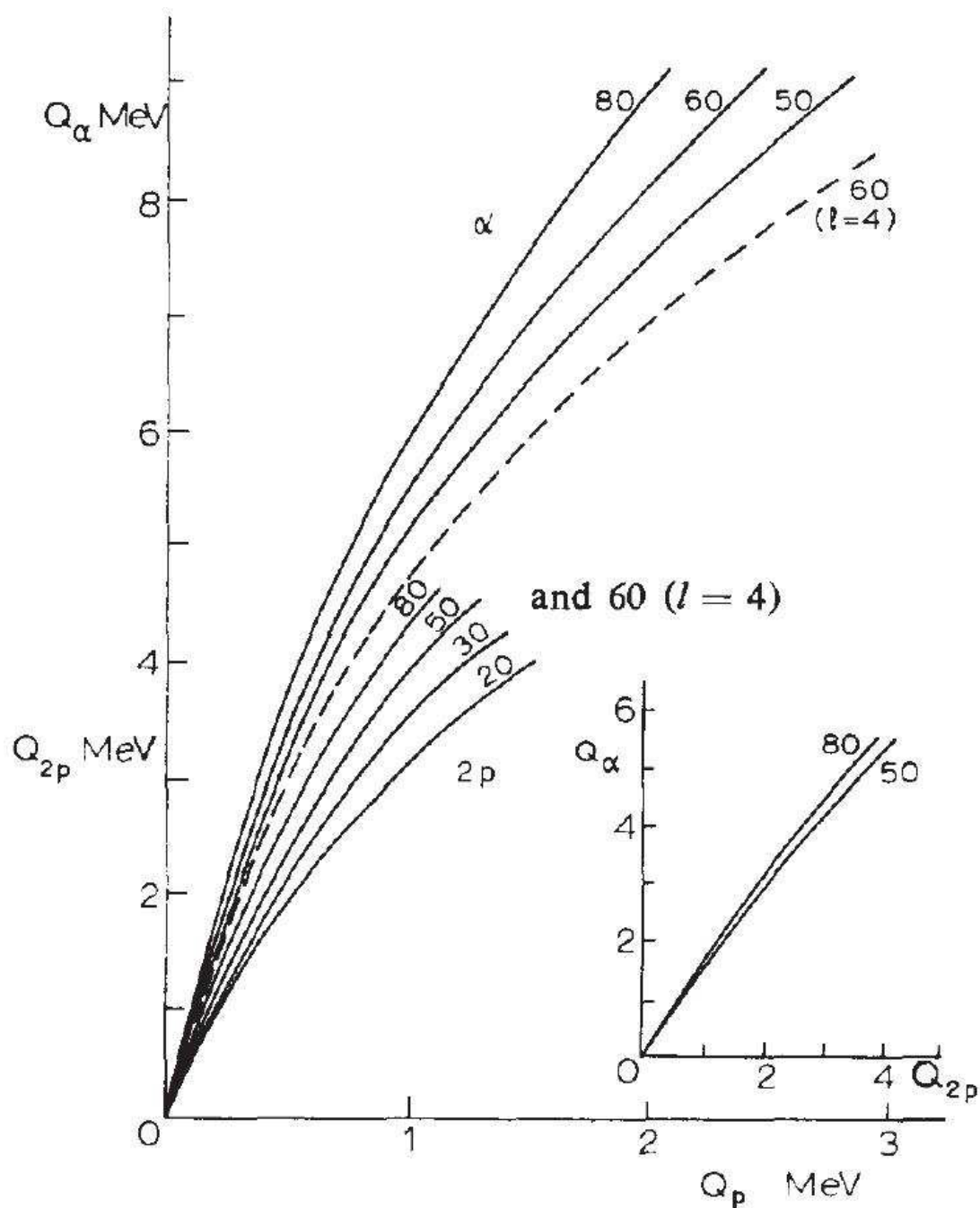


Figure 5.1: Connection between the energies of α -, two-proton- and proton-decay (Q_α , Q_{2p} and Q_p , respectively) - The curves correspond to the case of equal rates of these decays for a purely Coulomb barrier as well as for a particular case $l=4$ ($Z=60$) when there is also a centrifugal barrier for single protons. In the main section of the graph the upper curves give the connection between Q_α and Q_p and the lower curves between Q_{2p} and Q_p . The right section gives the connection between Q_α and Q_{2p} . The figure is taken from [104, 105].

Table 5.9: Comparison of the $T_{\frac{1}{2},p}$ values - The experimental $T_{\frac{1}{2},p}$ values of the 13 spherical proton emitters with $Z = 75-81$ of table I in [27] are compared with the $T_{\frac{1}{2},p}$ values $T_{\frac{1}{2},p}^{DV}$ (cf. Eq. (2.61)), $T_{\frac{1}{2},p}^{DR}$ (cf. Eq. (2.62)) and their geometric mean $\overline{T}_{\frac{1}{2},p}$ (equation (5.3)). $\overline{\delta}$ is the average of absolute values of discrepancies, rms is the root-mean-square value of these discrepancies and $\overline{f} = 10^{\overline{\delta}}$.

N	$T_{\frac{1}{2},p}^{DV}$			$T_{\frac{1}{2},p}^{DR}$			$\sqrt{T_{\frac{1}{2},p}^{DV} \cdot T_{\frac{1}{2},p}^{DR}}$		
	$\overline{\delta}$	rms	\overline{f}	$\overline{\delta}$	rms	\overline{f}	$\overline{\delta}$	rms	\overline{f}
13	0.184	0.213	1.53	0.194	0.229	1.56	0.185	0.219	1.53

in Eqs. (2.61) and (2.62) in order to estimate the proton emission half-lives of the so far unknown neutron deficient isotopes:

$$\overline{T}_{\frac{1}{2},p} = \sqrt{T_{\frac{1}{2},p}^{DV} \cdot T_{\frac{1}{2},p}^{DR}} \quad (5.3)$$

Similarly as in the previous subsection, the Q_p values obtained with equation (2.44) from the theoretical masses calculated by Möller and Nix (cf. section 2.8.1) and Goriely *et al.* (cf. section 2.8.2) were averaged arithmetically whenever possible:

$$\overline{Q}_p = \frac{Q_p^{MN} + Q_p^G}{2} \quad (5.4)$$

As discussed in subsection 2.7.2 the angular momentum l carried away by the emitted proton cannot be predicted exactly in all cases. The problem is then that a change of angular momentum transfer from zero to five corresponds to a half-life increase of 3–4 orders of magnitude. We therefore chose to calculate a lower $T_{\frac{1}{2},p}^L$ and an upper limit $T_{\frac{1}{2},p}^U$ of proton emission partial half-life corresponding to the extreme values of l i.e. $l=0$ and $l=5$, respectively.

For odd- Z isotopes, the estimated values of $T_{\frac{1}{2},p}^L$ and $T_{\frac{1}{2},p}^U$ for all the unknown neutron deficient isotopes with $N < 126$ and $Z = 74-92$ for which at least one mass value was calculated by Möller and Nix or Goriely *et al.* are reported in table 5.10.

5. HALF-LIVES

5.5 $T_{\frac{1}{2},2p}$

To analyze the competition between two-proton emission decay and the other decay modes we will consider again table 5.8 and figure 5.1:

- Even-Z isotopes: all Q_{2p} values are clearly under the corresponding Q_α values (table 5.8) for equal decay rate according to the right section of figure 5.1. This means that the partial α -decay half-lives are much smaller than the partial two-proton emission decay half-lives. As this is also true for the other isotopes of table 5.7 because the Q_{2p} values decrease much faster than the Q_α values, we decided not to take into consideration the possibility of two-proton emission decay for the even-Z neutron deficient isotopes of table 5.7.
- Odd-Z isotopes: the Q_{2p} are never more than 35% higher than the Q_p values (table 5.8). According to the lower curves of the main section of figure 5.1, such a relationship between Q_{2p} and Q_p is insufficient for two-proton decay to be dominant as a factor of 3–4 would be needed for this to happen. This isn't the case for the other isotopes of table 5.10 either. We therefore decided not to take into consideration the possibility of two-proton emission decay for the odd-Z neutron deficient isotopes of table 5.10.

5.6 Total $T_{\frac{1}{2}}$

For the unknown even-Z neutron deficient isotopes with $N < 126$ and $Z = 74-92$ the main decay modes are α - and β^+/EC -decay.

As can be deduced from Eqs. (2.18) and (2.20), for these isotopes the total half-lives $T_{\frac{1}{2}}$ shown in table 5.7 are calculated from the partial α - and β^+/EC -decay half-lives according to:

$$T_{\frac{1}{2}} = \frac{T_{\frac{1}{2},\alpha} \cdot T_{\frac{1}{2},\beta}}{T_{\frac{1}{2},\alpha} + T_{\frac{1}{2},\beta}}. \quad (5.5)$$

According to table 5.7, 73 unknown even-Z isotopes could be detected if one considered that $1\mu s < T_{\frac{1}{2}} < 1s$ or even 84 if $0.1\mu s < T_{\frac{1}{2}} < 1s$. One can observe that only for the lighter elements (W, Os, Pt and Hg), β^+/EC -decay can dominate over

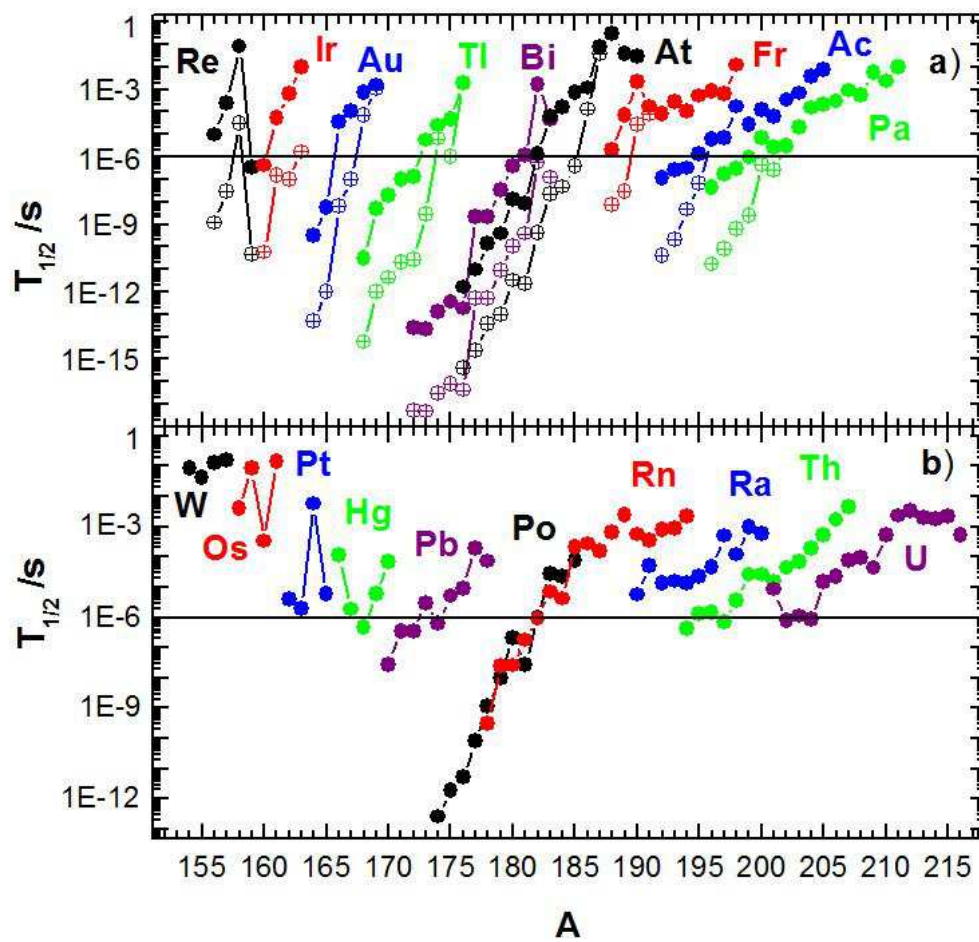


Figure 5.2: Expected total half-lives for the unknown neutron deficient isotopes with $N < 126$ and $Z = 74-92$ - (a) odd- Z isotopes: the full circles represent the upper limits $T_{\frac{1}{2}}^U$ ($\Delta I = 5$) while the empty circles represent the lower limits $T_{\frac{1}{2}}^L$ ($\Delta I = 0$) of the total half-lives; (b) even- Z isotopes

5. HALF-LIVES

α -decay because the values of Q_α are under 8 MeV. For heavier isotopes where $Q_\alpha > 8$ MeV, α -decay is clearly the predominant decay mode with half-lives in the $[1\mu\text{s}, 1\text{ms}]$ interval. The total half-lives of all these unknown even-Z isotopes are plotted in figure 5.2b.

For the unknown odd-Z neutron deficient isotopes with $N < 126$ and $Z = 74-92$ the main decay modes are α -, β^+ / EC - and proton emission decay. As can be deduced from Eqs. (2.18) and (2.20), for these isotopes the total half-lives $T_{\frac{1}{2}}$ are calculated from the partial α -, β^+ / EC - and proton emission decay half-lives according to:

$$T_{\frac{1}{2}} = \frac{T_{\frac{1}{2},\alpha} \cdot T_{\frac{1}{2},\beta} \cdot T_{\frac{1}{2},p}}{T_{\frac{1}{2},\alpha} \cdot T_{\frac{1}{2},\beta} + T_{\frac{1}{2},\alpha} \cdot T_{\frac{1}{2},p} + T_{\frac{1}{2},\beta} \cdot T_{\frac{1}{2},p}}. \quad (5.6)$$

But since there are two values for $T_{\frac{1}{2},p}$, namely a lower limit $T_{\frac{1}{2},p}^L$ and an upper limit $T_{\frac{1}{2},p}^U$, we also have two values for the total half-life $T_{\frac{1}{2}}$, namely a lower limit $T_{\frac{1}{2}}^L$ and an upper limit $T_{\frac{1}{2}}^U$ for the total half-life:

$$T_{\frac{1}{2}}^L = \frac{T_{\frac{1}{2},\alpha} \cdot T_{\frac{1}{2},\beta} \cdot T_{\frac{1}{2},p}^L}{T_{\frac{1}{2},\alpha} \cdot T_{\frac{1}{2},\beta} + T_{\frac{1}{2},\alpha} \cdot T_{\frac{1}{2},p}^L + T_{\frac{1}{2},\beta} \cdot T_{\frac{1}{2},p}^L}. \quad (5.7)$$

$$T_{\frac{1}{2}}^U = \frac{T_{\frac{1}{2},\alpha} \cdot T_{\frac{1}{2},\beta} \cdot T_{\frac{1}{2},p}^U}{T_{\frac{1}{2},\alpha} \cdot T_{\frac{1}{2},\beta} + T_{\frac{1}{2},\alpha} \cdot T_{\frac{1}{2},p}^U + T_{\frac{1}{2},\beta} \cdot T_{\frac{1}{2},p}^U}. \quad (5.8)$$

For odd-Z isotopes, the estimated values of $T_{\frac{1}{2}}^L$ and $T_{\frac{1}{2}}^U$ for all the so far unknown neutron deficient isotopes with $N < 126$ and $Z = 74-92$ for which at least one mass value was calculated by Möller and Nix or Goriely *et al.* are reported in table 5.10. According to it, 41 so far unknown odd-Z isotopes have both limits $T_{\frac{1}{2}}^L$ and $T_{\frac{1}{2}}^U$ that belong to the interval $[1\mu\text{s}, 1\text{s}]$. They are therefore from the decay point of view very likely to be detected at SHIP. They are marked with an asterisk in the table. The 19 isotopes marked with a “ - ” are those where only $T_{\frac{1}{2}}^U$ belongs to that interval, $T_{\frac{1}{2}}^L$ being too small and therefore these isotopes have a smaller chance of being identified. Finally, 31 unmarked isotopes have both limits below $1\mu\text{s}$ which are not accessible at SHIP. It can be observed that proton emission decay is generally the predominant decay mode as soon as the Q_p value of an isotope is well over 2 MeV, in agreement with the upper curves of the main section of figure 5.1. In the rest of the cases where Q_p

values are smaller, α -decay is predominant because of its high Q_α values well over 8 MeV explaining why there is very small room for β^+ / EC -decay to take place predominantly.

The lower and upper limits of the total half-lives of all these so far unknown odd-Z isotopes are plotted in figure 5.2a. The lowest values of $T_{\frac{1}{2}}^L$ go down to 5E-18s while the highest values of $T_{\frac{1}{2}}^U$ go up to 1s.

5. HALF-LIVES

Table 5.10: Estimated Q_α , Q_p , partial α -decay half-lives $T_{\frac{1}{2},\alpha}$, partial β^+/EC -decay half-lives $T_{\frac{1}{2},\beta}$, lower and upper limits for proton emission partial half-lives $T_{\frac{1}{2},p}$ and lower and upper limits for total half-lives $T_{\frac{1}{2}}$ for so far unknown odd-Z neutron deficient isotopes with $N < 126$ and $Z = 74-92$

- The isotopes marked with an asterisk are those where both limits $T_{\frac{1}{2}}^L$ and $T_{\frac{1}{2}}^U$ belong to the interval $[1\mu\text{s}, 1\text{s}]$ while those marked with a “ - ” are those where only $T_{\frac{1}{2}}^U$ belongs to it, $T_{\frac{1}{2}}^L$ being too small. The unmarked ones have both limits under $1\mu\text{s}$. The partial β^+/EC -decay half-lives that were not taken from [24] but calculated according to [26] are marked with superscripts: an “ A ” when the transition is allowed, or a number to indicate their order of forbiddenness. The lower and upper limits for total half-lives are colored according to the decay mode that corresponds to the smallest partial half-life used for their calculation: red for β^+/EC -decay, orange for proton emission and black for α -decay.

Z	A	Q_α	Q_p	$T_{\frac{1}{2},\alpha}/\text{s}$	$T_{\frac{1}{2},\beta}/\text{s}$	$T_{\frac{1}{2},p}^L/\text{s}$	$T_{\frac{1}{2},p}^U/\text{s}$	$T_{\frac{1}{2}}^L/\text{s}$	$T_{\frac{1}{2}}^U/\text{s}$	Z	A	Q_α	Q_p	$T_{\frac{1}{2},\alpha}/\text{s}$	$T_{\frac{1}{2},\beta}/\text{s}$	$T_{\frac{1}{2},p}^L/\text{s}$	$T_{\frac{1}{2},p}^U/\text{s}$	$T_{\frac{1}{2}}^L/\text{s}$	$T_{\frac{1}{2}}^U/\text{s}$
75	156 ⁻	4.54	1.92	3E7	3E-2	1E-9	1E-5	1E-9	1E-5	182 ⁻	7.50	1.80	6E-3	2E-1	5E-7	2E-3	5E-7	2E-3	
	157 ⁻	3.95	1.70	2E11	1E-1	3E-8	2E-4	3E-8	2E-4	183 ⁻	8.13	1.89	5E-5	4E-1	1E-7	5E-4	1E-7	4E-5	
	158*	4.92	1.34	2E5	1E-1	3E-5	2E-1	3E-5	8E-2	85	176	10.5	4.55	4E-10	6E-6 ¹	4E-16	2E-12	4E-16	2E-12
	159	6.99	2.18	2E-4	2E-1	4E-11	4E-7	4E-11	4E-7	177	9.81	4.15	1E-8	1E-5 ¹	2E-15	9E-12	2E-15	9E-12	
77	160	5.51	2.25	2E3	8E-4 ²	6E-11	4E-7	6E-11	4E-7	178	9.28	3.63	3E-7	2E-5 ¹	4E-14	1E-10	4E-14	1E-10	
	161 ⁻	7.41	1.67	5E-5	9E-4 ¹	1E-7	1E-3	1E-7	5E-5	179	8.78	3.46	4E-6	8E-5 ^A	1E-13	4E-10	1E-13	4E-10	
	162 ⁻	6.49	1.70	1E-1	2E-1	9E-8	7E-4	9E-8	6E-4	180	7.74	2.96	7E-3	1E-5 ^A	3E-12	1E-8	3E-12	1E-8	
	163*	6.50	1.54	6E-2	2E-1	2E-6	1E-2	2E-6	9E-3	181	9.04	3.01	9E-7	3E-4 ^A	2E-12	8E-9	2E-12	8E-9	
79	164	7.13	3.20	4E-3	3E-4 ²	5E-14	3E-10	5E-14	3E-10	182 ⁻	8.67	2.43	1E-5	4E-5 ^A	4E-10	2E-6	4E-10	1E-6	
	165	7.31	2.79	7E-4	3E-4 ¹	1E-12	6E-9	1E-12	6E-9	183 ⁻	8.17	2.09	2E-4	6E-4 ¹	2E-8	8E-5	2E-8	5E-5	
	166 ⁻	7.13	1.95	4E-3	6E-4 ¹	6E-9	4E-5	6E-9	3E-5	184 ⁻	7.93	2.04	1E-3	9E-2	5E-8	2E-4	5E-8	2E-4	
	167 ⁻	7.52	1.76	1E-4	1E-1	1E-7	6E-4	1E-7	1E-4	185 ⁻	7.88	1.89	1E-3	1E-1	4E-7	1E-3	4E-7	7E-4	
	168*	7.33	1.41	7E-4	1E-1	8E-5	4E-1	7E-5	7E-4	186*	7.96	1.56	1E-3	1E-1	1E-4	5E-1	1E-4	1E-3	
	169*	7.19	1.25	2E-3	2E-1	4E-3	2E1	1E-3	2E-3	187*	7.36	1.29	8E-2	2E-1	8E-2	3E2	3E-2	6E-2	
81	168	8.80	3.69	3E-7	1E-4 ³	6E-15	3E-11	6E-15	3E-11	188*	7.07	1.00	1E0	4E-1	1E3	5E6	3E-1	3E-1	
	169	8.59	2.90	7E-7	5E-4 ³	1E-12	5E-9	1E-12	5E-9	189*	7.45	0.86	4E-2	5E-1	8E5	3E9	3E-2	3E-2	
	170	8.89	2.72	1E-7	4E-4 ³	4E-12	2E-8	4E-12	2E-8	190*	7.52	0.57	3E-2	3E-1	3E14	1E18	3E-2	3E-2	
	171	8.45	2.54	2E-6	2E-3 ³	2E-11	1E-7	2E-11	1E-7	87	188 ⁻	9.16	2.26	2E-6	8E-4 ²	7E-9	2E-5	7E-9	2E-6
	172	8.39	2.51	3E-6	1E-3 ³	3E-11	1E-7	3E-11	1E-7	189 ⁻	8.33	2.15	3E-4	9E-2	3E-8	1E-4	3E-8	7E-5	
	173 ⁻	8.16	2.09	9E-6	1E-1	3E-9	1E-5	3E-9	6E-6	190*	8.09	1.71	2E-3	1E-1	3E-5	9E-2	3E-5	2E-3	
	174*	8.05	1.58	2E-5	1E-1	9E-6	4E-2	6E-6	2E-5	191*	8.42	1.62	2E-4	2E-1	1E-4	5E-1	8E-5	2E-4	
	175*	7.91	1.69	5E-5	2E-1	1E-6	5E-3	1E-6	5E-5	192*	8.58	1.37	8E-5	2E-1	4E-2	1E2	8E-5	8E-5	
	176*	7.43	1.08	2E-3	4E-1	3E0	2E4	2E-3	2E-3	193*	8.34	1.17	3E-4	3E-1	1E1	4E4	3E-4	3E-4	
83	172	10.8	5.62	4E-11	3E-6 ^A	5E-18	2E-14	5E-18	2E-14	194*	8.52	1.02	1E-4	3E-1	3E3	9E6	1E-4	1E-4	
	173	11.5	6.65	2E-12	7E-5 ^A	5E-18	2E-14	5E-18	2E-14	195*	8.25	0.88	5E-4	3E-1	2E6	5E9	5E-4	5E-4	
	174	10.8	5.08	3E-11	1E-5 ^A	3E-17	1E-13	3E-17	1E-13	196*	8.22	0.79	8E-4	5E-1	2E8	6E11	8E-4	8E-4	
	175	10.9	4.79	2E-11	2E-4 ^A	8E-17	4E-13	8E-17	4E-13	197*	8.22	0.70	6E-4	6E-1	6E10	2E14	6E-4	6E-4	
	176	10.8	4.97	3E-11	4E-5 ^A	4E-17	2E-13	4E-17	2E-13	198*	7.85	0.35	1E-2	7E-1	2E28	5E31	1E-2	1E-2	
	177	9.11	3.09	1E-7	2E-3 ⁴	5E-13	2E-9	5E-13	2E-9	89	192	9.32	2.86	4E-6	1E-4 ¹	4E-11	1E-7	4E-11	1E-7
	178	9.36	3.10	4E-8	7E-2	5E-13	2E-9	5E-13	2E-9	193	9.64	2.68	4E-7	2E-4 ¹	2E-10	6E-7	2E-10	2E-7	
	179	8.96	2.73	3E-7	9E-2	9E-12	4E-8	9E-12	3E-8	194	9.73	2.38	3E-7	4E-4 ¹	5E-9	1E-5	5E-9	3E-7	
	180	8.65	2.46	2E-6	1E-1	1E-10	5E-7	1E-10	4E-7	195 ⁻	9.44	2.16	1E-6	1E-1	7E-8	2E-4	7E-8	1E-6	
	181 ⁻	8.54	2.34	4E-6	2E-1	4E-10	2E-6	4E-10	1E-6	196*	9.21	1.72	6E-6	1E-1	7E-5	2E-1	6E-6	6E-6	

5.6 Total $T_{\frac{1}{2}}$

Z	A	Q_α	Q_p	$T_{\frac{1}{2},\alpha}/s$	$T_{\frac{1}{2},\beta}/s$	$T_{\frac{1}{2},p}^L/s$	$T_{\frac{1}{2},p}^U/s$	$T_{\frac{1}{2}}^L/s$	$T_{\frac{1}{2}}^U/s$	Z	A	Q_α	Q_p	$T_{\frac{1}{2},\alpha}/s$	$T_{\frac{1}{2},\beta}/s$	$T_{\frac{1}{2},p}^L/s$	$T_{\frac{1}{2},p}^U/s$	$T_{\frac{1}{2}}^L/s$	$T_{\frac{1}{2}}^U/s$
89	197*	9.15	1.61	7E-6	2E-1	6E-4	2E0	7E-6	7E-6	200 ⁻	9.44	2.09	7E-6	1E-1 ¹	5E-7	1E-3	5E-7	7E-6	
	198*	8.69	1.32	2E-4	3E-1	5E-1	1E3	2E-4	2E-4	201 ⁻	9.55	2.13	3E-6	2E-1 ²	3E-7	7E-4	2E-7	3E-6	
	199*	8.93	1.26	3E-5	3E-1	3E0	8E3	3E-5	3E-5	202*	9.58	1.76	3E-6	2E-1 ¹	1E-4	3E-1	3E-6	3E-6	
	200*	8.73	1.23	1E-4	5E-1	7E0	2E4	1E-4	1E-4	203*	9.21	1.53	2E-5	3E-1 ²	1E-2	3E1	2E-5	2E-5	
	201*	8.79	1.19	6E-5	7E-1	2E1	7E4	6E-5	6E-5	204*	8.94	1.27	1E-4	3E-1 ¹	8E0	2E4	1E-4	1E-4	
	202*	8.57	0.92	3E-4	7E-1	1E6	3E9	3E-4	3E-4	205*	8.84	1.32	2E-4	4E-1 ²	2E0	5E3	2E-4	2E-4	
	203*	8.43	0.79	7E-4	1E0	1E9	3E12	7E-4	7E-4	206*	8.82	1.14	3E-4	4E-1 ¹	6E2	1E6	3E-4	3E-4	
	204*	8.23	0.36	4E-3	1E0	1E29	3E32	4E-3	4E-3	207*	8.62	1.02	9E-4	7E-1 ²	5E4	1E8	9E-4	9E-4	
	205*	8.09	0.47	7E-3	2E0	2E21	6E24	7E-3	7E-3	208*	8.73	0.80	6E-4	7E-1 ¹	4E9	9E12	6E-4	6E-4	
91	196	9.80	3.07	9E-7	8E-5 ³	2E-11	4E-8	2E-11	4E-8	209*	8.34	0.72	6E-3	1E0 ²	5E11	1E15	6E-3	6E-3	
	197	9.72	2.88	1E-6	3E-4 ⁴	8E-11	2E-7	8E-11	2E-7	210*	8.52	0.65	2E-3	1E0 ¹	1E14	3E17	2E-3	2E-3	
	198	9.95	2.66	4E-7	1E-4 ¹	6E-10	2E-6	6E-10	3E-7	211*	8.26	0.46	1E-2	2E0 ²	4E22	1E26	1E-2	1E-2	
	199	9.71	2.52	1E-6	1E-3 ²	3E-9	6E-6	3E-9	9E-7										

5. HALF-LIVES

6

Cross-sections

This Chapter's subject is to study the synthesis of new neutron deficient isotopes with $N < 126$ and $Z = 74-92$ from the perspective of their production cross-sections σ . Indeed, if this value is below 1 pb synthesis at SHIP is not considered due to the long irradiation times needed. Therefore one has to be able to predict more or less reliable values for the cross-sections. A cross-section with an error of one or two orders of magnitude is still a very useful result, that can guide the experiment preparations. For cross-section predictions we used the statistical evaporation code HIVAP (cf. section 2.4).

6.1 HIVAP benchmark

To make sure to obtain reliable results using the statistical evaporation code HIVAP (cf. section 2.4) for the prediction of the cross-sections of new neutron deficient isotopes with $Z = 74-92$ we first had to compare its results with production cross-sections measured for isotopes of similar atomic number Z and neutron number N . For this purpose, we collected the cross-sections values of different reactions reported in 12 reviewed papers from several laboratories and added our own values from our two experiments R263 and R266 (cf. Chapter 4). The knowledge of the beam-target combination, the synthesized isotopes and the energy values at which the reaction took place was essential for the comparison with the results obtained with HIVAP. To illustrate the discrepancies between the HIVAP calculated σ_{calc} and the experimental σ_{exp} cross-section values, we plotted in figure 6.1 the logarithm of their ratio $\sigma_{calc}/\sigma_{exp}$ as

6. CROSS-SECTIONS

a function of the neutron number N of the synthesized isotopes. Each one of the 70 different configurations of beam, target, synthesized isotope and energy appears as a different colored point in figure 6.1. There, the 14 different atomic numbers of the synthesized isotopes comprised between 72 and 92 can be identified by the colored written element names. In the 70 configurations studied, 53 different isotopes and 20 different beam-target combinations were used, some of them reported by several authors. The cross-section results obtained in Chapter 4 in tables 4.1 and 4.5 contributed to eight of these 70 configurations. The considered isotopes were obtained through different reaction channels that include xn, pxn and α xn channels. The excitation energies varied between 24.5 and 80 MeV and the experimentally measured cross-sections ranged from 25 pb to 12 mb. The arithmetic mean of the logarithm of the ratios $\sigma_{calc}/\sigma_{exp}$ is 0.04. This shows that, on average, HIVAP is able to make reliable predictions by neither over- nor underestimating. The average of absolute values of discrepancies $\bar{\delta}$ equals 0.58 with $\bar{f} = 3.8$ and $rms = 0.68$. A mean discrepancy factor \bar{f} of under 4 is a very good value for cross-section predictions. Furthermore, by looking at figure 6.1, one can appreciate that there is not a single case where the absolute value of the logarithm of $\sigma_{calc}/\sigma_{exp}$ is larger than 1.2 which is the equivalent of a maximum factor of 16 between HIVAP calculated and experimentally measured cross-sections. This value may seem elevated, but is actually very acceptable when one takes into account the difficulties associated with cross-section predictions. We notice that HIVAP tends to overestimate the cross-sections for Tl, Fr and Ra while the contrary is true for Bi and Po.

In conclusion, after taking a wide experimental range of reactions, beams, targets, reaction energies, synthesized isotopes, cross-sections, reaction channels and of papers from different laboratories, the obtained results are very satisfactory if one takes into account the uncertainties of these predictions. We can therefore conclude that HIVAP can be used for the estimation of the different cross-sections of the neutron deficient isotopes with $N < 126$ and $Z = 74-92$ produced through xn, pxn and α xn channels.

6.2 New isotopes

6.2.1 Reactions

To produce new neutron-deficient isotopes with $Z = 74-92$, 117 reactions were studied. They are listed in table 6.1. 28 different beams and 24 different targets were

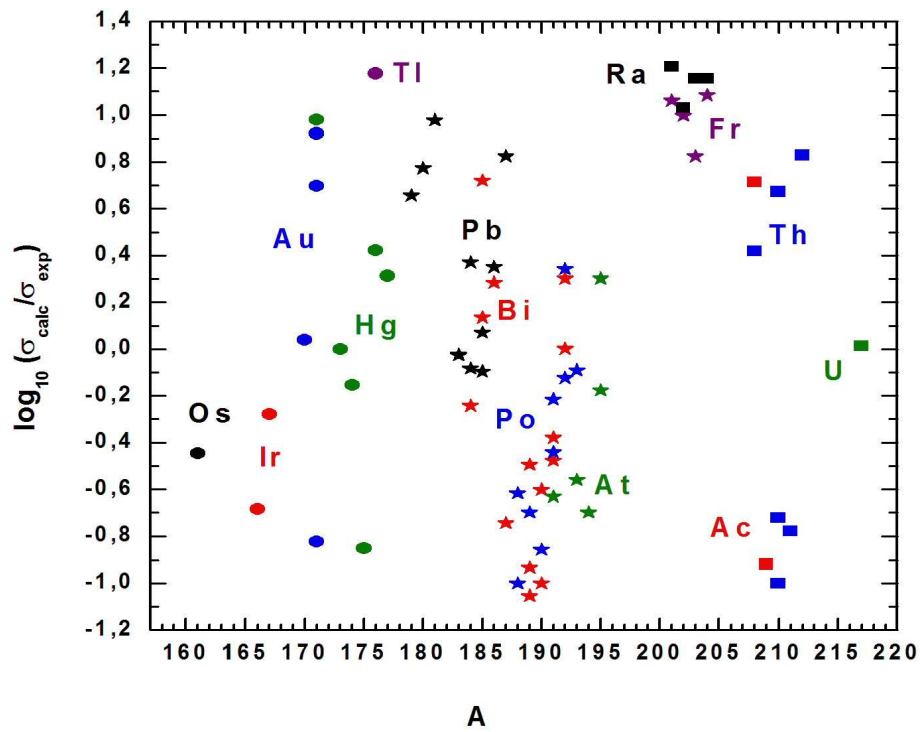


Figure 6.1: HIVAP benchmark - Discrepancies between the HIVAP calculated σ_{calc} and the experimental σ_{exp} cross-section values are illustrated by plotting the logarithm of their ratio $\sigma_{\text{calc}}/\sigma_{\text{exp}}$ as a function of the atomic number A of the same synthesized isotopes.

6. CROSS-SECTIONS

considered. The projectiles range from ^{40}Ca to ^{124}Xe while the targets range from ^{58}Ni to ^{158}Dy . These reactions cover very asymmetrical ones like $^{40}\text{Ca} + ^{144}\text{Sm}$ or $^{124}\text{Xe} + ^{58}\text{Ni}$ as well as symmetrical reactions like $^{92}\text{Mo} + ^{92}\text{Mo}$ or $^{96}\text{Ru} + ^{96}\text{Ru}$. They were chosen to produce a compound nucleus that after evaporation of some nucleons would likely end in a new isotope as evaporation residue. An interesting feature of these beam-target combinations is the fact that the compound nuclei always have an even number of protons Z because no beam-target combination led to an odd- Z compound nucleus with the required number of neutrons. This is achieved both through the fusion of two even- Z isotopes and two odd- Z isotopes. Therefore all xn and α xn channels will result in even- Z isotopes while all pxn channels will result in odd- Z isotopes.

6.2.2 xn channels

As mentioned in the previous subsection, all xn channels result in even- Z isotopes since all compound nuclei of the studied reactions have an even atomic number. In table 6.2 several reactions are shown that could lead to the synthesis of 41 new isotopes with reaction cross-sections higher than 1pb. In fact some σ values go up to 1 μb . For each new isotope only the reaction with the highest cross-section is listed in table 6.2 even if it could be synthesized in other ways, some times even with similar values of σ . The energy range of the proposed reactions goes from 20 (1n channel) to 77 (5n channel) MeV. New isotopes for all 10 even- Z elements lying between $Z=74$ and $Z=92$ could be synthesized according to these HIVAP calculations. For three elements (Rn, Ra and U) even 6 new isotopes are possible.

6.2.3 pxn channels

As mentioned in subsection 6.2.1, all pxn channels result in odd- Z isotopes since all compound nuclei of the studied reactions have an even atomic number. In table 6.3 several reactions are shown that could lead to the synthesis of 32 new isotopes with reaction cross-sections higher than 1pb. In fact some σ values go up to 70 nb. For each new isotope only the reaction with the highest cross-section is given even if it could be synthesized in other ways, some times even with similar values of σ . The energy range of the proposed reactions goes from 20 MeV (p channel) to 77 MeV (p5n channel). New isotopes for 8 of the 9 odd- Z elements lying between $Z=74$ and $Z=92$ (no Ir) could be

Table 6.1: Reactions calculated with HIVAP - Beam, target and compound nucleus.

Beam	Target	CN	Beam	Target	CN	Beam	Target	CN	Beam	Target	CN			
^{40}Ca	^{144}Sm	^{184}Pb		^{144}Sm	^{208}U		^{150}Sm	^{220}U		^{130}Ba	^{208}U			
^{46}Ti	^{156}Dy	^{202}Ra		^{147}Sm	^{211}U	^{69}Ga	^{141}Pr	^{210}Th	^{84}Sr	^{92}Mo	^{176}Hg			
^{50}Cr	^{112}Sn	^{162}W		^{148}Sm	^{212}U	^{70}Ge	^{92}Mo	^{162}W		^{96}Ru	^{180}Pb			
	^{144}Sm	^{194}Rn		^{149}Sm	^{213}U		^{96}Ru	^{166}Os		^{102}Pd	^{186}Po			
	^{156}Dy	^{206}Th		^{150}Sm	^{214}U		^{102}Pd	^{172}Pt		^{106}Cd	^{190}Rn			
	^{158}Dy	^{208}Th		^{152}Sm	^{216}U		^{106}Cd	^{176}Hg		^{112}Sn	^{196}Ra			
^{52}Cr	^{156}Dy	^{208}Th		^{154}Sm	^{218}U		^{112}Sn	^{182}Pb		^{120}Te	^{204}Th			
^{54}Fe	^{106}Cd	^{160}W	^{66}Zn	^{144}Sm	^{210}U		^{130}Ba	^{200}Ra	^{90}Zr	^{92}Mo	^{182}Pb			
	^{112}Sn	^{166}Os		^{147}Sm	^{213}U		^{136}Ce	^{206}Th		^{96}Ru	^{186}Po			
	^{130}Ba	^{184}Pb		^{148}Sm	^{214}U		^{142}Nd	^{212}U		^{102}Pd	^{192}Rn			
	^{142}Nd	^{196}Rn		^{149}Sm	^{215}U	^{72}Ge	^{142}Nd	^{214}U		^{106}Cd	^{196}Ra			
	^{144}Sm	^{198}Ra		^{150}Sm	^{216}U	^{73}Ge	^{142}Nd	^{215}U		^{112}Sn	^{202}Th			
	^{156}Dy	^{210}U		^{152}Sm	^{218}U	^{74}Ge	^{142}Nd	^{216}U		^{120}Te	^{210}U			
	^{58}Ni	^{102}Pd		^{160}W		^{154}Sm	^{220}U	^{76}Ge		^{142}Nd	^{218}U	^{92}Mo	^{92}Mo	^{184}Po
		^{106}Cd		^{164}Os	^{67}Zn	^{144}Sm	^{211}U	^{75}As		^{141}Pr	^{216}U		^{96}Ru	^{188}Rn
		^{112}Sn		^{170}Pt		^{147}Sm	^{214}U	^{74}Se		^{92}Mo	^{166}Os		^{102}Pd	^{194}Ra
		^{136}Ce		^{194}Rn		^{148}Sm	^{215}U			^{96}Ru	^{170}Pt		^{106}Cd	^{198}Th
^{142}Nd		^{200}Ra	^{149}Sm	^{216}U			^{102}Pd	^{176}Hg	^{112}Sn	^{204}U				
^{144}Sm		^{202}Th	^{150}Sm	^{217}U			^{106}Cd	^{180}Pb	^{96}Ru	^{96}Ru	^{192}Ra			
^{147}Sm		^{205}Th	^{152}Sm	^{219}U			^{112}Sn	^{186}Po		^{102}Pd	^{198}Th			
^{60}Ni		^{144}Sm	^{204}Th	^{68}Zn		^{144}Sm	^{212}U		^{120}Te	^{194}Rn	^{106}Cd		^{202}U	
^{63}Cu		^{141}Pr	^{204}Ra			^{147}Sm	^{215}U		^{130}Ba	^{204}Th	^{102}Pd		^{204}U	
^{64}Zn		^{96}Ru	^{160}W			^{148}Sm	^{216}U		^{136}Ce	^{210}U	^{124}Xe		^{58}Ni	^{182}Pb
	^{102}Pd	^{166}Os		^{149}Sm		^{217}U	^{78}Kr	^{84}Sr	^{162}W	^{70}Ge		^{194}Rn		
	^{106}Cd	^{170}Pt		^{150}Sm	^{218}U	^{92}Mo		^{170}Pt	^{74}Se	^{198}Ra				
	^{112}Sn	^{176}Hg		^{152}Sm	^{220}U	^{96}Ru		^{174}Hg	^{78}Kr	^{202}Th				
	^{120}Te	^{184}Pb	^{70}Zn	^{144}Sm	^{214}U	^{102}Pd		^{180}Pb	^{84}Sr	^{208}U				
	^{130}Ba	^{194}Rn		^{147}Sm	^{217}U	^{106}Cd		^{184}Po						
	^{136}Ce	^{200}Ra		^{148}Sm	^{218}U	^{112}Sn		^{190}Rn						
	^{142}Nd	^{206}Th		^{149}Sm	^{219}U	^{120}Te		^{198}Ra						

6. CROSS-SECTIONS

Table 6.2: New isotopes obtained through xn channels - Beam-Target combinations, new synthesized isotopes, reaction cross-sections and excitation energies of the compound nuclei. Isotopes for which an appropriate half-life for detection at SHIP (cf. Chapter 5) is expected are marked in red.

Beam	Target	Isotope	σ /pb	E/MeV	Beam	Target	Isotope	σ /pb	E/MeV		
^{54}Fe	^{106}Cd	^{155}W	80	77			^{192}Rn	90	29		
		^{156}W	1E4	62			^{193}Rn	1E3	20		
		^{157}W	1E6	50	^{54}Fe	^{142}Nd	^{194}Rn	2E3	29		
^{58}Ni	^{96}Ru	^{159}Os	80	74			^{144}Sm	^{195}Ra	4	41	
		^{160}Os	8E3	62	^{196}Ra	20		29			
		^{161}Os	4E5	47	^{197}Ra	200		20			
		^{165}Pt	200	74	^{58}Ni	^{142}Nd		^{198}Ra	30	26	
^{78}Kr	^{96}Ru	^{169}Hg	6	77			^{46}Ti	^{156}Dy	^{199}Ra	70	41
		^{170}Hg	700	62	^{200}Ra	20			29		
^{74}Se	^{106}Cd	^{175}Pb	4	77	^{58}Ni	^{147}Sm	^{203}Th	1	29		
		^{176}Pb	400	62			^{50}Cr	^{156}Dy	^{204}Th	1	29
		^{177}Pb	1E4	47					^{52}Cr	^{205}Th	40
		^{178}Pb	4E5	35			^{206}Th	100		29	
^{92}Mo	^{92}Mo	^{181}Po	10	44	^{69}Ga	^{141}Pr	^{207}Th	200	41		
		^{182}Po	200	29			^{70}Zn	^{144}Sm	^{211}U	1	41
		^{183}Po	3E3	20					^{68}Zn	^{147}Sm	^{212}U
^{90}Zr	^{96}Ru	^{184}Po	900	29	^{70}Zn	^{148}Sm	^{213}U	30			41
		^{185}Po	7E3	20			^{214}U	20	50		
	^{102}Pd	^{189}Rn	2	44			^{215}U	200	38		
		^{190}Rn	4	29			^{149}Sm	^{216}U	400	38	
^{50}Cr	^{144}Sm	^{191}Rn	5	41							

synthesized according to these HIVAP calculations. For Ac even 7 new isotopes can be expected.

Table 6.3: New isotopes obtained through pxn channels - Beam-Target combinations, new synthesized isotopes, reaction cross-sections and excitation energies of the compound nuclei. Isotopes for which an appropriate half-life for detection at SHIP (cf. Chapter 5) is expected are marked in red.

Beam	Target	Isotope	σ /pb	E/MeV	Beam	Target	Isotope	σ /pb	E/MeV
^{58}Ni	^{106}Cd	^{158}Re	300	77			^{190}At	2E3	32
		^{159}Re	7E4	68	^{54}Fe	^{144}Sm	^{195}Fr	10	38
^{78}Kr	^{96}Ru	^{168}Au	20	77			^{196}Fr	600	26
		^{169}Au	4E3	68			^{197}Fr	100	20
^{74}Se	^{106}Cd	^{174}Tl	10	77	^{58}Ni	^{142}Nd	^{198}Fr	1E3	29
		^{175}Tl	2E3	71		^{144}Sm	^{199}Ac	4	41
		^{176}Tl	5E4	56			^{200}Ac	30	29
^{78}Kr		^{179}Bi	2	68	^{60}Ni		^{201}Ac	1	41
		^{180}Bi	90	56			^{202}Ac	70	29
^{92}Mo	^{92}Mo	^{181}Bi	6E3	41	^{50}Cr	^{156}Dy	^{203}Ac	50	41
		^{182}Bi	6E4	29				^{204}Ac	200
		^{183}Bi	7E4	20	^{52}Cr	^{205}Ac	1E3	41	
^{84}Sr	^{106}Cd	^{186}At	10	56	^{54}Fe		^{208}Pa	200	32
		^{187}At	100	41	^{68}Zn	^{144}Sm	^{209}Pa	4	41
		^{188}At	500	32			^{70}Zn	^{210}Pa	4
^{90}Zr	^{102}Pd	^{189}At	400	41			^{211}Pa	40	41

6.2.4 α xn channels

In our study we wanted to investigate the cross-section values of the α xn channels. For this purpose, we analyzed the results of the same 117 reactions that were used to predict the synthesis of 41 and 32 new isotopes through xn and pxn channels, respectively, with higher cross-sections than 1pb. As mentioned in subsection 6.2.1, all α xn channels result in even-Z isotopes since all compound nuclei of the studied reactions have an even atomic number. Through α xn channels only 17 new isotopes could be produced with $\sigma_{\alpha xn}$ higher than 1pb. But these same 17 isotopes could be produced through xn channels with higher cross-sections σ_{xn} . To illustrate this, in figure 6.2 we

6. CROSS-SECTIONS

plotted the 17 logarithms of the ratios $\sigma_{xn}/\sigma_{\alpha xn}$ as a function of the neutron number N of the same synthesized isotopes. The results clearly show that σ_{xn} is $\sim 1-2$ orders higher than $\sigma_{\alpha xn}$. We obtained an interesting information out of this analysis: according to HIVAP, no improvement in the number of new isotopes or in the cross-section values can be achieved through the αxn channels of these reactions in comparison with the xn channels.

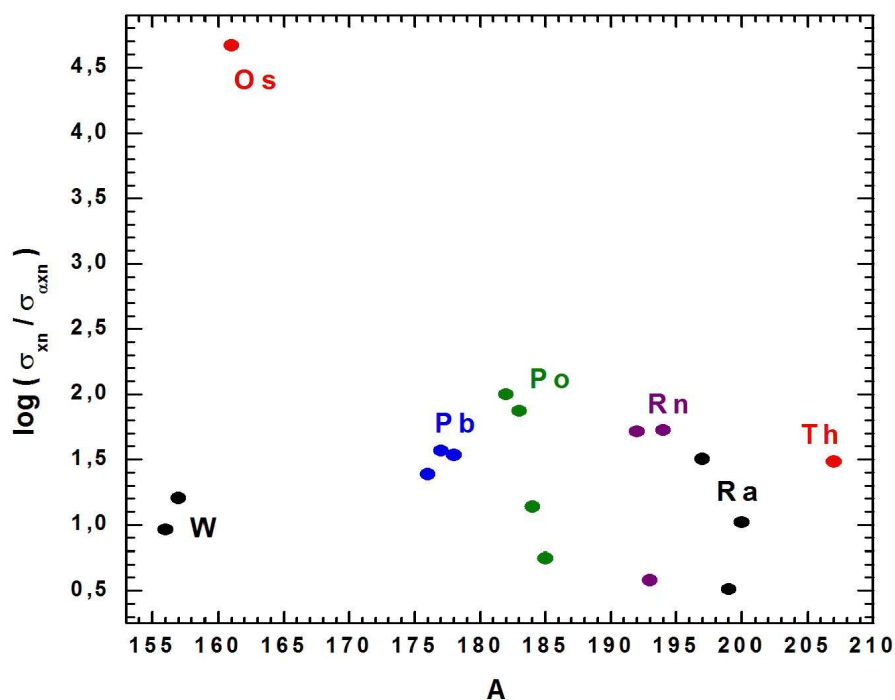


Figure 6.2: Comparison of σ_{xn} with $\sigma_{\alpha xn}$ - The 17 logarithms of the ratios $\sigma_{xn}/\sigma_{\alpha xn}$ are plotted as a function of the atomic number A of the same synthesized isotopes.

6.3 Reactions with RIBs

Today, Radioactive Ion Beams are still of low intensity in comparison with stable beams, but in the future one could imagine that the intensities could be similar and then their use for the production of new isotopes could be of paramount interest. We

therefore studied the possible values of reaction cross-sections using RIBs.

6.3.1 Reactions, new isotopes and higher cross-sections

Table 6.4: Reactions calculated with HIVAP using radioactive beams

Beam	Target	Beam	Target	Beam	Target	Beam	Target	Beam	Target
^{44}Ti	^{158}Dy	^{56}Ni	^{102}Pd	^{62}Zn	^{96}Ru	^{72}Se	^{96}Ru		^{108}Cd
^{48}Cr	^{158}Dy		^{104}Pd		^{98}Ru		^{98}Ru	^{82}Sr	^{96}Ru
	^{160}Dy		^{106}Cd		^{106}Cd		^{106}Cd		^{98}Ru
^{52}Fe	^{106}Cd		^{108}Cd		^{108}Cd		^{108}Cd	^{86}Zr	^{102}Pd
	^{108}Cd		^{112}Sn		^{132}Ba	^{76}Kr	^{92}Mo	^{88}Zr	^{98}Ru
	^{144}Nd		^{114}Sn		^{148}Sm		^{94}Mo		^{102}Pd
	^{144}Sm		^{144}Nd		^{149}Sm		^{96}Ru		^{104}Pd
	^{147}Sm		^{147}Sm		^{150}Sm		^{98}Ru	^{90}Mo	^{92}Mo
	^{156}Dy		^{148}Sm		^{152}Sm		^{102}Pd		^{94}Mo
	^{158}Dy		^{149}Sm		^{154}Sm		^{104}Pd		

To produce new neutron-deficient isotopes with $Z = 74\text{--}92$, 49 reactions with RIBs were studied. They are listed in table 6.4. 11 different beams and 22 different targets were used. They all represent combinations of isotopes with an even atomic number. Thus, all compound nuclei having an even number of protons Z , all xn and α xn channels will result in even- Z isotopes while all pxn channels will result in odd- Z isotopes. The projectiles range from ^{44}Ti to ^{90}Mo while the targets range from ^{92}Mo to ^{160}Dy . The considered reactions range from very asymmetrical ones like $^{44}\text{Ti} + ^{158}\text{Dy}$ to more symmetrical reactions like $^{90}\text{Mo} + ^{92}\text{Mo}$. They were chosen to produce a compound nucleus that after evaporation of some nucleons would likely end in a new isotope as evaporation residue.

In table 6.5 several reactions with RIBs are shown that could lead to the synthesis of 21 new isotopes with reaction cross-sections higher than 1 pb that cannot be synthesized with the reactions of section 6.2. In fact some σ values go up to 5 nb. For each new isotope only the reaction with the highest cross-section is listed in table 6.5 even if it could be synthesized in other ways, some times even with similar values of σ . The energy range of the proposed reactions goes from 29 MeV (2n and p1n channels) to 77 MeV (5n and p5n channels). New isotopes for all 15 elements lying between

6. CROSS-SECTIONS

Table 6.5: New isotopes obtained with radioactive beams - Beam-Target combinations, new synthesized isotopes, reaction cross-sections and excitation energies of the compound nuclei. Isotopes marked with an asterisk are obtained through pxn channels while those unmarked are obtained through xn channels. Isotopes for which an appropriate half-life for detection at SHIP (cf. Chapter 5) is expected are marked in red.

Beam	Target	Isotope	σ /pb	E/MeV	Beam	Target	Isotope	σ /pb	E/MeV
^{52}Fe	^{106}Cd	^{154}W	100	65	^{82}Sr	^{96}Ru	^{174}Pb	30	62
^{56}Ni		$^{156}\text{Re}^*$	1	77	^{90}Mo	^{92}Mo	$^{178}\text{Bi}^*$	10	53
		$^{157}\text{Re}^*$	2E3	68			^{179}Po	2	47
		^{158}Os	300	62			^{180}Po	30	32
	^{112}Sn	$^{162}\text{Ir}^*$	20	77	^{86}Zr	^{102}Pd	$^{184}\text{At}^*$	2	59
		$^{163}\text{Ir}^*$	5E3	68			$^{185}\text{At}^*$	10	44
		^{163}Pt	6	77	^{88}Zr		^{188}Rn	1	29
		^{164}Pt	700	62	^{52}Fe	^{144}Sm	$^{193}\text{Fr}^*$	1	38
^{76}Kr	^{96}Ru	$^{167}\text{Au}^*$	300	68			$^{194}\text{Fr}^*$	30	29
		^{168}Hg	40	62			^{194}Ra	3	29
^{72}Se	^{106}Cd	$^{173}\text{Tl}^*$	200	71					

Z=74 and Z=88 could be synthesized according to these HIVAP calculations. Isotopes marked with an asterisk are obtained through pxn channels while those unmarked are obtained through xn channels.

With RIBs, besides possibly reaching 21 new isotopes as mentioned in the last paragraph, 24 isotopes that were already mentioned in section 6.2 with their respective cross-sections σ (c.f. tables 6.2 and 6.3) could be produced with much higher cross-sections σ_R . These improvements are shown in table 6.6 through the logarithms of the ratios σ_R/σ . They range from 0.1 to 2.8 which correspond to factors of 1.3 to 631, respectively. The average of absolute values of discrepancies $\bar{\delta}$ equals 2.06 with $\bar{f} = 115$ and rms = 2.2. So, on average the cross-sections obtained with RIBs are 115 times higher than with stable beams. Also noticeable is the relatively low value of rms which shows that these improved values have a good homogeneity. The expected cross-sections range from 30 pb to 20 μb . For each new isotope only the reaction with the highest cross-section is listed even if it could be synthesized in other ways, some times even with similar values of σ . The energy range of the proposed reactions goes from 20 (1n channel) to 56 (p3n channel) MeV. New isotopes for 11 of the 12 elements

Table 6.6: Higher cross-sections with radioactive beams for 24 new isotopes of section 6.2 Beam-Target combinations, new synthesized isotopes, reaction cross-sections, excitation energies of the compound nuclei and logarithms of the ratios σ_R/σ . Isotopes marked with an asterisk are obtained through pxn channels while those unmarked are obtained through xn channels. Isotopes for which an appropriate half-life for detection at SHIP (cf. Chapter 5) is expected are marked in red.

Beam	Target	Isotope	σ_R/pb	E/MeV	$\log \frac{\sigma_R}{\sigma}$	Beam	Target	Isotope	σ_R/pb	E/MeV	$\log \frac{\sigma_R}{\sigma}$
^{52}Fe	^{106}Cd	^{155}W	3E4	50	2.6			^{170}Hg	2E5	35	2.5
^{62}Zn	^{96}Ru	^{156}W	2E6	38	2.3	^{72}Se	^{106}Cd	$^{174}\text{Tl}^*$	7E3	56	2.8
		^{157}W	2E7	29	1.3			$^{175}\text{Tl}^*$	4E5	44	2.3
^{56}Ni	^{106}Cd	$^{158}\text{Re}^*$	1E5	53	2.5			$^{176}\text{Tl}^*$	3E6	32	1.8
		$^{159}\text{Re}^*$	2E7	41	2.5	^{82}Sr	^{96}Ru	^{175}Pb	2E3	50	2.7
		^{159}Os	3E4	47	2.6			^{176}Pb	8E4	35	2.3
		^{160}Os	2E6	35	2.4			^{177}Pb	2E5	23	1.3
		^{161}Os	8E6	26	1.3	^{90}Mo	^{92}Mo	$^{179}\text{Bi}^*$	800	41	2.6
	^{112}Sn	^{165}Pt	5E4	47	2.4			$^{180}\text{Bi}^*$	8E3	29	1.9
^{76}Kr	^{96}Ru	$^{168}\text{Au}^*$	1E4	56	2.7			^{181}Po	80	20	0.9
		$^{169}\text{Au}^*$	1E6	41	2.4	^{86}Zr	^{102}Pd	$^{186}\text{At}^*$	30	35	0.5
		^{169}Hg	3E3	47	2.7	^{88}Zr		$^{188}\text{At}^*$	700	32	0.1

lying between $Z=74$ and $Z=85$ (no Ir) could be synthesized with higher cross-sections according to these HIVAP calculations. Isotopes marked with an asterisk are obtained through pxn channels while those unmarked are obtained through xn channels.

As in section 6.2.4, we studied the cross-sections with RIBs of αxn channels. We could not find an improvement neither for the number of possible new isotopes nor for the cross-section values through these evaporation channels.

6.3.2 Study to increase the cross-sections with RIBs for a given compound nucleus

Let's consider the following pair of reactions:

$${}^{A_1}X + {}^{A_2}Y = {}^{A_1+A_2}W^* \tag{6.1}$$

$${}^{A_1-2}X + {}^{A_2+2}Y = {}^{A_1+A_2}W^* \tag{6.2}$$

6. CROSS-SECTIONS

Table 6.7: Beam-target combinations of the type described in Eq. 6.2 belonging to the 27 pairs of reactions calculated with HIVAP described in subsection 6.3.2

Beam	Target	Beam	Target	Beam	Target	Beam	Target	Beam	Target
^{44}Ti	^{158}Dy	^{56}Ni	^{104}Pd		^{108}Cd		^{108}Cd	^{88}Zr	
^{48}Cr			^{108}Cd		^{132}Ba	^{76}Kr	^{94}Mo		^{104}Pd
	^{160}Dy		^{114}Sn		^{150}Sm		^{98}Ru	^{90}Mo	^{94}Mo
^{52}Fe	^{108}Cd		^{144}Nd		^{152}Sm		^{104}Pd		
	^{144}Nd		^{149}Sm		^{154}Sm		^{108}Cd		
	^{158}Dy	^{62}Zn	^{98}Ru	^{72}Se	^{98}Ru	^{82}Sr	^{98}Ru		

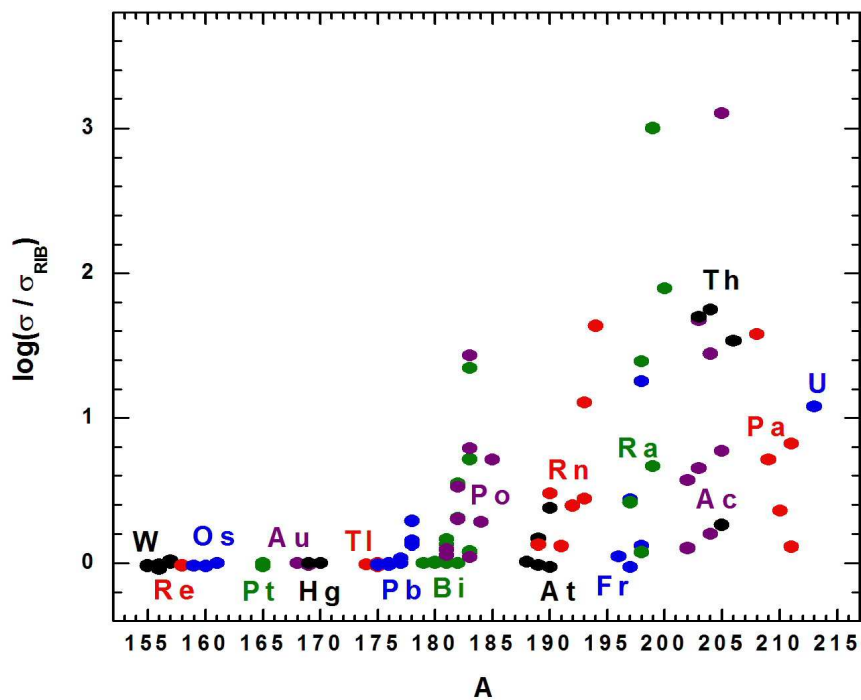


Figure 6.3: Comparison of σ with σ_{RIB} - The 27 logarithms of the ratios σ/σ_{RIB} are plotted as a function of the atomic number A of the same synthesized isotopes.

where ^{A_1}X is a stable beam isotope, ^{A_2}Y and $^{A_2+2}\text{Y}$ are stable target isotopes and $^{A_1-2}\text{X}$ is a radioactive beam isotope.

As can be seen the compound nucleus is the same in both reactions. This is achieved in the first case with the use of a given stable beam-target combination and in the second case by the use of a radioactive beam with two neutrons less than in the first case and a stable target nucleus with two neutrons more.

Since it is interesting if for the same compound nuclei the use of RIBs could increase the cross-sections in comparison with stable beam-target combinations, we studied 27 pairs of reactions of the kind discussed above. The second members of these pairs can be found in table 6.7 and the first members can be deduced from them. 10 different pairs of beams ^{A_1}X – $^{A_1-2}\text{X}$ and 13 different pairs of targets ^{A_2}Y – $^{A_2+2}\text{Y}$ were considered. In these 27 pairs of reactions, all used isotopes have an even atomic number. Thus, all compound nuclei having an even number of protons Z , all xn and α xn channels will result in even- Z isotopes while all pxn channels will result in odd- Z isotopes. The projectiles range from ^{44}Ti to ^{92}Mo while the targets go from ^{92}Mo to ^{160}Dy . These reactions range from very asymmetric ones like $^{44}\text{Ti} + ^{158}\text{Dy}$ to symmetric reactions like $^{92}\text{Mo} + ^{92}\text{Mo}$. They were mainly chosen to perform the aforementioned comparison but also keeping in mind the task of synthesizing a compound nucleus that after evaporation of some nucleons would end in a new isotope as evaporation residue.

For each pair, we calculated with HIVAP the cross-sections σ and σ_{RIB} for the reactions corresponding to Eqs. 6.1 and 6.2, respectively. To compare them, we plotted in figure 6.3 the logarithms of the ratios σ/σ_{RIB} as a function of the neutron number N of the same synthesized isotopes. The plot shows that for $74 \leq Z \leq 81$ the results are quite similar while for $82 \leq Z \leq 92$ the results obtained from reactions of type Eq. 6.1 without the use of RIBs are generally better. We obtained an interesting information out of this analysis: according to HIVAP, for reactions leading to the same compound nuclei, no improvement in the cross-section values can be achieved through the use of RIBs instead of the corresponding stable beams with 2 neutron heavier isotopes.

6. CROSS-SECTIONS

7

Summary and Outlook

7.1 Summary

Neutron deficient isotopes with $N < 126$ and $74 \leq Z \leq 92$ were synthesized in two experiments: R263 and R266. In the first, the new isotope ^{208}Th was produced in a complete-fusion reaction and unambiguously identified on the basis of energy-, position- and time-correlated α -decay chains. Also improved data on the α decay of $^{209,210,212}\text{Th}$, $^{208g,208m,209}\text{Ac}$ and ^{208}Ra were obtained using complete fusion reactions of ^{64}Ni with $^{147,150,152}\text{Sm}$ targets. In R266 the isotope ^{179}Pb was identified for the first time while improved data on the α decay of $^{180,181}\text{Pb}$, ^{181g}Tl , ^{177g}Au , $^{174,172}\text{Pt}$ and ^{177}Hg were also obtained.

Q_α and, for odd- Z isotopes, Q_p values of new neutron deficient isotopes with $N < 126$ and $74 \leq Z \leq 92$ were determined by averaging the data collected in the aforementioned experiments and the literature. New parameters for semi-empirical α -decay formulae for our region of interest were calculated. The partial α -, β^+ / EC -, and proton-decay half-lives $T_{\frac{1}{2},\alpha}$, $T_{\frac{1}{2},\beta}$ and $T_{\frac{1}{2},p}$, respectively, were estimated to obtain total half-lives $T_{\frac{1}{2}}$. With these values, 73 new even- Z (or even 84 if $0.1\mu\text{s} < T_{\frac{1}{2}} < 1\text{s}$) and 41 new odd- Z isotopes have a good probability of being detected and identified at SHIP. They are marked in red, orange and yellow in figure 7.1.

The statistical evaporation code HIVAP was tested positively with experimental results, both from our two experiments and from the literature. According to it, using stable beams, 73 new neutron deficient isotopes with $N < 126$ and $Z = 74\text{--}92$ could be produced with cross-sections higher than 1 pb, which was set as the lower limit for

7. SUMMARY AND OUTLOOK

production at SHIP. Of these, 65 would have at the same time an appropriate half-life for detection (colored in red in figure 7.1). Considering that one day the intensities of RIBs could match the ones of present stable beams, 21 more new isotopes, of which 9 (colored in orange in figure 7.1) would also satisfy the half-live detection condition, would fulfill the same 1pb-synthesis constraint. The use of RIBs would allow the production with higher cross-sections of 24 of the 73 new aforementioned isotopes.

7.2 Outlook

Now that the cross-sections and the half-lives of so many new neutron-deficient isotopes have been estimated, experiments to produce them could be carried out. Their synthesis and the detailed study of their properties could be a step towards a better understanding of the nuclear force. The use of fragmentation reactions could be another way to reach this region of nuclei as the promising application of the projectile fragmentation method at FRS (GSI) to produce neutron-deficient Fr-Th nuclei was demonstrated [106, 107]. The methods employed in this thesis could be used on another region of the chart of nuclides to predict both half-lives and cross-sections.

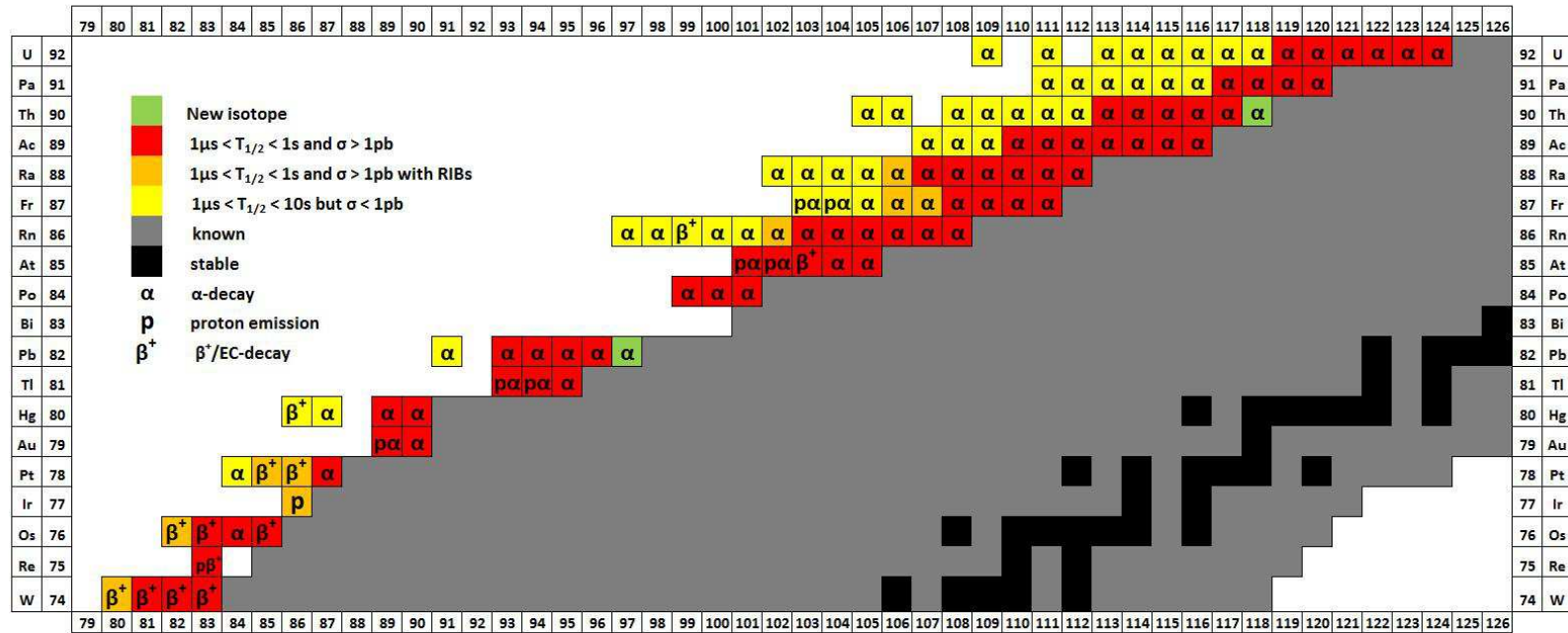


Figure 7.1: Results concerning the production and decay properties of neutron deficient isotopes with $N < 126$ and $74 \leq Z \leq 92$. - The main decay modes (smallest partial half-lives) are indicated by letters: α , β^+ and p for α -, β^+ /EC- and proton emission decay, respectively. For an odd- Z isotope, if the main decay modes that correspond to $T_{1/2}^L$ and $T_{1/2}^U$ are different, both decay modes are indicated, the first and second letter corresponding to the lower and upper limit, respectively. If the decay modes are identical, only one letter is used. See section 7.1 for an explanation of the colors.

7. SUMMARY AND OUTLOOK

References

- [1] J.C. CORNELL. **Radioactive Ion Beam Facilities in Europe: current status and future development.** GANIL, BP 55027, Caen 14076 cedex 5, France (2005).
- [2] M. FACINA. **A gas catcher for the selective production of radioactive beams through laser ionization.** PhD thesis, Instituut voor Kern- en Stralingsfysica, Departement natuurkunde en sterrenkunde, Faculteit Wetenschappen, K.U. Leuven, Belgium (2004).
- [3] B. STREICHER. **Synthesis and spectroscopic properties of transfermium isotopes with $Z = 105, 106$ and 107 .** PhD thesis, Department of Nuclear Physics, Faculty of Mathematics, Physics and Informatics, Comenius University Bratislava, Slovakia (2006).
- [4] G. GIARDINA *et al.* **Effect of the entrance channel on the synthesis of superheavy elements.** European Physical Journal A **8**, 205 (2000).
- [5] W. REISDORF. **Analysis of Fissionability Data at High Excitation Energies.** Zeitschrift für Physik A **300**, 227 (1981).
- [6] D. VERMEULEN. **Erzeugung schwerer Kerne in ^{40}Ar -induzierten Fusionsreaktionen.** Dissertation, Fachbereich Physik, Technische Hochschule Darmstadt, Germany (1984).
- [7] H. KETTUNEN. **Decay Spectroscopy of heavy nuclei beyond the proton drip line.** PhD thesis, Department of Physics, University of Jyväskylä, Finland (2003).
- [8] I. PERLMAN AND J.O. RASMUSSEN. **Alpha Radioactivity.** Handbuch der Physik, Band XLII, Edited by S. Flügge, Springer-Verlag, Berlin-Göttingen-Heidelberg, 109 (1957).
- [9] J.O. RASMUSSEN. **Alpha-, Beta- and Gamma-Ray Spectroscopy,** Edited by K. Siegbahn, North-Holland, Amsterdam, 701 (1966).
- [10] H. GEIGER AND J.M. NUTTALL. **LVII. The ranges of the α particles from various radioactive substances and a relation between range and period of transformation.** Philosophical Magazine Series 6, **22**, 613 (1911).

REFERENCES

- [11] R. TAAGEPERA AND M. NURMIA. **On the relations between half-life and energy release in alpha decay.** *Annales academiæ Scientiarum fennicæ, Series A VI* **78**, 1 (1961).
- [12] G. GAMOW. **Zur Quantentheorie der Atomzertrümmerung.** *Zeitschrift für Physik* **52**, 510 (1928).
- [13] R.W. GURNEY AND E.U. CONDON. **Quantum Mechanics and Radioactive Disintegration.** *Physical Review* **33**, 127 (1929).
- [14] W.D. LOVELAND *et al.* **Modern nuclear chemistry.** A John Wiley & Sons, Inc., Publication, 193 (2006).
- [15] J.O. RASMUSSEN. **Alpha-Decay Barrier Penetrabilities with an Exponential Nuclear Potential: Even-Even Nuclei.** *Physical Review* **113**, 1593 (1959).
- [16] G. IGO. **Optical Model Potential at the Nuclear Surface for the Elastic Scattering of Alpha Particles.** *Physical Review Letters* **1**, 72 (1958).
- [17] V.E. VIOLA AND G.T. SEABORG. **Nuclear systematics of the heavy elements–II, Lifetimes for alpha, beta and spontaneous fission decay.** *Journal of Inorganic and Nuclear Chemistry* **28**, 741 (1966).
- [18] D.N. POENARU *et al.* **A new semiempirical formula for the alpha decay half-lives.** *Journal Physique Lettres* **41**, L-589 (1980).
- [19] E. RURARZ. **Alpha emitters in the region from Ce to Os.** *Acta Physica Polonica B* **14**, 917 (1983).
- [20] G. ROYER. **Alpha emission and spontaneous fission through quasi-molecular shapes.** *Journal of Physics G* **26**, 1149 (2000).
- [21] A. PARKHOMENKO AND A. SOBICZEWSKI. **Phenomenological formula for α -decay half-lives of heaviest nuclei.** *Acta Physica Polonica B* **36** (10), 3095 (2005).
- [22] T.D. LEE AND C.N. YANG. **Question of Parity Conservation in Weak Interactions.** *Physical Review* **104**, 254 (1956).
- [23] C.S. WU *et al.* **Experimental Test of Parity Conservation in Beta Decay.** *Physical Review* **105**, 1413 (1957).
- [24] P. MÖLLER *et al.* **Nuclear Properties for Astrophysical and Radioactive-Ion-Beam Applications.** *Atomic Data and Nuclear Data Tables* **66**, 131 (1997).
- [25] P. MÖLLER AND J.R. NIX. **Nuclear ground-state Masses and Deformations.** *Atomic Data and Nuclear Data Tables* **59**, 185 (1995).

-
- [26] X. ZHANG *et al.* **Simple Formula of β^+ -Decay Half-Lives of Nuclei Far From β -Stable Line.** Communications in Theoretical Physics (Beijing, China) **48**, 1072 (2007).
- [27] J.M. DONG *et al.* **Proton radioactivity within a generalized liquid drop model.** Physical Review C **79**, 054330 (2009).
- [28] S. ÅBERG *et al.* **Spherical proton emitters.** Physical Review C **56**, 1762 (1997).
- [29] D.S. DELION *et al.* **Theories of proton emission.** Physics Reports **424**, 113 (2006).
- [30] R. BARTH *et al.* **GSI Multi-Branch System User Manual.** GSI Darmstadt, (2000).
- [31] C.N. DAVIDS AND H. ESBENSEN. **Particle-vibration coupling in proton decay of near-spherical nuclei.** Physical Review C **64**, 034317 (2001).
- [32] K. HAGINO. **Role of dynamical particle-vibration coupling in reconciliation of the $d_{3/2}$ puzzle for spherical proton emitters.** Physical Review C **64**, 041304(R) (2001).
- [33] D.N. BASU *et al.* **Folding model analysis of proton radioactivity of spherical proton emitters.** Physical Review C **72**, 051601(R) (2005).
- [34] M. BHATTACHARYA AND G. GANGOPADHYAY. **Microscopic calculation of half lives of spherical proton emitters.** Physics Letters B **651**, 263 (2007).
- [35] M. BALASUBRAMANIAM AND N. ARUNACHALAM. **Proton and α -radioactivity of spherical proton emitters.** Physical Review C **71**, 014603 (2005).
- [36] S. HOFMANN. **Alpha-, Proton-, and Heavy Ion-Radioactivities.** Particle Emission from Nuclei, Vol. II, Edited by D.N. Poenaru and M.S. Ivascu, CRC Press, Boca Raton, Florida, 25 (1988).
- [37] F.D. BECCHETTI AND G.W. GREENLEES. **Nucleon-Nucleus Optical-Model Parameters, $A > 40$, $E < 50$ MeV.** Physical Review **182**, 1190 (1969).
- [38] E. MAGLIONE AND L.S. FERREIRA. **New developments in the theory of proton radioactivity.** European Physical Journal A **15**, 89 (2002).
- [39] J. DONG *et al.* **Alpha-decay for heavy nuclei in the ground and isomeric states.** Nuclear Physics A **832**, 198 (2010).
- [40] Y.Z. WANG *et al.* **Fine structure of α decay to rotational states of heavy nuclei.** Physical Review C **81**, 067301 (2010).
- [41] S. GORIELY *et al.* **Recent breakthroughs in Skyrme-Hartree-Fock-Bogoliubov mass formulas.** European Physical Journal A **42**, 547 (2009).

REFERENCES

- [42] G. AUDI *et al.* **The AME2003 atomic mass evaluation, (II). Tables, graphs and references.** Nuclear Physics A **729**, 337 (2003).
- [43] P. SPÄDTKE *et al.* **Ion source development at GSI.** Review of Scientific Instruments **69**, 1079 (1998).
- [44] S. HOFMANN AND G. MÜNZENBERG. **The discovery of the heaviest elements.** Reviews of Modern Physics **72**, 733 (2000).
- [45] R. GELLER *et al.* **Metal ion production in ECRIS (invited).** Review of Scientific Instruments **63**, 2795 (1992).
- [46] N. ANGERT *et al.* **A New 1.4 MeV/u Injector for the Unilac.** GSI Scientific Report **89-1**, 372 (1989).
- [47] J. BOSSLER *et al.* **Ion Source Development and Operation.** GSI Scientific Report **97-1**, 155 (1997).
- [48] B. KINDLER *et al.* **Chemical compound targets for SHIP on heated carbon backings.** Nuclear Instruments and Methods in Physics Research A **561**, 107 (2006).
- [49] G. MÜNZENBERG *et al.* **The velocity filter SHIP, a separator of unslowed heavy ion fusion products.** Nuclear Instruments and Methods **161**, 65 (1979).
- [50] S. ANTALIC. **Synthesis and properties of neutron deficient isotopes of elements around $Z = 100$.** PhD thesis, Department of Nuclear Physics and Biophysics, Faculty of Mathematics, Physics and Informatics, Comenius University Bratislava, Slovakia (2005).
- [51] M. MAZZOCCO *et al.* **Extension of the Monte-Carlo code MOCADI to fusion-evaporation reactions.** European Physical Journal Special Topics **150**, 363 (2007).
- [52] A. POPEKO. private communication (2008).
- [53] B. SULIGNANO. **Search for K isomers in $^{252,254}\text{No}$ and ^{260}Sg and investigation of their nuclear structure.** PhD thesis, Department of Chemistry, Pharmacy, and geosciences of the Johannes Gutenberg-University, Mainz , Germany (2007).
- [54] Š. ŠÁRO *et al.* **Large size foil-microchannel plate timing detectors.** Nuclear Instruments and Methods in Physics Research A **381**, 520 (1996).
- [55] S. HOFMANN *et al.* **The reaction $^{48}\text{Ca} + ^{238}\text{U} \rightarrow ^{286}\text{112}^*$ studied at the GSI-SHIP.** European Physical Journal A **32**, 251 (2007).
- [56] J.A. HEREDIA *et al.* **The new isotope ^{208}Th .** European Physical Journal A **46**, 337 (2010).
- [57] F.P. HESSBERGER. private communication (2004).

-
- [58] J. HOFFMANN AND W. OTT. **Development of new readout processor SAM3**. GSI Scientific Report (2002).
- [59] J. HOFFMANN *et al.* **Development of ADC multiplexer for SHIP**. GSI Scientific Report (2004).
- [60] J. ADAMCZEWSKI-MUSCH *et al.* **The Go4 Analysis Framework Introduction V3.4**. GSI Darmstadt, (2008).
- [61] R. BRUN AND F. RADEMAKERS. **ROOT – An object oriented data analysis framework**. Nuclear Instruments and Methods in Physics Research A **389**, 81 (1997).
- [62] S. HOFMANN. **New elements - approaching $Z = 114$** . Reports on Progress in Physics **61**, 639 (1998).
- [63] K.H. SCHMIDT *et al.* **Some Remarks on the Error Analysis in the Case of Poor Statistics**. Zeitschrift für Physik A **316**, 19 (1984).
- [64] D. VERMEULEN *et al.* **^{212}Th , a New Isotope**. Zeitschrift für Physik A **294**, 149 (1980).
- [65] J. UUSITALO *et al.* **α decay of the new isotopes ^{210}Th and ^{211}Th** . Physical Review C **52**, 113 (1995).
- [66] H. IKEZOE *et al.* **α decay of a new isotope ^{209}Th** . Physical Review C **54**, 2043 (1996).
- [67] M. LEINO *et al.* **Alpha decay studies of neutron-deficient radium isotopes**. Zeitschrift für Physik A **355**, 157 (1996).
- [68] F.G. KONDEV. **Nuclear Data Sheets for $A = 201$** . Nuclear Data Sheets **108**, 365 (2007).
- [69] A.H. WAPSTRA *et al.* **The AME2003 atomic mass evaluation, (I). Evaluation of input data, adjustment procedures**. Nuclear Physics A **729**, 129 (2003).
- [70] G. AUDI *et al.* **The NUBASE evaluation of nuclear and decay properties**. Nuclear Physics A **729**, 3 (2003).
- [71] C.J. CHIARA AND F.G. KONDEV. **Nuclear Data Sheets for $A = 204$** . Nuclear Data Sheets **111**, 141 (2010).
- [72] K. ANDGREN *et al.* **Excited states in the neutron-deficient nuclei $^{197,199,201}\text{Rn}$** . Physical Review C **77**, 054303 (2008).
- [73] J.O. RASMUSSEN. **Alpha-Decay Barrier Penetrabilities with an Exponential Nuclear Potential: Odd-Mass Nuclei**. Physical Review **115**, 1675 (1959).
- [74] J.KHUYAGBAATAR *et al.* **Isomeric states in ^{214}Th and ^{213}Th** . European Physical Journal A **34**, 355 (2007).

REFERENCES

- [75] A.N. ANDREYEV *et al.* **Shell effects and cross sections of formation of neutron-deficient isotopes of Ac, Ra and Fr in $^{20}\text{Ne} + ^{197}\text{Au}$ reaction.** Nuclear Physics A **568**, 323 (1994).
- [76] F.P. HESSBERGER *et al.* **Decay properties of neutron-deficient nuclei in the region $Z = 86-92$.** European Physical Journal A **8**, 521 (2000).
- [77] M. LEINO *et al.* **Alpha decay of the new isotopes $^{207,208}\text{Ac}$.** Zeitschrift für Physik A **348**, 151 (1994).
- [78] K. VALLI *et al.* **On-Line Alpha Spectroscopy of Neutron-Deficient Actinium Isotopes.** Physical Review **167**, 1094 (1968).
- [79] K. VALLI *et al.* **On-Line Alpha Spectroscopy of Neutron-Deficient Radium Isotopes.** Physical Review **161**, 1284 (1967).
- [80] A.N. ANDREYEV *et al.* **α decay of $^{180,181}\text{Pb}$.** Physical Review C **80**, 054322 (2009).
- [81] A.N. ANDREYEV *et al.* **Identification and decay of the 0.48 ms $13/2^+$ isomer in ^{181}Hg .** Physical Review C **80**, 044334 (2009).
- [82] A.N. ANDREYEV *et al.* **Decay of the $9/2^-$ isomer in ^{181}Tl and mass determination of low-lying states in ^{181}Tl , ^{177}Au , and ^{173}Ir .** Physical Review C **80**, 024302 (2009).
- [83] A.N. ANDREYEV *et al.* **The new isotope ^{179}Pb and α -decay properties of $^{179}\text{Tl}^m$.** Journal of Physics G: Nuclear and Particle Physics **37**, 035102 (2010).
- [84] K.S. TOTH *et al.* **Identification of ^{181}Pb in ^{40}Ca irradiations of ^{144}Sm .** Physical Review C **39**, 1150 (1989).
- [85] K.S. TOTH *et al.* **α -decay properties of ^{181}Pb .** Physical Review C **53**, 2513 (1996).
- [86] K.S. TOTH *et al.* **Identification of ^{180}Pb .** Zeitschrift für Physik A **355**, 225 (1996).
- [87] K.S. TOTH *et al.* **α -decay rates of $^{180,182,184}\text{Pb}$ and the $Z=82$ shell closure.** Physical Review C **60**, 011302 (1999).
- [88] V.A. BOLSHAKOV *et al.* **Nuclei Far From Stability/Atomic Masses and Fundamental Constants 1992.** Proceedings of the 6th International Conference on Nuclei Far From Stability and of the 9th International Conference on Atomic Masses and Fundamental Constants, Bernkastel-Kues, 1992, Edited by R. Neugart and A. Wöhr, IOP Conference Proceedings **132**, Institute of Physics and Physical Society, Bristol, 743 (1993).
- [89] K.S. TOTH *et al.* **Identification of ^{180}Tl α decay.** Physical Review C **58**, 1310 (1998).

-
- [90] F.G. KONDEV *et al.* **Identification of excited structures in proton unbound nuclei $^{173,175,177}\text{Au}$: shape co-existence and intruder bands.** *Physics Letters B* **512**, 268 (2001).
- [91] R.D. PAGE *et al.* **Radioactivity of neutron deficient isotopes in the region $N > 82 > Z$.** *Physical Review C* **53**, 660 (1996).
- [92] F.G. KONDEV. **Nuclear Data Sheets for $A = 177$.** *Nuclear Data Sheets* **98**, 801 (2003).
- [93] E. HAGBERG *et al.* **Alpha decay of neutron-deficient mercury isotopes and their daughters.** *Nuclear Physics A* **318**, 29 (1979).
- [94] G.L. POLI *et al.* **Proton and α radioactivity below the $Z=82$ shell closure.** *Physical Review C* **59**, R2979 (1999).
- [95] J.R.H. SCHNEIDER. GSI Scientific Report **84-3** (unpublished) (1984).
- [96] A. MELERANGI *et al.* **Shape isomerism and spectroscopy of ^{177}Hg .** *Physical Review C* **68**, 041301(R) (2003).
- [97] D. O'DONNELL *et al.* **First observation of excited states in $^{175}\text{Hg}_{95}$.** *Physical Review C* **79**, 051304(R) (2009).
- [98] E. ACHTERBERG *et al.* **Nuclear Data Sheets for $A = 178$.** *Nuclear Data Sheets* **110**, 1473 (2009).
- [99] M.W. ROWE *et al.* **Decay of ^{178}Tl .** *Physical Review C* **65**, 054310 (2002).
- [100] F.G. KONDEV *et al.* **First observation of excited structures in neutron-deficient ^{179}Hg : evidence for multiple shape coexistence.** *Physics Letters B* **528**, 221 (2002).
- [101] R. GRZYWACZ *et al.* **Applications of digital pulse processing in nuclear spectroscopy.** *Nuclear Instruments and Methods in Physics Research B* **204**, 649 (2003).
- [102] R. GRZYWACZ *et al.* **Rare isotope discoveries with digital electronics.** *Nuclear Instruments and Methods in Physics Research B* **261**, 1103 (2007).
- [103] M. PFÜTZNER *et al.* **First evidence for the two-proton decay of ^{45}Fe .** *European Physical Journal A* **14**, 279 (2002).
- [104] V.I. GOLDANSKY. **Two-Proton Radioactivity of Heavier-than-Tin Nuclei.** *Nuclear Physics* **78**, 233 (1966).
- [105] V.I. GOLDANSKII. **Modes of Radioactive Decay Involving Proton Emission.** *Annual Review of Nuclear Science* **16**, 1 (1966).

REFERENCES

- [106] J. KURCEWICZ *et al.* **Production cross-sections of protactinium and thorium isotopes produced in fragmentation of ^{238}U at 1 A GeV.** Nuclear Physics A **767**, 1 (2006).
- [107] Z. LIU *et al.* **Decay spectroscopy of suburanium isotopes following projectile fragmentation of ^{238}U at 1 GeV/u.** Nuclear Instruments and Methods in Physics Research A **543**, 591 (2005).

Curriculum Vitae



Figure 7.2: The Author -

Family names: Heredia Cardona
First Names: Julio Antonio
Marital Status: married
Nationality: Cuban
Place of birth: Havana
Date of birth: 25/01/1981

Education

- **Sep. 2003 to June 2005:** Two year Master in Sciences in the specialty of Experimental Nuclear Physics, Higher Institute of Technologies and Applied Sciences (InSTEC), Academic Tutor: Prof. Dr. Oscar Díaz Rizo
- **Sep. 1998 to July 2003:** Five year Bachelor in Sciences in the specialty of Nuclear Physics, Higher Institute of Technologies and Applied

Sciences (InSTEC/ISCTN), Golden Diploma, Academic Tutor: Prof.
Dr. Oscar Díaz Rizo

- **July 1998:** Baccalauréat with *Mention Très Bien* at the Lycée Français de Vienne

Present Professional Status

- PhD student at the Goethe Universität Frankfurt am Main with a scholarship from HGS-HIRe
- Email: j.heredia@gsi.de
- Telephone: +49 516971-2788
- Address: Planckstrasse 1, 64291, Darmstadt.

Professional Experience

- Teacher Assistant from Sep. 2003 to Jan. 2008 (Nuclear Physics Experimental Methods, Nuclear Physics, Quantum Mechanics I)

Awards

- First Prize: 2003 Forum Estudiantil ISCTN/INTEC in Nuclear Experimental Physics
- Third Prize: 2003 Forum Estudiantil ISCTN/INTEC in Nuclear Experimental Physics
- First Prize: Rallye Alsace Mathématiques 1998

Languages

- **Spanish:** mother tongue
- **French:** mother tongue
- **German:** fluent
- **English:** fluent
- **Italian:** fluent

- **Portuguese:** fluent
- **Russian:** basic

Computing

- Windows (+Office), Linux
- C++
- MCNP
- Go4

Publications

- K.Nishio, S.Hofmann, H.Ikezoe, F.P Heßberger, D.Ackermann, S. Antalic, V.F.Comas, Z.Gan, S.Heinz, **J.A.Heredia**, J.Khuyagbaatar, B.Kindler, I.Kojouharov, P.Kuusiniemi, B. Lommel, R. Mann, M. Mazzocco, S. Mitsuoka, Y. Nagame, T. Ohtsuki, A. G. Popeko, Š. Šáro, H. J. Schött, B. Sulignano, A. Svirikhin, K. Tsukada, K. Tsuruta and A. V. Yeremin. *Measurement of evaporation residue cross-sections of the reaction $^{30}\text{Si} + ^{238}\text{U}$ at subbarrier energies*, European Physical Journal A **29**, 281 (2006).
- S.Hofmann, D.Ackermann, S. Antalic, H.G. Burkhard, V.F.Comas, R.Dressler, Z.Gan, S.Heinz, **J.A.Heredia**, F.P Heßberger, J.Khuyagbaatar, B.Kindler, I.Kojouharov, P.Kuusiniemi, M. Leino, B. Lommel, R. Mann, G. Münzenberg, K.Nishio, A.G. Popeko, Š. Šáro, H.J Schott, B.Streicher, B. Sulignano, J. Uusitalo and A.V Yeremin. *Studies of Superheavy Elements at SHIP*, International Journal of Modern Physics E **16**, 937 (2007).
- S.Hofmann, D.Ackermann, S. Antalic, H.G. Burkhard, V.F.Comas, R.Dressler, Z.Gan, S.Heinz, **J.A.Heredia**, F.P Heßberger, J.Khuyagbaatar, B.Kindler, I.Kojouharov, P.Kuusiniemi, M. Leino, B. Lommel, R. Mann, G. Münzenberg, K.Nishio, A.G. Popeko, Š. Šáro, H.J Schött, B.Streicher, B. Sulignano, J. Uusitalo, M. Venhart and A.V Yeremin. *The reaction $^{48}\text{Ca} + ^{238}\text{U} \rightarrow ^{286}112^*$ studied at the GSI-SHIP*, European Physical Journal A **32**, 51 (2007).
- S. Heinz, V. Comas, F. P. Heßberger, S. Hofmann, D. Ackermann, H. G. Burkhard, Z. Gan, **J. Heredia**, J. Khuyagbaatar and B. Kindler. *Di-nuclear systems studied with the velocity filter SHIP*, European Physical Journal A **38**, 227 (2008).
- **Julio Heredia Carmona**, Oscar Díaz Rizo. *Experimental and Monte Carlo determination of mass absorption coefficients for $^{90}\text{Sr}/^{90}\text{Y}$ beta particles in organic compounds*, Nucleus **45**, 26 (2009).
- A.N. Andreyev, S. Antalic, D. Ackermann, T. E. Cocolios, V. F. Comas, J. Elseviers, S. Franchoo, S. Heinz, **J. A. Heredia**, F. P. Heberger, S. Hofmann, M. Huyse, J. Khuyagbaatar, I.Kojouharov, B. Kindler, B. Lommel, R. Mann, R. D. Page, S. Rinta-Antilla, P. J. Sapple, Š. Šáro, P. Van Duppen, M. Venhart, and H. V. Watkins. *α decay of $^{180,181}\text{Pb}$* , Physical Review C **80**, 054322 (2009).

- A.N. Andreyev, S. Antalic, D. Ackermann, T. E. Cocolios, V. F. Comas, J. Elseviers, S. Franchoo, S. Heinz, **J. A. Heredia**, F. P. Heberger, S. Hofmann, M. Huyse, J. Khuyagbaatar, I.Kojouharov, B. Kindler, B. Lommel, R. Mann, R. D. Page, S. Rinta-Antilla, P. J. Sapple, Š. Šáro, P. Van Duppen, M. Venhart, and H. V. Watkins. *Identification and decay of the 0.48 ms $13/2^+$ isomer in ^{181}Hg* , Physical Review C **80**, 044334 (2009).
- A.N. Andreyev, S. Antalic, D. Ackermann, T. E. Cocolios, V. F. Comas, J. Elseviers, S. Franchoo, S. Heinz, **J. A. Heredia**, F. P. Heberger, S. Hofmann, M. Huyse, J. Khuyagbaatar, I.Kojouharov, B. Kindler, B. Lommel, R. Mann, R. D. Page, S. Rinta-Antilla, P. J. Sapple, Š. Šáro, P. Van Duppen, M. Venhart, and H. V. Watkins. *Decay of the $9/2^-$ isomer in ^{181}Tl and mass determination of low-lying states in ^{181}Tl , ^{177}Au , and ^{173}Ir* , Physical Review C **80**, 024302 (2009)
- A.N. Andreyev, S. Antalic, D. Ackermann, T. E. Cocolios, V. F. Comas, J. Elseviers, S. Franchoo, S. Heinz, **J. A. Heredia**, F. P. Heberger, S. Hofmann, M. Huyse, J. Khuyagbaatar, I.Kojouharov, B. Kindler, B. Lommel, R. Mann, R. D. Page, S. Rinta-Antilla, P. J. Sapple, Š. Šáro, P. Van Duppen, M. Venhart, and H. V. Watkins. *The new isotope ^{179}Pb and α -decay properties of $^{179}\text{Tl}^m$* , Journal of Physics G: Nuclear and Particle Physics **37**, 035102 (2010).
- **J.A. Heredia**, A.N. Andreyev, S. Antalic, S. Hofmann, F.P. Heßberger, D.Ackermann, V.F. Comas, S.Heinz, B. Kindler, B. Lommel, R. Mann. *The new isotope ^{208}Th* , European Physical Journal A **46**, 337 (2010).
- S. Heinz, V. Comas, S. Hofmann, D. Ackermann, **J. Heredia**, F. P. Heberger, J. Khuyagbaatar, B. Kindler, B. Lommel and R. Mann. *Investigation of di-nuclear systems as entrance channel to fusion*, European Physical Journal A **43**, 181 (2010).
- J. Khuyagbaatar, F. P. Heßberger, S. Hofmann, D. Ackermann, V. S. Comas, S. Heinz, **J. A. Heredia**, B. Kindler, I. Kojouharov, B. Lommel, R. Mann, K.Nishio, and A. Yakushev. *The new isotope ^{236}Cm and new data on ^{233}Cm and $^{237,238,240}\text{Cf}$* , European Physical Journal A **46**, 59 (2010).
- A. N. Andreyev, J. Elseviers, M. Huyse, P. Van Duppen, S. Antalic, A. Barzakh, N. Bree, T. E. Cocolios, V. F. Comas, J. Diriken, D. Fedorov, V. Fedosseev, S. Franchoo, **J. A. Heredia**, O. Ivanov, U. Köster, B. A. Marsh, K. Nishio, R. D. Page, N. Patronis, M. Seliverstov, I. Tsekhanovich, P. Van den Bergh, J. Van De Walle, M. Venhart, S. Vermote, M. Veselsky, C. Wagemans, T. Ichikawa, A. Iwamoto, P. Möller, and A. J. Sierk. *New Type of Asymmetric Fission in Proton-Rich Nuclei*, Physical Review Letters **105**, 252502 (2010).
- S. Heinz, V. Comas, S. Hofmann, D. Ackermann, **J. Heredia**, F. P. Heberger, J. Khuyagbaatar, B. Kindler, B. Lommel and R. Mann. *Transfer reaction studies in the region of heavy and superheavy nuclei at SHIP*, Journal of Physics: Conference Series **282**, 012007 (2011).